Development of Wearable, Screen-Printable Conductive Polymer Biosensors on Flexible and Textile Substrates

by

Yohan Laffitte

B.A.Sc., University of Waterloo, 2017

Thesis Submitted in Partial Fulfillment of the
Requirements for the Degree of
Master of Applied Science

in the
School of Engineering Science
Faculty of Applied Sciences

SIMON FRASER UNIVERSITY
Summer 2021

Declaration of Committee

Name:	**Yohan Laffitte**
Degree:	**Master of Applied Science**
Title:	**Development of Wearable, Screen-Printable Conductive Polymer Biosensors on Flexible and Textile Substrates**
Examining Committee:	**Chair:** Rodney Vaughan Professor, Engineering Science
	Bonnie L. Gray Supervisor Professor, Engineering Science
	Ash Parameswaran Committee Member Professor, Engineering Science
	Michael Adachi Examiner Assistant Professor, Engineering Science

Abstract

Wearable biosensors have great potential for real-time diagnostics, but have been encumbered by costly fabrication processes, rigid materials, and inadequate sensitivity for physiological ranges. Sweat has hitherto been an understudied sample for measurement of components like pH and lactate, which can provide meaningful guidance for wound healing, eczema, and sports medicine applications. This thesis presents the development of a flexible, textile-based, screen-printed electrode system for biosensing applications. Furthermore, a flexible, pH-sensitive composite for textile substrates is developed by mixing polyaniline with dodecylbenzene sulfonic acid and textile screen-printing ink. The optimized composite's pH response is compared to electropolymerized and drop-cast polyaniline sensors via open circuit potential measurements. A linear response is observed for all sensors between pH 3-10, with the composite demonstrating sufficient response time and a sensitivity better than -20 mV/pH, exceeding existing flexible screen-printed pH sensors. Investigations into a potentiometric, non-enzymatic lactate sensor using polyaminophenylboronic acid are also discussed.

Keywords: wearable biosensors; flexible electronics; screen-printed electrodes; polyaniline; conductive polymer composite

Acknowledgements

I would like to thank my family for allowing me to pursue my studies and interests throughout this degree. I am very grateful for their continued support regardless of the physical distance between us.

I would equally like to thank my senior supervisor Prof. Bonnie L. Gray for her continued support throughout my project and studies. Additionally, I want to acknowledge the members of my evaluation committee for taking the time to review my thesis.

For the regular discussions, answers to my questions, and support, I would like to greatly thank my group members, particularly Chelsey Currie, David Stevens, and Juan Ferrer. For a number of incredibly helpful conversations and helping me get started in various labs and equipment, I would like to thank Tyler Cuthbert, Jasbir Patel, Armin Hatami, Joyce Leung, among others.

For making Burnaby feel like a second home and keeping me sane during the COVID pandemic, I would like to thank the numerous people who have shown me kindness and friendship throughout my degree, most notably, the community at the SFU Climbing Wall.

Table of Contents

List of Tables

List of Figures

List of Acronyms

3-APBA	3-Aminophenylboronic Acid
APS	Ammonium Persulfate
BA	Boronic Acid
BSA	Bovine Serum Albumin
CE	Counter Electrode
CSA	Camphosulfonic Acid
CNT	Carbon Nanotubes
CV	Cyclic Voltrammetry
DI	Deionized Water
DMF	Dimethylformamide
DMSO	Dimethylsulfoxide
DMM	Digital Multimeter
DBSA	Dodecylbenzene Sulfonic Acid
EB	Emeraldine Base
EIS	Electrical Impedance Spectroscopy
ES	Emeraldine Salt
FET	Field Effect Transistor
GO	Graphene Oxide
H_2O_2	Hydrogen Peroxide
HCl	Hydrochloric Acid
IDE	Interdigitate Electrode
IPA	Isopropanol
ISE	Ion-Sensitive Electrode
ISFET	Ion-Sensitive Field Effect Transistor
LDH	Lactate Dehydrogenase
LOD	Limit of Detection
LOX	Lactate Oxidase
NAD+	Nicotinamide Dinucleotide (Oxidized Form)
NADH	Nicotinamide Dinucleotide (Reduced Form)
NaF	Sodium Fluoride
NF	Nanofiber
NFC	Near-Field Communication

NMP	N-Methyl-2-pyrrolidone
NP	Nanoparticle
PANI	Polyaniline
PAPBA	Poly(3-aminophenylboronic acid)
PBS	Phosphate Buffered Saline
PEDOT:PSS	Poly(3,4-ethylenedioxythiophene) Polystyrene Sulfonate
PEN	Polyethylene Naphthalate
PET	Polyethylene Terephthalate
PMMA	Polymethyl Methacrylate
PPY	Polypyrrole
PS	Polystyrene
PVB	Polyvinyl Butyral
PVC	Polyvinyl Chloride
PVDF	Polyvinylidene Fluoride
RE	Reference Electrode
SFU	Simon Fraser University
SPE	Screen-Printed Electrode
THF	Tetrahydrofuran
TTF	Tetrathiafulvene
WE	Working Electrode
V_G	Gate Voltage
V_{DS}	Drain-Source Voltage

Chapter 1. Introduction

1.1. Wearable Sensors

Healthcare treatment has generally consisted of patients seeking out healthcare centers to receive testing and treatment from medical practitioners. As a growing percentage of the population ages and health issues become more prevalent, it becomes increasingly difficult to provide the same level of medical attention to all patients, which presents a severe concern to our social infrastructure [1]. Consequently, healthcare has been trending towards rapid tests and point-of-care diagnostics to ease these challenges and accelerate the diagnosis step [2-5]. This shift has been highlighted during the recent COVID-19 pandemic where rapid testing has been critical to identifying those infected and prevent the further spreading of the disease [6]. Although rapid and point-of-care methods are well suited for certain diagnostic tests such as infectious diseases, genetic conditions, or other illnesses, they still present challenges for long term monitoring of people with chronic and rapidly fluctuating conditions. Chronic diseases such as diabetes, which requires continuous monitoring of blood-glucose levels, is a well-known example [7, 8]. Furthermore, the body's physiological parameters and biochemical balances are important parameters in determining the health of patients [9-11] or optimizing performance in athletes [12].

The advent of new wearable technologies, facilitated by recent advances in miniaturization and materials development provides an opportunity for bridging this gap. Wearable technologies encompass all technology which can be worn by a user to receive information about or treatment for a physiological or environmental condition. Many examples can be found in use today ranging from devices such as smartwatches to pacemakers. Countless other examples can be found at various stages of commercialization and research. From a biomedical standpoint, wearables have enabled the recording of many physiological parameters. For instance, the recording of biopotentials provides information on muscle activity and heart activity using EMG and ECG technologies, respectively. These have even been integrated into commercially available wearable articles and technologies [13-16]. Similarly, tactile and strain sensors have enabled the tracking of movements and sensations which has led to prosthetics which can interface with human skin to provide tactile feedback capabilities [17, 18]. These

technologies have also been used for tracking of movements and potential falls in the elderly, those with Parkinson's, or other people at risk of injury [19, 20]. These wearable devices monitoring biopotentials and body movements have readily been implemented in a non-invasive fashion by interfacing electrodes with the skin.

On another note, the ability to monitor the body's biochemistry has also been of significant interest. Traditionally, this has been done through blood sampling. Blood serves the vital purpose of transporting blood cells, nutrients, and oxygen throughout the body and as such, it contains a great deal of information about a person's physiological condition. However, at this time, continuous blood sampling presents a set of inherent challenges which make its integration into practical wearable devices infeasible [21]. Namely, blood is only present in blood vessels which cannot be accessed without the use of invasive techniques. Thus, there are various levels of pain associated with blood sampling as to access blood vessels, we must first penetrate through the skin's epidermis layer to at least the dermis layer which is interlaced with various nerve endings. Additionally, continuous sampling of blood results in fouling of sensor surfaces as the body's natural defense mechanism tries to shelter itself from these external probes. If not healed properly or exposed to unsanitary conditions, blood sampling can also lead to infections [22, 23]. To maintain contact with blood vessels while not necessitating an open wound site, implantable devices have also been explored. However, similar sensor fouling issues and challenges still arise [24]. Another consideration is that of micro and macro shocks in which the body becomes part of the conduction pathway for electrical current and can lead to tissue burns or undesired action potentials in muscles like the heart.

Overall, blood does not make for the most convenient analyte for continuous, non-invasive, wearable applications. For this reason, many other bodily fluids have garnered interest for biosensing applications, including wearable biosensors. Great efforts have been invested into exploring these bodily fluids as alternatives to blood diagnostics or monitoring of additional physiologic conditions. These bodily fluids have included saliva, sweat, urine, mucus, interstitial fluid, among others. These distinct body fluids differ in function and thus evidently also differ in composition. Consequently, information that can be obtained from one, may not be obtainable through another. Yet, many of the same biomarkers can be found between some of these which can be correlated to similar physiological pathways and conditions given the body's interconnectedness.

Perspiration, or sweat, presents an attractive alternative given that it can be collected non-invasively and contains many useful biomarkers (glucose, lactate, electrolytes, urea, drugs, etc.). It can be collected passively or extracted via electrochemical stimulation in cases where insufficient sweat is produced [25]. Clinically, potassium levels in sweat are already used for cystic fibrosis diagnosis [26]. Skin pH is another parameter of significant interest as it has been used for monitoring the progression and infection of healing wounds [27], as an indicator of dermatitis [28], and linked to dehydration levels in the field of sports medicine [29]. Lactate equally provides important information with regards to tissue oxidation, physical exertion, and wound healing [30-32].

Yet, despite the availability of sweat and the information it can provide as a biofluid, challenges revolving around reliable sample collection, flexible materials, cost-effective fabrication methods, and complete device integration with other sensors have hindered its progression. Diving into the literature surrounding existing wearable technologies for monitoring pH and lactate revealed deficiencies in the processing and practicality of prior implementations. Many flexible devices have been developed, although relatively few have been created using methods that could easily be translated to fabrication outside of research labs. Furthermore, even fewer have developed sensors which can be applied to textile substrates.

1.2. Thesis Scope and Contributions

This thesis looks at developing wearable technologies which can be used for continuous monitoring of physiologically relevant biomarkers. Sweat was first identified as an attractive alternative for collecting physiological information in a non-invasive manner. The constituents of sweat were then reviewed, and their physiological relevance was assessed. Of particular interest, sweat pH and lactate levels were viewed to have important repercussions to the field of sports medicine and skin care. Upon studying the state of the art of these sensors, wound healing was recognized as an additional application which would benefit from the tracking of these same biomarkers. These applications are highlighted to a greater extent in the ensuing chapter.

The focus of this thesis pertains to the development of flexible sensors which can be applied to textile substrates using a scalable fabrication method, with a greater emphasis being placed on the development of the pH sensor. The decision to prioritize

the pH sensor development was made as the lactate sensor was essentially building on the processing of materials required for the pH sensor. Briefly, the conducting polymer polyaniline (PANI) was selected as a material of interest for the development of the pH sensor, whereas a modified PANI functionalized with a boronic acid group, polyaminophenylboronic acid (PAPBA), was selected as a lactate binding element. By the same token, the fabrication, materials, and methods surrounding the development of the pH sensor could potentially be applied to various other biochemical sensors.

The scope of this project is limited to the development of materials and integration of these onto a textile substrate for the application of sensing lactate and pH in sweat. Therefore, the electrical integration such as signal recording, processing, and display have not been addressed at this time. Similarly, power requirements and sample collection have also not been addressed. These represent their own set of challenges which are outside the scope of this thesis.

Screen-printing technology is a well-established patterning technique applicable to textile and electrodes devised for electrochemical characterization. Our research group has also recently explored its use for fabrication of textile-based ECG electrodes and wearable microfluidics [16, 33]. In continuation with these methods, the development of a flexible, screen-printable, textile-based PANI composite pH sensor was thus the primordial goal of this thesis.

The following chapter, Chapter 2, reviews sweat as a sample and the application of pH and lactate sensors to sports medicine, skin disorders, and wound healing. Chapter 3 evaluates the existing body of research conducted on pH and lactate sensors, beginning with a review of typical sensor architectures. Following this review, Chapter 4 discusses the methods and materials used for the sensors fabricated as part of this thesis to overcome the deficiencies highlighted in literature. The results of the fabrication and the sensor responses are then given and discussed in Chapter 5. The closing chapter, Chapter 6, will summarize the main conclusions of this thesis and discuss the next steps in pursuing the project.

The overall contributions of this thesis are as follows:

1) Development of a textile-based screen-printed electrode system for continuous chemical/biochemical monitoring.

2) Development of a flexible, screen-printable, pH-sensing composite ink using PANI particles which could be applied to textiles.

3) Investigation of a non-enzymatic, potentiometric lactate sensor based on electrochemically synthesized PAPBA on screen-printed electrodes on textiles.

4) Establishing a platform for the development of a comprehensive multi-analyte textile biosensor system for sweat diagnostics.

A peer-reviewed conference paper on the development of a screen-printable PANI composite ink was presented via poster at the 2021 International Conference on Flexible, Printed Sensors and Systems (FLEPS 2021) [34].

Chapter 2. Background

This chapter serves to provide the background information for understanding the applications, existing sensing technology, and previous literature relating to pH and lactate sensors.

2.1. Sweat Diagnostics

Sweat is produced by the body mainly as a means of temperature regulation, but it also plays a role in emotional response and excretion [35, 36]. It is produced by sweat glands located just below the surface of the skin and is excreted through pores in the skin and along hair follicles as seen in Figure 1. It also helps with the excretion of certain waste from the body. Overall, sweat is mainly a product of cell metabolism.

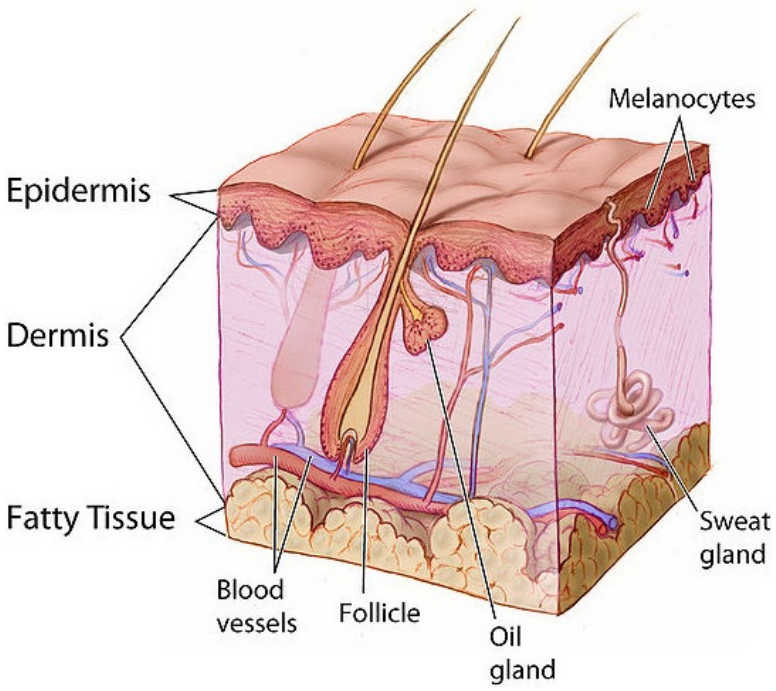

Figure 1. Anatomy of skin and sweat glands reprinted with permission from [37]

Compositionally, sweat is primarily composed of water, yet it also contains many electrolytes, metabolic by-products, proteins, and amino acids in various quantities. An exhaustive review by Baker et al. [35] discusses the major components of sweat. The components present at concentrations greater than 10 μM are summarized in Table 1.

Table 1. Sweat composition and approximate concentrations [36]

Component	Concentration (mmol/L)
Sodium, Na^+	10-90
Chloride, Cl^-	10-90
Lactate	5-40
Urea	4-12
Ethanol	2-30
Potassium, K^+	2-8
Ammonia, NH_3^+	1-8
Bicarbonate, HCO_3^-	0.5-5
Calcium, Ca^{2+}	0.2-2
Magnesium, Mg^{2+}	0.02-0.4
Glucose	0.01-0.2

Currently, sweat plays a limited role in clinical diagnostics, with the main example being the diagnosis of cystic fibrosis wherein sweat tests are used to measure the concentration of sweat chloride. Cystic fibrosis is a genetic condition which affects the production of sweat, digestive fluids, and mucus leading to digestive and respiratory complications [38]. Those with the condition have abnormally elevated concentrations of chloride in their sweat because of defective chloride channels which hinder the flow of chloride through cells. Nevertheless, many studies [39] have reported correlations between other sweat parameters and physiological conditions which has highlighted its potential for other applications, particularly in relation to skin conditions, hydration monitoring, and other health issues.

2.1.1. Lactate

When the body cannot supply enough oxygen to the bloodstream to metabolize energy sources, it starts using the less efficient anaerobic metabolic pathway. Lactate is a by-product of this anaerobic pathway which impedes cell function. Consequently, blood lactate concentration is a strong indicator of a person's physical state and it is widely used in sports medicine to determine athletes' levels of physical conditioning, performance, and exercise intensity [30]. Additionally, prolonged high blood lactate levels, or lactic acidosis, has also been linked to common cardiovascular diseases, diabetes, sepsis, and tumor proliferation in cancerous patients [40-43]. It is therefore imperative to have methods that measure blood lactate levels. As previously mentioned, using blood as a sample for continuous monitoring presents many practical challenges due to its inherent invasiveness. For this reason, sweat provides a more attractive non-invasive alternative

to monitoring lactate levels. Some studies have shown that sweat lactate levels correlate to blood lactate levels [44-47]. However, this correlation remains somewhat debated as others have concluded that no correlation between these exist [36, 48-50]. Instead, they found that that while some blood lactate may be excreted in sweat, sweat lactate is instead produced in the sweat glands as a by-product of sweat production [51]. Despite this controversy, lactate remains an important indicator of the body's oxygenation and metabolic operation and the sensing of this biomolecule is still relevant. Others have also suggested a link between sweat lactate concentration and fitness levels and intensity of physical activity [45, 52, 53]. Numerous studies have highlighted lactate levels as an important indicator to identify reduced oxygen tissue perfusion for detection of pressure ischemia or ulcers [31, 54, 55]. Consequently, the relation between sweat lactate and other physiological parameters warrants further investigation as this presents an attractive alternative to blood sampling.

2.1.2. Sweat pH

The pH range for healthy skin typically lies between a pH of 4 and 6 and is primordially maintained by the free amino acids produced as a by-product of skin flora metabolism [56-58]. This acidic environment inhibits pathogenic bacterial activity and helps regulate the activity of proteins responsible for maintaining the thickness and integrity of the stratum corneum. In fact, disruptions to normal skin pH have been associated with cutaneous diseases such as dermatitis, also known as eczema. Through murine models, it was shown that maintaining an acidic pH has helped prevent atopic dermatitis [28, 59]. Yet, according to the National Eczema Association, about 31.6 million people in the USA suffer from some form of eczema [60]. Consequently, monitoring of skin pH via sweat represents an ideal application for maintaining healthy skin.

On another note, sweat pH has been shown to correlate to the concentration of sodium ions which has in turn been related to dehydration [61-63]. Thus, sweat pH can be used as an indirect measurement of hydration. Additionally, sweat pH can be used to identify metabolic alkalosis [64], and increases in sweat rate [61, 65] demonstrating potential application in the field of sports medicine. However, further investigation is required as there is a great deal of interindividual differences [66].

2.1.3. Other Sweat Biomarkers of Interest

The two main parameters to be discussed in this thesis are sweat pH and lactate, however, a great deal of other potentially useful information can be gleaned from sweat as was highlighted in Table 1.

In terms of biomarkers, glucose is an obvious component of interest in relation to monitoring diabetes. Potentially useful correlations between blood glucose and sweat glucose have been reported further highlighting its appeal [67]. However, many challenges still exist when it comes to sweat glucose analysis. The activity of the glucose oxidase enzyme typically used for glucose sensors is greatly hindered by the presence of lactate and at normal pH of sweat. Additionally, the concentration of sweat glucose is far lower than that of blood necessitating much more sensitive sensors with lower limits of detection [67, 68]. Another biomolecule of potential interest is urea. Urea is a produced when ammonia is broken down during protein digestion. Ammonia is typically metabolised to urea in the liver where it can then be excreted in urine. However, when concentrations are too high or renal failure occurs, it will instead be excreted via sweat. As such, some have studied the link between kidney diseases and sweat levels of urea or ammonia [69, 70].

Many proteomic analyses have been conducted on sweat to try and identify useful biomarkers for diagnostics. In comparing sweat proteome to serum proteome, many different proteins were found [71]. The function of most of these sweat proteins identified pertain to the maintenance of the chemical skin barrier through pH regulation [72]. However, possible links to diagnosing conditions such as schizophrenia have also been suggested [71]. On another note, monitoring of the amino acid tyrosine in sweat has also shown strong correlation to that of serum and can be used to assist in diagnosing liver diseases as well as metabolic, neuropsychiatric, and eating disorders [73].

Various electrolytes are present in sweat and offer meaningful physiological insight. Electrolytes help to maintain proper fluid levels within cells. Thus, sweat rate and electrolyte concentration, particularly sodium, chloride and potassium are highly correlated and serve to give an indication of level of physical exertion and hydration [50]. This information is relevant to athletes in establishing hydration schedules. Electrolytes are typically detected via ionophores, molecules which bind to ions reversibly and can

create a measurable change in potential. For instance, valinomycin and calixarene can be used to measure the concentration of potassium and sodium ions, respectively [74].

Given that sweat also plays a role in excretion, it could also potentially be used for determining the presence of toxicants and intoxicants [75]. Sweat has been examined as a method to test exposure to heavy metals like mercury, cadmium, arsenic, and lead [76, 77]. However, concentrations for these are in the nanomolar to picomolar concentrations, which currently still necessitates highly precise analytical methods for accurate detection. Sweat samples can also be used to test for recent use of drugs including amphetamines/methamphetamines/ecstasy, opiates, cocaine, and cannabis among many others [78]. Products such as the DrugWipe ® have even been developed to screen for these using sweat and are currently in use in locations such as airports. Similarly, ethanol levels can also be detected via sweat sampling [79]. Despite the presence of these in sweat, other body fluids obtainable non-invasively such as saliva or breath tend to be more reliable indicators of consumption and have thus been the preferred means for screening.

Various other compounds exist in sweat at relatively lower levels which could also provide valuable medical information. Cortisol levels in sweat and serum have also shown a strong correlation and could potentially be used for monitoring of stress levels [80]. Gout, a form of arthritis, has also been managed clinically via tracking of uric acid levels in serum, which have been shown to correlate with sweat levels [73].

2.1.4. Sweat Sampling Considerations

Given that sweat is a physiological by-product of thermoregulation, physical exertion, or emotional stimuli, the collection of sweat still requires some sort of stimulus to be excreted continuously. This can be done by exposing subjects to prolonged periods of heat or physical activity, although this can be somewhat inconvenient for more vulnerable patients. Alternatively, sweat can also be extracted through iontophoresis. This process applies an electrical potential gradient over the skin allowing the electrophoretic transport of chemical stimulants to sweat glands. Upon stimulation, the sweat glands then produce sweat. Acetylcholine, pilocarpine, and carbachol are all examples of chemical stimulants that have been used to generate continuous sweat production, some for up to 24 hours [25].

Beyond the excretion of sweat at the surface of the skin, reliable collection methods must equally be considered. External contaminations at the surface of the skin can potentially interfere with measurement accuracy. Localized differences between sweat composition can also create inaccuracies if sweat is simply pooled together for sampling. Local variations in sweat rate and losses due to evaporation can also lead to errors in measurement.

Methods currently used for the collection of sweat with relevance to wearable applications generally involve some sort of absorbent patch which collects sweat from a select regions and pools it together for analysis. This has been the standard for cystic fibrosis tests and can be done using systems such as the Macroduct and Nanoduct ® sweat collector system which uses a hydraulic pressure to draw sweat into a hollow tube used for sampling [26].

2.2. Wound Healing

Typically, wound dressings need to be regularly changed to monitor the progression of wound healing. However, this can lead to reopening of the wounds and provide complications for chronic wounds [32]. In the US alone, about 5.7 million people are affected by chronic wounds annually resulting in a total of approximately $20 billion in costs, with comparable numbers also found in the UK [81-83]. Hence, being able to track the wound healing process without changing dressings as frequently would be highly beneficial.

Normal wound healing is characterized by the sequential progression of the following phases: hemostasis, inflammation, proliferation, and remodeling [32, 84, 85]. Hemostasis is initiated at the time of injury and lasts between three to five minutes. Here, the body tries to mitigate blood loss through vasoconstriction, platelet aggregation, and blood clotting. Additionally, a fibrin matrix is laid out to serve as a scaffold for tissue reconstruction and cell transport. Following this, the inflammation phase is initiated and typically lasts 2-3 days. In this phase, various cells arrive to the wound site and generate an inflammatory response to prevent bacterial infection and help with tissue repair. Next, in the proliferation phase (also referred to as granulation), which can last up to a year later, various types of cells deposit collagen, fibrin, and extracellular matrix to help with tissue regeneration and angiogenesis. Finally, in the remodeling phase, the inflammatory

response subsides, re-epithelialization takes place, and scarring helps restore the tissue's mechanical properties at the wound site.

In chronic wounds, the inflammatory response is extended and maintains an elevated pH range of 7.15-8.90 [32]. This leaves it exposed to bacterial infection further increasing the inflammatory response while consuming nutrients and oxygen generating the potential for tissue hypoxia. A consequence of increased tissue hypoxia is increased lactate levels from their standard 1-3 mM. At lactate levels above 7 mM, fibroblast operation is impaired restricting the deposition of collagen fibers essential to restoring mechanical strength to the tissue. Consequently, wound sites become more susceptible to damage and re-instigating the inflammatory response, preventing it from progressing to the next phase in normal healing.

Figure 2 (a) shows the progression of the skin pH at the wound site for the natural healing process. As mentioned, healthy skin pH is typically slightly acidic to help prevent bacterial proliferation. When the wound is created, the skin's epidermis layer is ruptured, and the dermis and subcutaneous tissue layers are both exposed. This increases the pH to about 7.4, namely that of normal blood. Upon healing of the wound, the pH then returns to its normal slightly acidic value. However, in chronic wounds where the healing process is interrupted, the pH at the wound site remains slightly alkaline as seen in Figure 2 (b) [27, 86]. As such, pH and lactate sensors incorporated on bandages for monitoring wound healing present a very useful additional application for these wearable sensors.

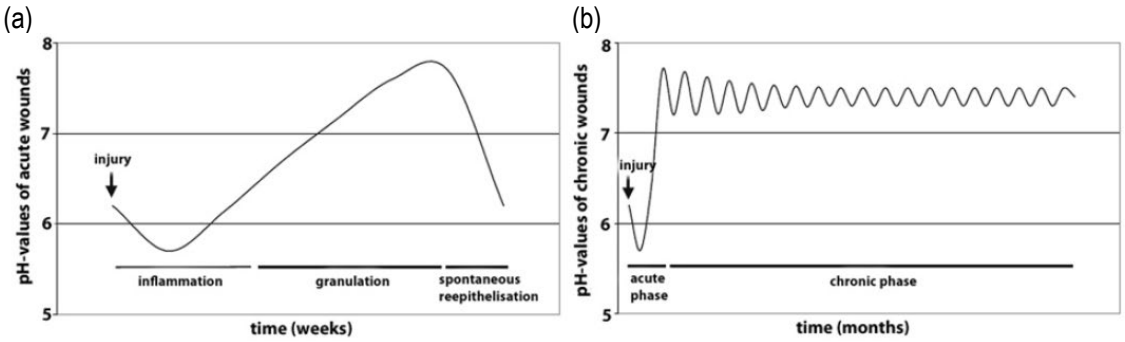

Figure 2. **(a) pH progression of acute wounds; (b) pH progression of chronic wounds reprinted with permission from Elsevier [85]**

2.3. Wearable Sensor Architectures and Materials

Prior to discussing the current state of the art of wearable pH and lactate sensors, an understanding of the underlying detection and transduction mechanisms is required. First generic sensor implementations will be discussed along with material considerations of these systems. Next, the sensor specific materials and implementations found in literature will be addressed for both pH and lactate.

2.3.1. Sensor Mechanisms Overview

Wearable biochemical sensors generally fall under one of the following two broad categories: electrochemical or optical. Optical methods tend to operate through colorimetric comparisons to colour standard charts and require an external image capturing device to make a measurement. Given this need, they tend to be more intermittent in nature and not as feasible for continuous real-time sensing applications. Henceforth, a greater focus will be placed on electrochemical sensors. These have been further subcategorized into potentiometric, amperometric, chemiresistive, and ion-sensitive field effect transistors (ISFETs).

Electrochemical sensors generally rely on the change in concentration of the chemical analyte to effect a detectable change in an electrical property of the sensing material. This transduction effect of the sensing material can be implemented in many different sensor architectures assuming the material can be processed accordingly. Figure 3 shows the general design for each of the electrochemical sensors to be discussed herein.

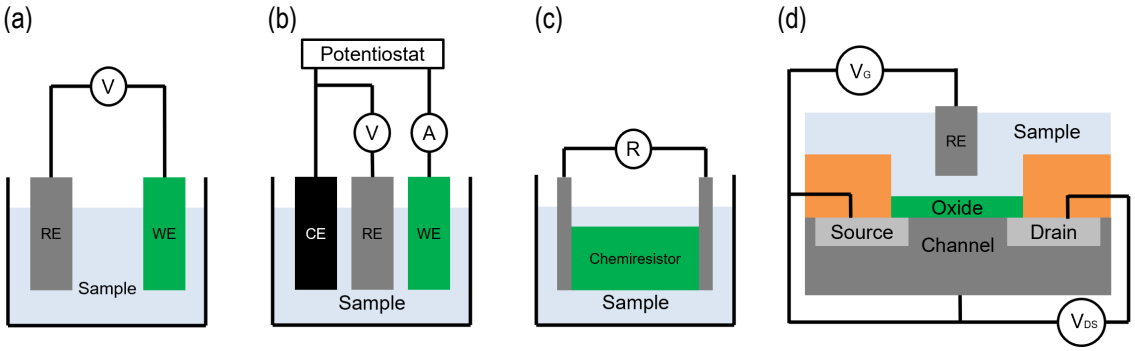

Figure 3. Electrochemical sensor designs: (a) Potentiometric sensor; (b) Amperometric sensor; (c) Chemiresistor; (d) ISFET

Potentiometric sensors measure the electric potential, or open circuit potential (OCP), generated across a pair of electrodes in the analyte solution. These electrodes are referred to as the working electrode (WE) and the reference electrode (RE). Together in solution, they make up what is called an electrochemical cell with each electrode representing a half-cell. The reference electrode provides a stable and known potential regardless of the analyte concentration, whereas the working electrode potential changes with the analyte concentration. The working electrode is sometimes also referred to as the sensing electrode in literature. Potentiometric sensors are simple to fabricate and require simple electronic systems for measurement but face a few challenges mainly with respect to the reference electrode.

Amperometric sensors instead record the current response over time upon application of an external potential. It can also be referred to as chronoamperometry (CA). A current is generated by a redox process occurring at the surface of the working electrode. This implementation uses a three-electrode system consisting of a working (or sensing), reference, and counter electrode (CE). The WE corresponds to the active site where the sensing reaction occurs. The RE fulfills the same purpose as that of the RE in potentiometric sensors and is kept at a constant known potential. The main difference here being that negligible current is passed through the RE in this configuration, and instead current flows between the CE and the WE. This helps ensure that no large fluctuations in potential occur at the RE from the redox reactions occurring at the WE. The reaction taking place at the WE is counteracted by the reaction taking place the CE. Amperometric sensors are also relatively simple to fabricate and build off potentiometric sensors by improving some of their stability issues. However, they require more complicated electronics and the presence of a redox active species for detection. This is

an issue as most biological species of interest are not redox active species themselves. Instead, a redox active species is typically generated as a by-product of an enzymatic reaction with the analyte. A relatively high potential is then required to measure this redox active by-product. This high potential is unfortunately prone to interference from other redox active species present in solution. For this reason, electron mediators such as ferrocene or ferro/ferricyanide have been added to be able to operate at a lower potential and generate a more specific response to the analyte. However, the addition of reagents to the sample is not an ideal implementation for wearable applications.

Chemiresistive, or conductimetric, sensors monitor the electrical resistance, or conductance, across the sensing material which changes in response to the analyte concentration. These are just as easy to implement as potentiometric sensors but can suffer from specificity issues and are more affected by mechanical deformations.

ISFETs are an adaptation of the classic field-effect transistor (FETs) for use as a chemical sensor. FETs monitor the potential (V_{DS}) between two electrodes commonly referred to as the source and drain. These terminals are separated by a semi-conducting channel whose conductivity can be modified by a potential, referred to as the gate potential (V_G). For FETs, the V_G is controlled by a second set of electrodes placed on the top and bottom of the semi-conductor channel and separated by a dielectric layer. For ISFETs, V_G is controlled by the build-up of charge at the dielectric membrane surface upon binding of the analyte to the sensor material deposited at this surface. In this way, analyte concentration is correlated to V_{DS}. This implementation is more fabrication-intensive and requires clean room processes, although much greater sensitivities are typically attainable.

2.3.2. Conductive Polymer Composites

In general, composites are used to obtain new materials which share the mechanical, electrical, and/or magnetic properties of the different materials which comprise it. The new material properties can also be tailored to be processed more readily or with sensing capabilities for a range of stimuli. For instance, piezoelectric particles can be used to create pressure sensitive materials [87]. Temperature responsive materials have also been achieved using carbon-based nanomaterials [88].

In terms of conductive composites, nano- or micro-sized conductive particles (metal, semiconductor, or conductive polymer) are typically dispersed within an insulating polymer matrix. In doing so, the aim to is achieve a material which shares the conductive properties of the filler particles and the mechanical properties or processability of the polymer matrix. In this way, typically rigid and brittle conductive materials can be made flexible, stretchable, and easy to pattern or form to desired shapes. The properties of the composite range between the values of the bulk constituents used and depend on their relative ratios. Below a certain threshold of conductive filler particles, the composite material will remain electrically insulating. As more conductive filler particles are added and are in closer proximity to each other, this threshold is exceeded, and more conductive pathways are created increasing the composite's conductivity. This threshold is referred to as the percolation threshold and is defined by the concentration of conductive filler particles at which one or more conductive pathways are created across it.

The conductivity of the composite is typically much lower than the bulk conductivity of its conductive filler particle as the conduction mechanism typically relies on the tunneling of electrons from one filler particle to the next. Percolation theory assumes that the conductive filler disperses homogenously throughout the polymer matrix. However, this is typically one of the main challenges with conductive composites. Often, particles will tend to aggregate and separate from the matrix when favoured by intermolecular forces. For this reason, blends involving multiple polymers can also be difficult to create.

The addition of solvents can be used to assist in the processing of polymer composites [16]. Proper solvent selection allows for loosening and uncoiling of the polymer chains. Upon addition of filler components and removal of the solvent, uniform composites can be achieved in this way. Yet, molecular interactions can still prevent components from dispersing uniformly upon solvent removal. In these cases, the addition of plasticizers or surfactants can be used to help blend the components together. In most cases, polymer components either have hydrophilic or lipophilic components. Surfactants are molecules with a polar head group and hydrocarbon tail. This dual nature allows them to be mixed with both compounds and can be used to stabilize particles within a matrix which otherwise would not be mixable.

2.3.3. Screen-Printing and Compatible Inks

Screen-printing is a widely used patterning technique for various substrates, including textiles. Figure 4 shows the basic principle of its operation. Essentially, ink is poured onto a patterned mesh screen which sits in proximity to the substrate. The viscosity and surface tension of the ink prevents it from leaking through the screen. Then to pattern the substrate, the screen is brought into contact with it and a blade or squeegee is pressed against the screen to squeeze the ink through the mesh holes and onto the fabric. The ink adheres to the substrate as the screen is removed, and the substrate is flash heated to quickly dry and set the ink. The mesh screen in typically patterned by coating it with a photosensitive polymer layer in a process similar to photolithography. A transparency film with the pattern printed with a dark ink is exposed to UV light to cross-link the regions left uncovered by the transparency. The uncross-linked regions are then washed away from the mesh leaving mesh holes for the ink to pass through. For the work done in this thesis, the mesh screen was replaced with an adhesive layer patterned using a laser cutter. This was done for rapid prototyping purposes as the screen-printed electrode patterns were changed several times throughout the design process.

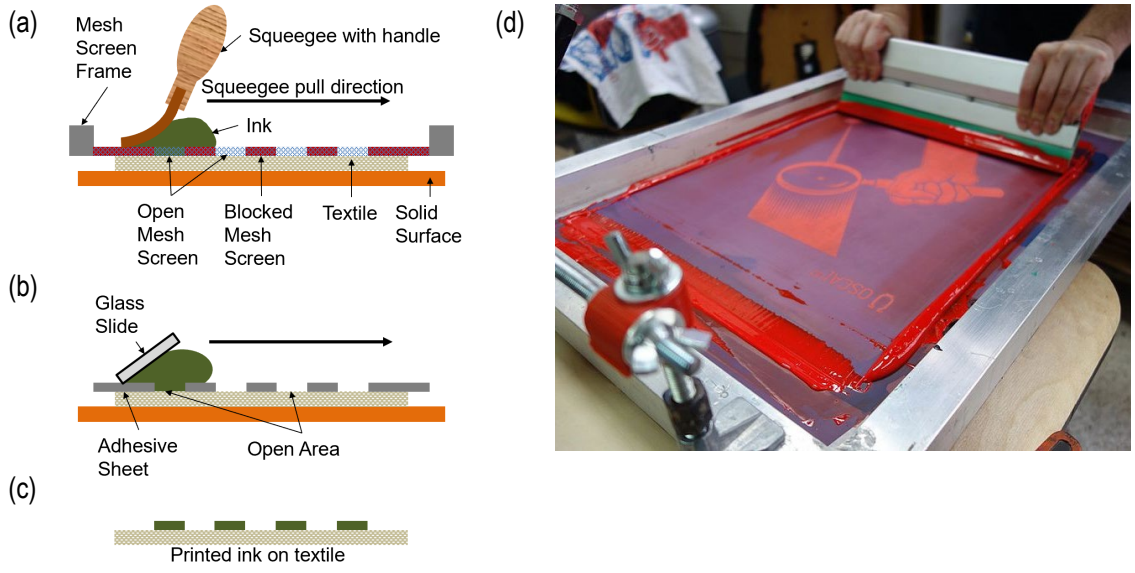

Figure 4. **(a) Graphical representation of typical textile screen-printing; (b) Graphical representation of thee screen-printing process used in this thesis, which replaced the mesh screen with a laser cut adhesive sheet; (c) Finished product of both above processes; (d) Real-life representation of screen-printing reprinted with permission from [89]**

The most popular ink used in the textile screen-printing industry at this time is plastisol-based ink. These inks are made up of plasticized PVC microparticles, contain no solvent, and cure upon heating. They do not dry on the screen and maintain their viscous fluid properties for many hours, even days after printing. This makes it easy to leave out and return to between screen-printing jobs as well as for clean up. They are also very affordable. The ink formulation and viscosity will affect the final print feel. More viscous inks tend to form a thin film which sits atop the textile, whereas lower viscosity inks will be absorbed into the fabric. Regardless of viscosity, plastisol inks are inherently flexible, and composites involving them have been shown to withstand many wash cycles [16]. Stretchable plastisol inks have also been created for printing on stretchable textiles such as Lycra or Spandex.

The second most popular category of screen-printing inks are water-based inks. These have plasticized PMMA particles and are more environmentally friendly due to the absence of PVC. They are equally inexpensive. Additionally, they share similar mechanical properties to plastisol-based inks being inherently flexible, but not stretchable. Their main limitation comes from the fact that they tend to dry up quicker, making them slightly less favourable to work with than plastisol inks.

Silicone inks also exist and rely on a 2-part mixing system for cross-linking meaning they need to be used within a few hours of mixing. But these can be used to create prints which are somewhat stretchable.

2.3.4. Screen-Printed Electrodes

A common feature of electrochemical sensors is their requirement for electrodes and conductive traces from which measurements can be recorded. The conductive traces form connection pathways to interface the sensors to equipment capable of measuring and recording the electrochemical changes. Electrode materials must provide stable electrochemical properties to not interfere with measurements. Furthermore, both electrodes and conductive traces need to be not only conductive, but also flexible to be comfortable to wearers. However, traditional bulk conductive materials such as metals or carbon-based materials are inherently rigid. Therefore, to overcome this intrinsic rigidity, many strategies for developing flexible conductive materials exist. For example, thin-film

processes, patterning onto pre-strained substrates [90], wavy patterns [91], polymer composites [16], and electrospinning [92] have all shown various levels of success.

Metals, such as gold and silver, are common given their high conductivity and chemical inertness. Other metals such as copper, aluminium, and chrome have also been used to a lesser extent. These metals are typically deposited via more complex fabrication methods such as sputtering or other thin film processes requiring clean room access. Thin-film processes generally produce higher quality films and electrical properties; however, they are not easily scalable and expensive. Conductive composites are a versatile alternative which can produce a broad range of properties and can be applied using various scalable processes including screen-printing, roll-to-roll printing, and inkjet printing. The concept involves blending conductive particles with an easily processable material, typically polymeric, to obtain a processable hybrid material exhibiting properties of both, as discussed earlier. For conductive traces of screen-printed electrodes (SPEs), numerous screen-printable silver inks are commercially available and provide a high level of conductivity and electrical stability. However, silver inks are not typically used as the electrode materials themselves as they may tarnish or corrode in solution over time.

To this end, organics such as graphene, carbon nanotubes (CNTs), carbon black, and graphite, are often used in screen-printable pastes for WEs and, in amperometric sensors, for CEs [93]. They provide greater stability and lower cost but generally at the expense of lower conductivity. For this reason, they tend not to be used as conductive traces as much. Platinum is also a popular choice for standard CEs and has been implemented in screen-printable inks but tends to be much more expensive. Conductive polymers have also been used as electrode materials and can provide greater biocompatibility and flexibility. However, these tend to be reserved for use as the sensing material at the WE. Polyaniline (PANI), polypyrrole (PPY), poly(3,4-ethylenedioxythiophene) polystyrene sulfonate (PEDOT: PSS), and polyacetylene are examples of conductive polymers which have also been widely studied. PEDOT: PSS has been used as a gate material for organic electrochemical transistors [94, 95]. Conductive polymers are typically processed by drop-casting, dip-coating, electrochemical deposition, or as composites.

2.3.5. Reference Electrodes

For potentiometric and amperometric sensors, great attention has to be taken when choosing materials for the RE. In standard chemistry labs, many choices exist including the saturated calomel electrode (SCE), the silver/silver chloride electrode (Ag/AgCl), copper-copper (II) sulfate electrode. Each of these have different standard potentials and chemical or temperature stabilities to be considered, but they generally have a similar design and operate similarly. The general design of a standard RE is shown through the silver/silver chloride RE in Figure 5.

Figure 5. Standard Ag/AgCl RE

A solid metal electrode is coated with its corresponding salt compound and placed in an isolated compartment filled with a saturated solution of this same salt. The saturated salt solution is then ionically connected to the solution of interest via a porous frit. Upon applying a potential, electrons flow from the metal electrode and are transferred through the salt solution via the metal-salt coating and the soluble salt before connecting to the solution of interest. A saturated salt solution is used to extend the lifetime of the electrode stability and to carry the current between electrodes. Using the Ag/AgCl RE with a half-cell potential of +0.222 V as an example, we have a Ag electrode coated with a layer of AgCl placed in an aqueous Cl^- saturated solution, typically 3M KCl. The flow of electrons (e^-) or current flow, then proceeds according to following half-reaction:

$$AgCl_{(s)} + e^- \leftrightarrow Ag_{(s)} + Cl^-_{(aq)}$$

Ag/AgCl is a common choice as it is relatively non-toxic compared to the mercury-containing calomel electrode and is relatively stable under numerous conditions.

For screen-printed electrodes, screen-printable Ag/AgCl inks are widely available and provide acceptable stability. When these inks are printed and used in analyte solutions without any additional components or salt solution, they are referred to as pseudo-REs. In consequence of the missing salt solution, they sacrifice some of their long-term stability and drift over extended periods of time. This drift is a result of the local electrolyte depletion at the AgCl surface given their exposed and miniaturized surface. Nevertheless, this implementation has often been used in literature due to its relative simplicity in fabrication [96] and will be used for the purpose of this thesis. Recently, groups have tried to recreate the saturated salt solution by depositing layers of entrapped electrolytes in polymer films to create electrolyte reservoirs and extend the RE lifetime [97].

2.3.6. Substrates

The substrate acts as the base of the material and provides much of the sensor device's overall properties. Again, flexibility is one of the primordial requirements for these to ensure wearer comfort. Accordingly, flexible polymers, like polyimide (PI), polyethylene terephthalate (PET), polyethylene naphthalate (PEN), as well as elastomers (such as polydimethylsiloxane (PDMS), EcoFlex, polyurethane (PU), and silicones) are popular choices [93]. Most materials can be made somewhat flexible if made thin enough, but this does not make them stretchable.

Paper also acts as a suitable, cost-effective substrate for disposable sensors. Using paper microfluidic concepts, channels that wick sweat and direct the flow of samples can be designed. In the same vein, textile channels can also be patterned [98]. These present a more suitable substrate for comfortable, long-term monitoring via wearable sensors given their existing everyday use as articles of clothing.

2.3.7. Dielectric Layers

Insulating layers are typically added overtop electrode traces to prevent them from corroding. The main requirement for these is that they form an impermeable, barrier to isolate the conductive materials. Non-conductive polymers with simple patterning or

deposition techniques are a common choice for this purpose. Parylene, epoxies, polyvinylidene fluoride (PVDF), thermoplastics, and elastomers represent examples of some of these [93]. The deposition process is dependent on the choice of material. For instance, parylene is deposited via chemical vapor deposition, whereas some epoxies, elastomers, and thermoplastics can simply be poured overtop, spin coated, or screen-printed.

2.4. pH Sensors

This section will look at the operating principle of pH electrodes and the existing literature on wearable pH electrodes.

2.4.1. Overview

The pH of a solution is established by its concentration of hydrogen ions, or protons *[H^+]*, and calculated according to the following relation:

$$pH = -\log[H^+]$$

It provides a measure of a solution's acidity (low pH) or alkalinity (high pH) and is typically rated between 1 to 14 for most common solutions. Glass pH electrodes are the standard pH measurement tools in analytical chemistry labs. These measure the potential difference with a set of electrodes across an ion-doped glass surface, typically as a bulb at the bottom of the electrode. The internal RE is placed in a solution of a known pH, typically a buffered, electrolyte-saturated solution. The external reference electrode is also placed in a saturated electrolyte solution but is ionically connected to the solution whose pH we are trying to measure via a porous frit. The REs used tend to be Ag/AgCl with a KCl electrolyte solution. The standard setup of a glass pH electrode is shown in Figure 6 along with a representation of the charge accumulation on the internal and external surfaces of the glass bulb.

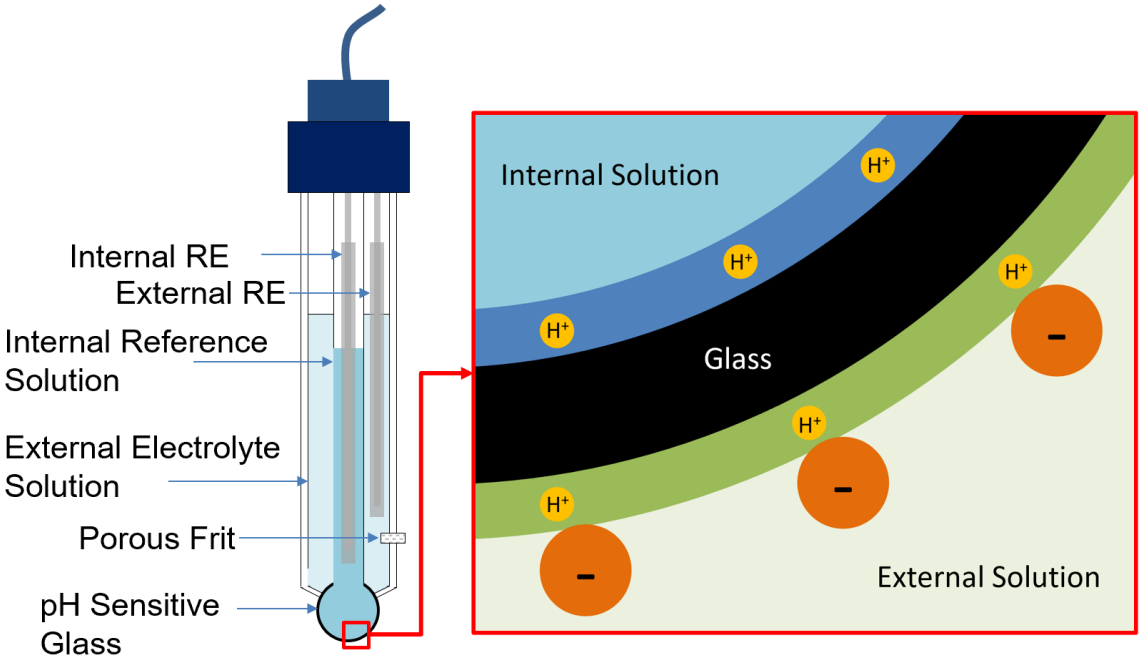

Figure 6. Glass electrode pH sensor

When the glass pH electrode is immersed in an aqueous solution, only the tiny protons can diffuse into the outer layer of the of the doped glass bulb. A corresponding layer of larger anions, such as Cl^-, which cannot diffuse into the outer glass surface then solvates it creating an electric double layer and a measurable charge separation. The same occurs at the internal surface of the glass bulb with the internal reference solution. The slow migration of dopants in the glass allows for a potential to be measured across its surface. The measured potential, *E*, is then governed by the Nernst equation:

$$E = E_0 - \frac{RT}{nF} logQ$$

where E_0 is the standard cell potential, *R* is the universal gas constant, *T* is the temperature, *n* is the ionic charge, *F* is the Faraday constant, and *Q* is the activity of the ionic species. Under standard conditions, this expression can be further simplified down to

$$E = E_0' - 0.0591 * \log\left(\frac{[H^+_{external}]}{[H^+_{internal}]}\right)$$

where E_0' is the standard cell potential under standard conditions (*T*= 25˚C, room temperature; *n* = +1 based on the ionic charge of the hydrogen ion; and *logQ* can be

rewritten as log $([H^+_{external}]/[H^+_{internal}])$, where $[H^+_{internal}]$ and $[H^+_{external}]$ are the concentrations of protons at the internal and external electrodes, respectively. These quantities are then related back to the pH. This expression also sets the theoretical limit for the sensitivity of single electron transfer events such as potentiometric pH sensors at 59.1 mV/pH. This value is thus used as a metric to gauge the quality of the sensitivity of electrochemical pH sensors.

Despite the reliability of glass pH sensors, this design is not readily implementable for wearable applications due to the need for frequent recalibration and the mechanical rigidity of glass. Instead, optical, and electrochemical sensors present interesting alternatives for wearable pH sensors. The focus herein will be on the electrochemical sensors, but for completeness, a few optical methods will also be discussed.

Electrochemical methods allow for continuous sampling over extended time periods making them more suitable to wearable applications. For this reason, many different materials have been explored for electrochemical pH sensing. In a potentiometric sensor and OCP measurements, the principle of operation is based on the electric double layer theory. When an electrode is placed in contact with a solution, a layer of ions is tightly adsorbed at the electrode-solution interface through chemical bonds to form what is called the Helmholtz layer. As a result of this first charged layer, a second more diffuse layer of counterions is attracted to the first via Coulombic forces. The properties of the electric double layer and the associated potential measured for the electrode will depend on the electrode material selected and its chemical reactivity towards the adsorbed species. [97] Common to most pH sensor materials, surface hydroxide groups will form at the electrode-solution interface and act as either proton acceptors or donors depending on the pH of the solution. The concept of the electric double layer is shown in Figure 7.

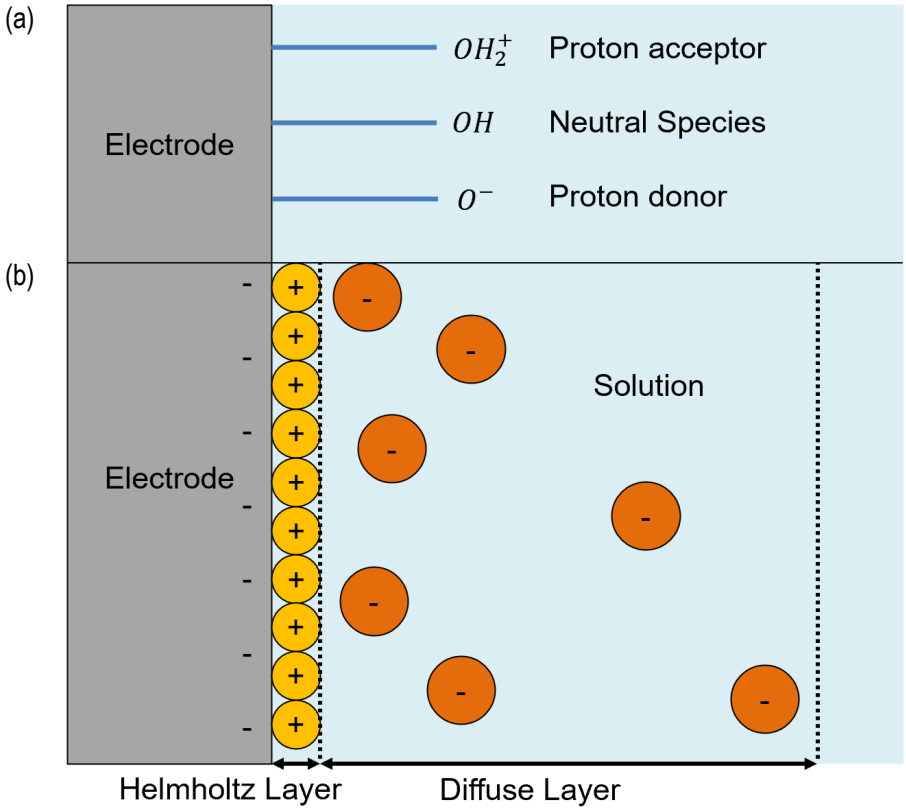

Figure 7. **(a) Hydroxyl groups at the surface of an electrode acting as proton acceptor and donor groups; (b) Electric double layer of an electrode in solution**

2.4.2. Metal Oxides

Metal oxides represent one subset of pH sensing materials. The exact mechanism for pH sensing is still somewhat debated, with some attributing it to the transition of redox states of the metal atom [99]. However, the more accepted mechanism is generally attributed to the formation of an electric double layer which was previously discussed. Here, the build up of surface hydroxyls on the metal oxide-solution interface, which is affected by pH, regulates the electrical properties and surface potential of the sensing electrode [100]. To this end, many different metal oxides with their own surface properties have been used with the most prevalent including platinum group metals like IrO2 [101,102] and RuO2 [103-105] among others [106]. Yet, numerous others metal oxides such as ZnO [107,108] have also been reported and reviewed [100, 109, 110]. One of the main advantages of metal oxides is that they can produce highly sensitive pH sensors,

even displaying super-Nernstian responses (above the Nernstian limit of 59.1 mV/pH) when synthesized electrochemically or with nanopatterned electrodes [111, 112]. However, given the more complex and costly clean-room fabrication processes and their inherently rigid nature, these tend to be less suitable to wearable applications.

2.4.3. Organics

Organic materials, including graphite, graphene, carbon black, and CNTs, represent another important subset of materials for electrochemical pH sensors. Like metal oxides, oxidized organic material operate based on the generation of an electric double layer whose potential will be governed by the surrounding pH [109]. Salvo et al. [113] drop-casted a dispersion of graphene oxide (GO) in water on rigid commercial DropSens screen-printed electrodes to obtain a sub-Nernstian response of -42 mV/pH. Others have incorporated organic materials into easily processable and flexible composites such as graphite-polyurethane composites [114]. However, sensitivity in these cases is greatly reduced to about 11 mV/pH. Overall, organic materials provide much greater ease in processing and flexibility than metal oxides, although, they provide much lower sensitivity. Additionally, toxicity and biocompatibility remain an issue surrounding these materials [115, 116].

2.4.4. Conductive Polymers

Finally, conductive polymers represent the final subset of materials used for electrochemical pH sensors to be discussed in this thesis. They have been extensively reviewed for numerous biomedical applications, including pH sensors [117-119]. In the context of the latter, these have shown great promise due to their tailorable mechanical and electrical properties, and general ease of synthesis. For instance, Gou et al. demonstrated a sensitivity of 52.5 mV/pH by coating poly(1-aminoanthracene) conductive polymer onto CNTs in an ISFET configuration [120] in a wireless configuration.

PPY is another conductive polymer which is often explored for sensors, however for pH sensors, these have been mostly limited to rigid electrodes and has generally reported a lower sensitivity to that of PANI pH sensors [121-122]. For that reason, many research groups have emphasized the potential for using PANI as a pH sensitive material as flexible electrochemical sensors [123-128]. Again, the pH response is brought about

by changes in the electric double layer at the polymer-solution interface. Although PANI has a unique conduction mechanism where doping through protons allows it to gain conductivity. This will be discussed to a greater extent in Chapter 4. Of note, PANI has shown a high sensitivity, even super-Nernstian when electropolymerized [129], is easily synthesized, and has been shown to be biocompatible [97, 127, 128]. Bandodkar et al. [123] implemented PANI into a temporary tattoo which could be directly adhered to the skin for monitoring pH as a potentiometric sensor. Yoon et al. [124] created a nanopillar array with a PANI coating to create a highly sensitive and flexible potentiometric pH sensors. Others have deposited PANI layers on various carbon-based electrodes such as graphene [125], CNTs [130], screen-printable carbon [126, 127], equally for use as a potentiometric pH sensor.

However, these incorporations of PANI use electrochemical polymerization or drop-casting methods which are not easily scalable and time consuming. Gill et al. [131-133] formulated a resistive pH sensor based on a PANI composite which could be screen-printed onto a rigid alumina substrate. They demonstrated a somewhat linear range between pH values of 2 and 11. The composite used PANI as the pH sensitive material, polyvinyl butyral (PVB) as the binder, and PS3 surfactant to help with the dispersion of PANI in PVB. This work demonstrated that PANI could be included into a composite and produced using a scalable approach via screen-printing. However, the alumina substrates used do not lend themselves well to wearable applications given their rigidity and the resistive sensing approach means it is highly dependent on the shape of the electrode. Others have attempted to integrate PANI into inkjet printing ink for facilitating the drop-casting approach [134-136]. Of note, Bao et. al [137] published on a screen-printable PANI-CNT composite for pH sensing on a PET substrate. Their composite was made up of PANI, CNTs and polyvinyl alcohol, a water-soluble polymer. They reported a sensitivity of 20.63 mV/pH. Examples of some of the existing PANI sensors are shown in Figure 8.

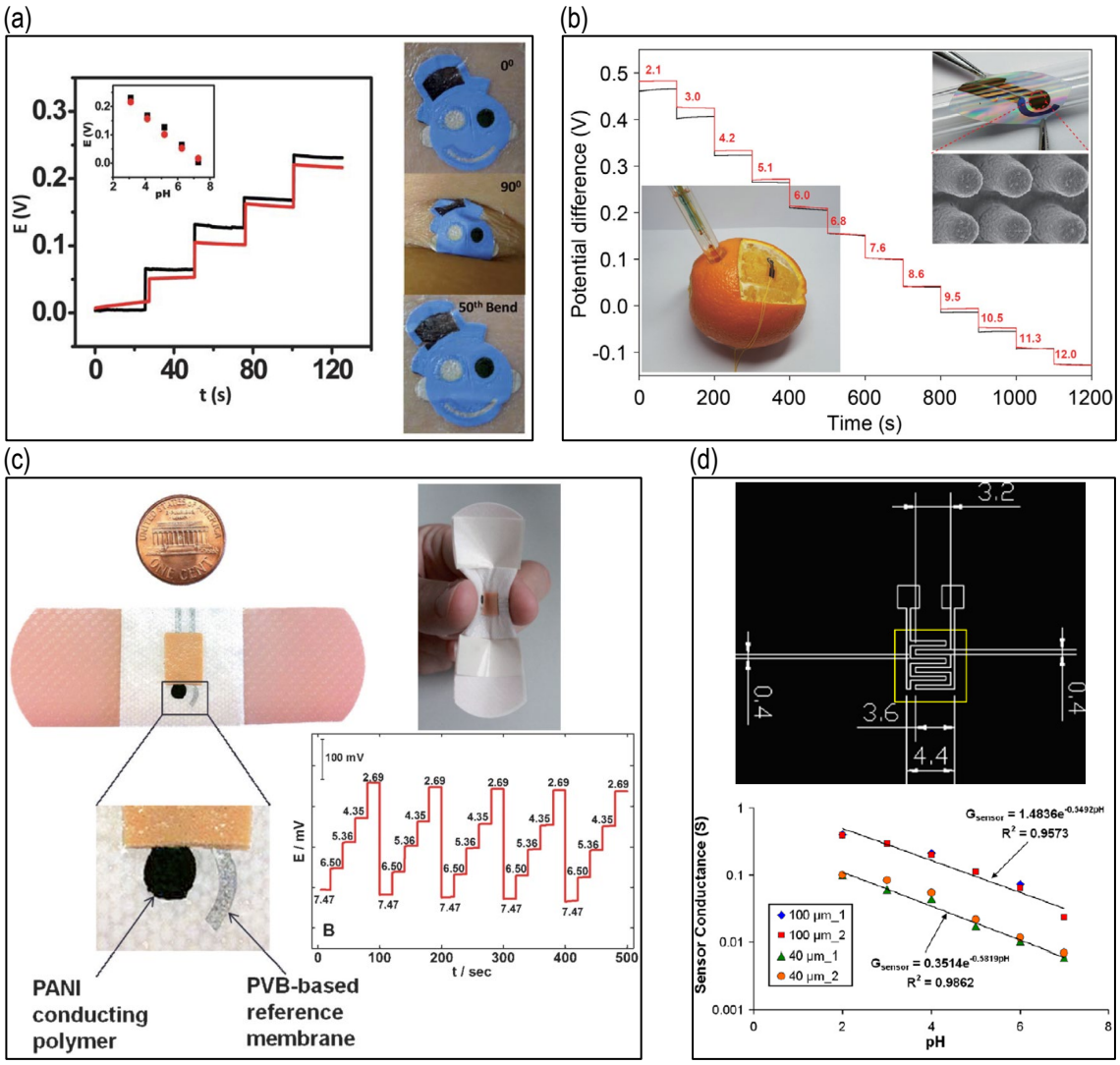

Figure 8. **(a) Tattoo-based, potentiometric, electropolymerized PANI pH sensor and response after 50 bend cycles by Bandodkar et al. reprinted with permission from the Royal Chemical Society [123]; (b) Flexible, potentiometric electropolymerized PANI on nanopillar array by Yoon et al. reprinted with permissions from Elsevier [124]; (c) Bandage-based, potentiometric, electropolymerized PANI pH sensor by Guinovart et al. reprinted with permissions from John Wiley and Sons [126]; (d) Conductimetric interdigitated electrode screen-printed PANI composite pH sensor on alumina substrate by Gill et al. reprinted with permissions from Elsevier [133].**

2.4.5. Optical

In general, pH probes based on optical methods rely on the colour change of pH-sensitive dyes and then locating these on a reference colour spectrum. Consequently, the focus of these methods has been on selection, incorporation, and retainment of these

dyes in appropriate matrixes. The main requirements for the selected dye are that it must be biocompatible and functional within the pH range of interest, specifically, pH level 3-9. To this end, various dyes have been used including curcurmin, phenol red, bromocresol green, methyl orange, azobenzene derivatives, litmus, and others [83, 138, 139]. Matrix materials have included various types of hydrogels, and cross-linked networks. The main drawback to these methods is that they typically require an external optical device such as a camera to make measurements and are often single use dyes making measurements intermittent in nature. As such, this implementation is generally favourable for intermittent monitoring, disposable single-use sampling, but not for real-time, long-term monitoring or repeated use. In 2019, l'Oreal launched research into skin pH sensors for the purpose of monitoring skin conditions such as eczema, also known as dermatitis [140]. They created a sensor which collects mircrodroplets of sweat using microfluidic technology to elicit color changes in pH-sensitive dyes within 5 to 15 minutes of application.

2.5. Lactate Sensors

This section will review the different methods used for wearable lactate sensors.

2.5.1. Lactate Oxidase

The most common approach to measuring the concentration of lactate has involved the use of an immobilized enzyme, generally lactate oxidase (LOX), in an amperometric sensor implementation [141-148]. LOX oxidizes lactate in the presence of oxygen to create pyruvate and hydrogen peroxide (H_2O_2), as shown in the reaction in Figure 9 (a). The applied potential oxidizes H_2O_2 dissociating it into oxygen gas, a pair of protons, and releasing a pair of electrons which get transferred to a set of electrodes in the process. This amperometric response is then indirectly correlated to the concentration of lactate analogously to the way glucose sensors first reported by Clark et al. with the glucose oxidase enzyme [149]. Jia et al. [141] was the first to report on the use of a real-time sweat-based wearable lactate sensor utilizing LOX. They designed a screen-printed three-electrode system which could be temporarily tattooed directly onto skin. The WE and CE were made of carbon ink, whereas the reference electrode was made of silver ink. This is shown in Figure 9 (b). The WE was then functionalized through a series of drop-casted solutions of tetrathiafulvene (TTF), multiwall carbon nanotubes (CNTs) in an

ethanol/acetone mixture, LOX with bovine serum albumin (BSA), and finally, chitosan in acetic acid with subsequent exposure to glutaraldehyde vapor for crosslinking. The TTF/CNT facilitated electron transduction to reduce the operating potential. BSA and glutaraldehyde were used to immobilize the LOX enzyme. Lastly, the chitosan layer was added to ensure biocompatibility and avoid irritation at the skin surface. They reported a limit of detection (LOD) of 1mM with a sensitivity of 644.2 nA/mM, or 10.31 uA/mM·cm^2, real-time sensing and a wide linear detection range between 1 and 20 mM (R^2=0.996).

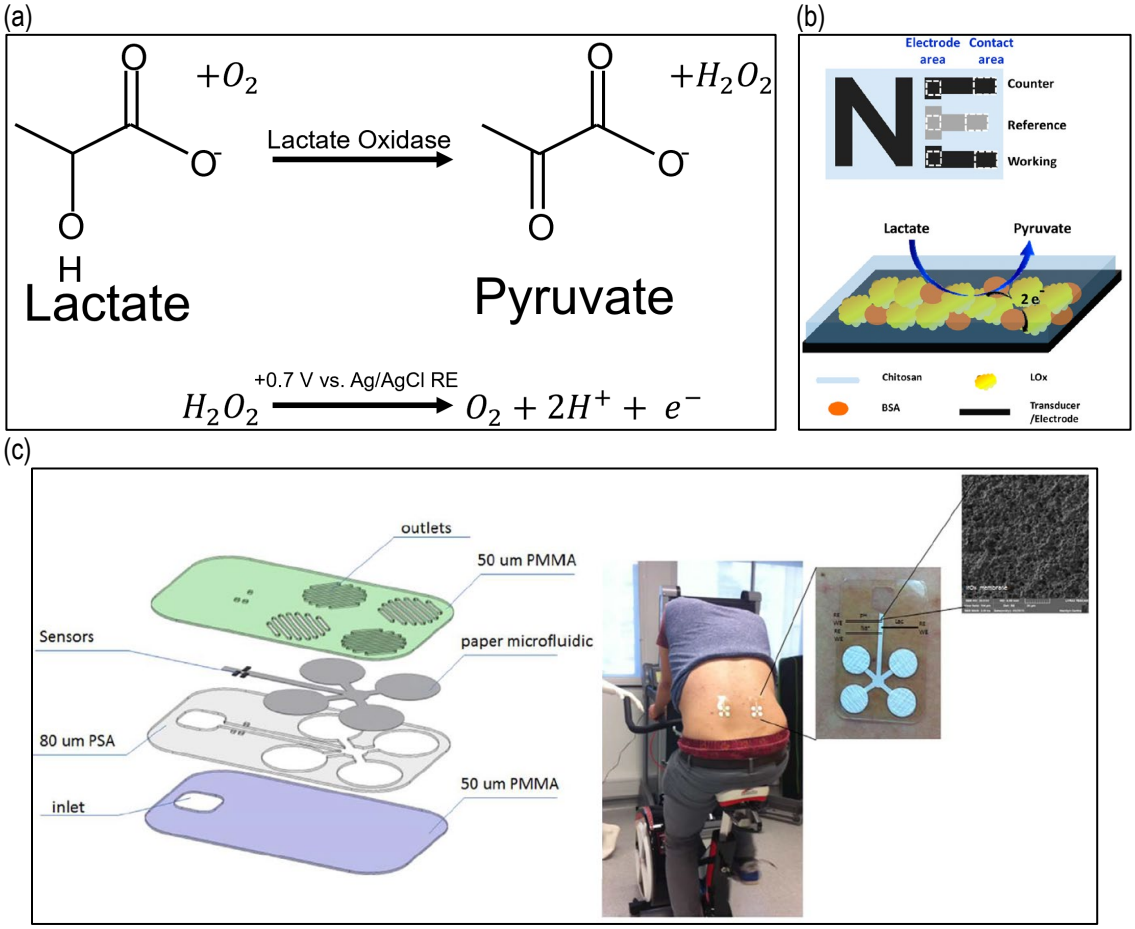

Figure 9. **(a) Lactate oxidase oxidation reaction mechanism for lactate generating pyruvate and hydrogen peroxide, whose electrochemical dissociation can be measured; (b) Jia's screen-printed tattoo sensor reprinted with permissions from the American Chemical Society [141] (c) Implementation of lactate sensor into wearable skin patch by Anastasova et al. reprinted with permissions from Elsevier [142]**

Following the work of Jia et al., numerous other groups have published wearable sweat-based lactate sensors using the same enzyme sensing mechanism albeit with different electrode materials, substrates, fabrication methods, sweat collection designs, or

levels of integration into wearable systems [142-148, 150, 151]. One notable design for collection and cycling of fresh localized sweat using a paper microfluidics concept is shown in Figure 9 (c) [142]. Detailed reviews of enzymatic sensors have been published [153-155]. Overall, some of these methods report similar sensitivities and LOD, and acceptable linear ranges [44, 92] although many show a saturation of signal at concentrations far too low to be relevant to sweat sensing [94, 143, 145, 150, 151]. The sensing mechanism relies on the electrooxidation of the by-products of the enzyme reaction. The enzymes themselves are quite selective, but the presence of other oxidizable species can create interference. Additionally, enzymes are inherently prone to environmental degradation, have strict storage requirements, are expensive, require pre-calibration, and frequent recalibration.

2.5.2. Other Electrochemical Methods

In place of LOX, lactate dehydrogenase (LDH) enzyme has also been used in wearable sensors [156, 157]. These require the addition of a co-enzyme such as nicotinamide dinucleotide (NAD+ in its oxidized form, and NADH in its reduced form) to transfers electrons to the electrode. The reaction catalyzed by LDH converts lactate to pyruvate and NAD+ to NADH. NADH is then oxidized back to NAD+ at the electrode generating a current which is correlated back to the lactate concentration. However, this approach has shown lower sensitivity than LOX-based sensors, requires the immobilization of both the enzyme and co-enzyme, and still suffers from many of the same issues associated with enzyme stability and high oxidation potentials. Similarly, others have tried increasing selectivity using bienzymatic systems combining LOX and lactate peroxidase [158] or LDH with pyruvate oxidase [159].

Nevertheless, other lactate sensing mechanisms exist. Recently, Zaryanov et al. [160] demonstrated the feasibility of using PAPBA for sensing lactate in sweat. PAPBA is essentially polyaniline (PANI), a conductive polymer, functionalized with a boronic acid groups which binds to lactate. Upon binding of lactate, a reconfiguration of the polymer's electrons occurs along the backbone of the polymer, increasing its conductivity and the measured current flow. PAPBA was electropolymerized onto the WE in the presence of fluorine ions. By adding lactate during electropolymerization, they reportedly increase selectivity by imposing a structure on the polymer in a way that mimics enzymes via polymer imprinting. Using this approach, they obtained a detection range of 3 to 100 mM

and a LOD of 1.5 mM using electrical impedance spectroscopy (EIS). However, EIS operates based on the increase in measured impedance between a set of electrodes as a result of the analyte binding to the target bound to the WE. This impedance increase is only observable through the addition of an aqueous soluble redox active species such as ferrocene or ferricyanide. Thus, this detection method is not suitable for wearable sensors. PAPBA has also been implemented as a potentiometric sensor for the detection of glucose and fructose, albeit with lower sensitivities of 1.5 mV/mM and 3.5 mV/mM, respectively [161].

On another note, certain metals can exhibit electrocatalytic activity and transform lactate to pyruvate through a measurable redox reaction. Wang et al. [162] reported using a metal organic framework (MOF) electrode for lactate detection in sweat. They fabricated their WE by dip-coating an amino-functionalized graphene paper (NH_2-GP) at the interface a copper-based emulsion of $Cu_3(btc)_2$, where btc is 1,3,5-benzene tricarboxylate. The $Cu_3(btc)_2$ self-assembled at the interface of the organic emulsion and an aqueous phase generating an aligned 2D structure on the NH_2-GP. They reported a detection limit of 5 μM with a linear range up of 50 μM to 22.6 mM and a relatively sensitivity. However, this is not a very scalable approach, and it was simultaneously used to detect glucose unselectively from lactate. Other reports using nickel oxide NPs [163-165] and cobalt phthalocyanine [166] have also been reported as lactate sensors, however their catalytic activities were only in non-physiologically relevant pH levels.

2.5.3. Optical

Some of the above lactate sensing binding and sensing mechanisms have been implemented such that they elicit a colorimetric or optical response alternatively to the above electrochemical approaches [167-170]. For example, Koh et al. used an enzyme with diaphorase to create a color change in a chromogenic dye upon lactate binding [169]. Sartain et al. [170] functionalized acrylamide hydrogels with boronic acid groups to create holographic sensors through changes in replay wavelength generated by lactate-dependent hydrogel swelling.

Chapter 3. Design, Fabrication, and Synthesis

Chapter 3 begins by outlining the ideal requirements for wearable pH and lactate sensors and how these were used to generate the plan for the project. The proposed solution is then elaborated by discussing the design process, materials selection, fabrication processes, synthesis conditions, and characterization methods used for creating the textile SPE, validating the PANI pH response, formulating the screen-printable PANI composite, and measuring the PAPBA lactate response.

3.1. Project Requirements

After examining the existing state of the art in the previous chapter of this thesis, a set of ideal characteristics for wearable pH and lactate sensors has been summarized in Table 2. Ultimately, the ideal sensor would be flexible and stretchable, have a linear and stable response within the physiologically relevant analyte range, high sensitivity, respond in a reasonable time span, and be fabricated using a cost-effective, scalable process, with materials that are biocompatible.

Table 2. Ideal properties of wearable pH and lactate sensors

Characteristic	Reasoning	Ideal Technical Requirement
Flexible and Stretchable	Functional while withstanding natural deformation of skin	Flexibility: Bends at least 90˚, radius of curvature < 1 cm Stretchiness: 25-30% strain [97, 171]
Lactate Sensor Requirements	Needs to be able to accurately determine lactate concentration at physiologically relevant conditions	Lactate: LOD smaller than 1mmol/L with a linear range between 1-40 mmol/L
pH Sensor Requirements	Needs to be able to accurately determine pH levels at physiologically relevant conditions	High sensitivity in the range of pH 3-9
Scalable Fabrication	Needs to be fabricated using a repeatable process which is cost effective	Scalable manufacturing approach (such as screen-printing) [172]
Biocompatible	Should not react with skin or body fluids in harmful manner	Biocompatible materials
Provides real-time sensing	Can provide continuous information in timely fashion	Delay in response no greater than 5 minutes
Stable operation	Avoiding the need for recalibration and erroneous data	Stable for at least 24 hours

As was discussed in Chapter 2, polyaniline-based potentiometric pH sensors were able to provide some of the highest reported sensitivities. However, polyaniline was either

formulated into non-flexible composites or using less scalable fabrication methods such as electropolymerization or drop-casting. As such, a project was formulated to bridge this gap and create a flexible PANI composite for pH sensing.

Screen-printed electrodes seemed to be the preferred implementation for designing electrode systems for biosensors. Additionally, screen-printing methods and flexible screen-printable composites applied to textile substrates previously been developed at the Microsintrumentation lab. Therefore, a screen-printable composite represented an ideal merger of these concepts to address the properties laid out by Table 2. However, upon examining the screen-printable materials that were commercially available, it was determined that the characteristic for creating a stretchable sensor system (conductive traces, RE, and CE) would not be feasible within the framework of this project and this property was thus omitted. The main mechanical requirement was that it could be flexible enough to be worn comfortably.

The first step of the project was to validate the textile SPE design and confirm the pH response of PANI. To do so, the textile SPE operation was compared to a commercial SPE through cyclic voltammetry (CV) and chronoamperometry (CA) of $K_3Fe(CN)_6$, a well-established redox mediator. It was believed that CA could be used for monitoring pH response of PANI [125]. Once the SPE design was confirmed with $K_3Fe(CN)_6$, PANI's pH response was to be confirmed. PANI was meant to be synthesized via chemical oxidative polymerization such that its properties could be tailored during synthesis and the optimal collected powders could then be used directly in the composite. However, it was found that electropolymerization and drop-casting were more favourable synthesis and fabrication approaches, and these were instead used for measuring the PANI's pH response. Measuring the OCP proved to be the more responsive implementation for monitoring the pH reaction of PANI and was thus used for characterization. PANI composites were then optimized by testing various formulations optimized by print quality and sensor response. Finally, the flexibility of the textile SPE with the PANI composite was demonstrated by recording the pH response while in a bent state.

In the early stages of this project, PAPBA, a polyaniline derivative with an additional boronic acid group, was seen in literature to be used as an impedimetric lactate sensor and as potentiometric sensor for diols and other compounds [173]. Therefore, its use as

a potentiometric lactate sensor was of interest. Similarly to PANI, PAPBA was synthesized onto a textile SPE and its lactate response was characterized.

3.2. Textile Screen-Printed Electrodes

This section discusses the design process, material selection, and fabrication process used to create the textile SPE system.

3.2.1. Design

To test the sensor materials developed in this thesis, a set of SPEs needed to be designed for use on textiles. These SPEs will henceforth be referred to as “textile SPEs”. The main design consideration takes place at the electrode area, and more specifically at the connection point between the electrode materials and the conductive traces. For testing, purposes, various WE designs were printed and tested with a standard Ag/AgCl RE to validate the proper operation of the individual electrodes. Figure 10 shows two of the designs that were considered for the WE connections to be used for the final two-electrode and three-electrode textile SPEs. The silver is typically printed under the WE layer, however in the right-most image of each design, it was printed overtop to demonstrate how far it extends past the plastisol cover layer.

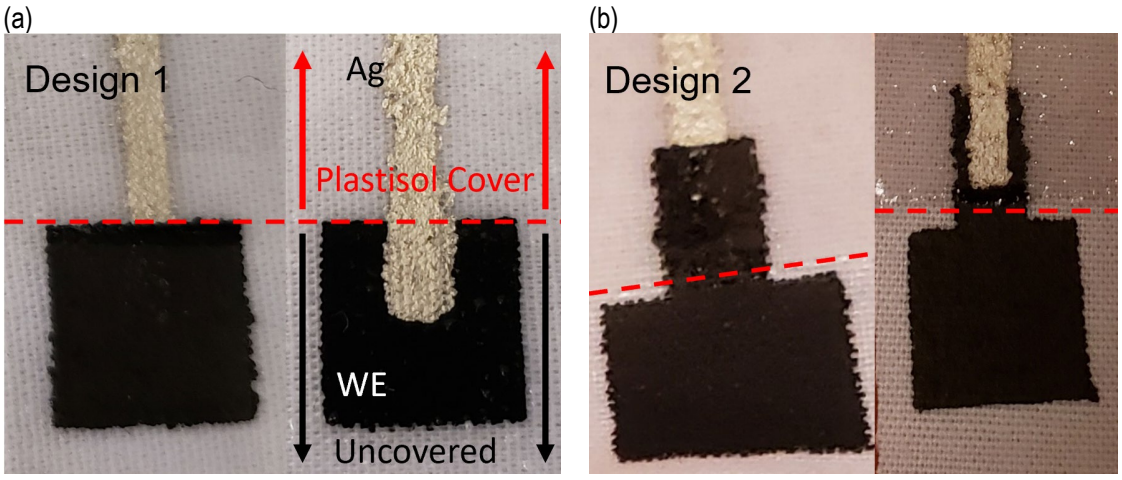

Figure 10. **(a) Design 1, and (b) Design 2, considered for the connection between the electrode and the conductive trace of the textile SPEs; the red dashed line indicates how far the plastisol cover extends over the Ag conductive trace**

In Design 1, the conductive silver trace extends past the plastisol cover layer. This design was considered as the WE ink (carbon screen-printing ink, 50 Ω/sq; or PANI composite, >10-1000 Ω/sq) had a much higher resistivity than the silver screen-printing ink (0.01 Ω/sq). So, to minimize the overall impedance of the sensor, the WE ink pathway was minimized. In Design 2, the conductive silver trace is shortened and instead the WE is extended such that the connection was instead made under the plastisol cover layer. This was done to isolate electrical measurements of the WE from any potentially interfering effects of the conductive silver ink.

Once this was done, a third design which builds on the second one was designed where the plastisol cover layer extends over the entire electrode area. Here, the electrodes instead contact the solution through the porous textile backside, not the side they are printed on. This was done to reduce stress on the printed layers thus potentially increasing flexibility while also protecting the sensor surface layer from direct contact. The final designs for the 2-electrode textile SPE and 3-electrode are shown in Figure 11.

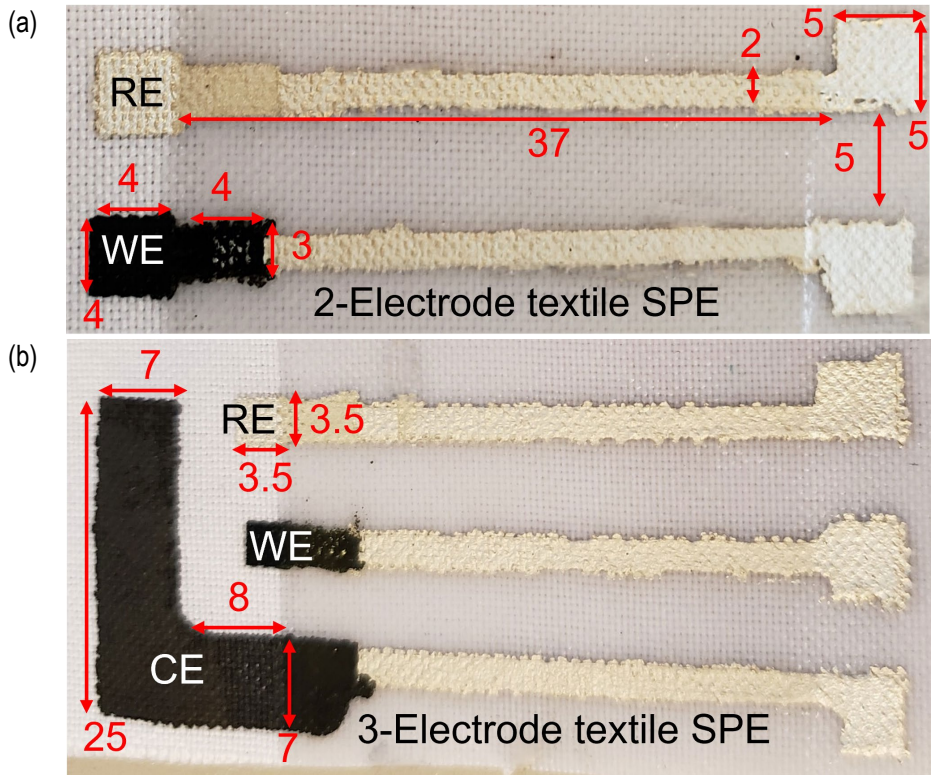

Figure 11. (a) 2- and (b) 3-electrode textile SPE designs; all dimensions in mm

The dimensions of the textile SPEs were optimized to fit the test setup and based on limitation of the outlined screen-printing approach. For instance, the dimensions and

spacing between contact pads was determined based on the size of the alligator clips used to connect the textile SPE to the potentiostat used for characterization. The 35 mm length of the contact traces was selected such that the electrodes could be submerged in a 20 mL beaker while the contact pads remained outside of the beaker. The 2 mm width and 5mm spacing of the contact traces was selected to ensure a reliable connection between the contact pads and the electrodes. At narrower widths and spacings, the adhesive mask would occasionally migrate during screen-printing causing the ink to be deposited in unwanted areas and potentially resulting in the separate electrodes short-circuiting.

In terms of dimensions for the three-electrode SPE, the CE must be at least 20 times greater in area than the WE to ensure that the measured current is that of the WE [174]. Therefore, to avoid making the overall device too big but still allowing for accurate alignment via manual fabrication, the WE was designed to be 3 mm x 3 mm. The CE was then designed to have an appropriate area based on the previous constraint. The RE was given the same size as the WE. In the two-electrode textile SPE design, the dimensions are relatively arbitrary and various sizes between 3 mmm x 3 mm and 5 mm x 5 mm were used, with no real differences between these. The three-electrode system was used for voltametric characterization whereas the two-electrode system was used for OCP characterization, both of which will be described in later sections in this chapter. The only difference between the two being that for the three-electrode system, an additional CE was required.

3.2.2. Textile SPE Materials

A discussion on material selection for SPEs was given in Section 3.1 but will be briefly expanded on here with regards to specific materials chosen.

For the conductive traces, AG-500A silver conductive ink by Kayaku Advanced Materials was chosen as it is designed for screen-printing, provides high conductivity, is flexible, and designed for polyester substrates. The RE was made of Ag/AgCl screen-printable ink, specifically, electrically conductive medical electrode ink 113-09 from Creative Materials. Similarly, this ink was selected for its high conductivity (0.05 Ω/sq), screen-printing capability, and flexibility. For the CE and the WE, a screen-printable carbon/graphite paste was purchased from Sigma Aldrich. The cover layer consisted of a

more viscous plastisol layer, LFP-1070 clear gel by QCM materials. This plastisol was selected as it tends to form a layer that sits atop the substrate instead of impregnating it making for a reliable insulating, impermeable cover over the conductive traces and connection points to the electrode materials.

Flexibility was highlighted as an important property for wearable sensors to ensure wearer comfort by having devices conform to the shape of the wearer, including on clothing that is form-fitting. To this end, the materials selected represent this choice. Stretchability is an ideal property for many wearable sensors, such as ECG, when good electrode-to-skin contact is required and for further wearer comfort. However, for the proposed sensor platform, this was determined to not to be essential given that the sample of interest is liquid perspiration. Additionally, given the lack of existing stretchable commercial screen-printing inks, this would have required substantial redesign solely for the sake of the stretchability. Therefore, the textile substrate was chosen to be flexible, but not stretchable, as stretchable substrates would lead to cracked prints with non-stretchable materials. A 100% polyester fabric purchased from Fabricana was selected as a substrate. This material was selected as it was thin, flexible, not stretchable, and the weave was not too dense. Other textiles were also tested including 100% cotton, cotton-polyester blends, and stretchable polyester-spandex blends. It was found that many of the textiles behaved similarly and could be used interchangeably. The only textiles to avoid were the ones that were woven too densely or too thick, or those that were stretchable. In terms of textile weave, the denser or thicker weaves simply required more processing to be made impermeable, so these were not selected for ease of fabrication. To make the textile impermeable a layer of low viscosity plastisol, P-5011 curable reducer purchased from the TheScreenPrintStore.ca, was printed on the blank textile as the first layer. As a result of the low viscosity and textile porosity from looser weaves, the plastisol layer impregnated the textile and rendered it impermeable, thus creating an insulating backing isolating the conductive traces from the test solution. Plastisol inks were selected as the backing and cover layer mainly due to availability and information from prior work conducted by the Microinstrumentation Lab [33].

Given the proprietary nature of textile screen-printing inks, their exact chemical make-up is not typically disclosed, thus making it challenging to predict which chemicals or solvents would interact favourably with them. However, it was previously reported that heptane could be used as a solvent for preparing plastisol-based composites [16]. Water-

based inks could logically be mixed with water-soluble solvents. Plastisol-based and water-based inks also had the advantage of not requiring the addition of a catalyst for curing, making these easier to work with. These factors ultimately led to the selection of plastisol and water-based inks for the preparation of PANI composites in this thesis.

For the screen-printable PANI composites, the WE consisted of composites containing plastisol P-5011 curable reducer or a screen-printable water-based ink, Speedball Transparent Base/White textile screen-printing ink. The Speedbal White ink was purchased initially due to in-store availability and used for some of the initial testing. Upon in-store availability, the Speedball Transparent Base was then purchased later and used in its place. It was believed that the absence of any pigment in the Transparent Base might allow for better mixing with PANI when creating a composite, allowing for greater conductivity and sensitivity. However, no discernible difference was observed when substituting the Transparent Base for the White ink. Therefore, the two will be used interchangeably and referred to as the Speedball water-based screen-printing ink, or simply the Speedball ink throughout this thesis.

3.2.3. Fabrication

The fabrication process for the textile SPE is displayed in Figure 12.

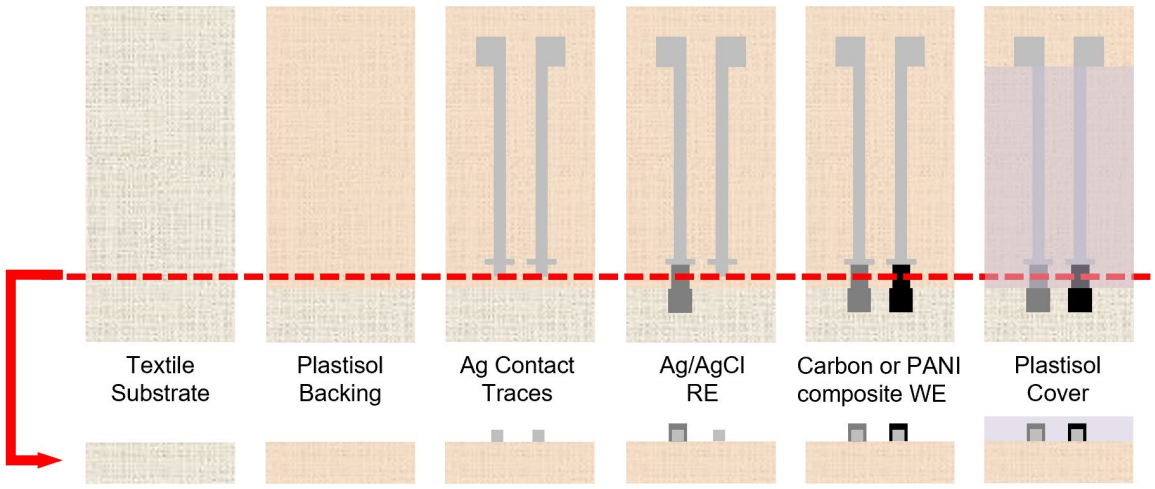

Figure 12. Fabrication process of textile SPE top (top row) and cross-sectional views (bottom row); all layers are screen-printed

As previously mentioned, no mesh screen was used when screen-printing. Instead, a sheet of adhesive (BC352 Clear Self-Adhesive Protective Film Book Cover

Tape) purchased from Staples Business Depot patterned using a Universal Laser Systems CO_2 laser cutter using a file designed in Corel Draw was used to create patterns on textiles. This adhesive film had a thickness of 50.8 µm (2 mil) and set the maximal thickness of the screen-printed layers. However, some layers would be as thin as 20 µm upon curing. The laser parameters used were 13% power and 100% speed. An example of the laser cut adhesive mask pattern is shown in Figure 13.

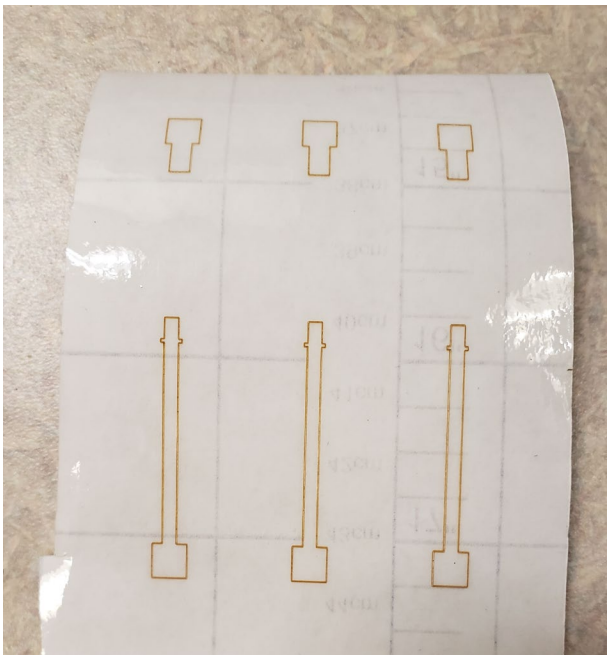

Figure 13. Laser-cut pattern of adhesive sheet used as mask pattern for screen-printing

Once all the mask patterns were cut out, the textile substrate was cut to workable dimensions and any large contaminants were removed or brushed off by hand. Next a layer of ScotchTM Magic Tape was used to block part of the textile for screen-printing a layer of P-5011 plastisol for creating the SPE backing. Next, the conductive silver traces would be screen-printed using one laser-cut pattern, followed by the Ag/AgCl ink using a second pattern, and then the carbon paste or PANI composite with an identical pattern to the previous one. Lastly, the thicker plastisol LFP-1070 would be printed overtop of the conductive traces and electrode connections, using the ScotchTM Magic Tape to protect the electrode area and contact pads.

The screen-printable inks and corresponding composites were screen-printed and cured on a Torrey-Pines programmable hotplate at 130°C for the times specified by the supplier. For the plastisol, speedball, and PANI composites, this was 30 to 60 seconds.

Local variations in the hotplate made the exact time and temperature slightly ambiguous. However, curing could be determined by hand by touching the screen-printing ink and seeing if no residue would remain on when touched. The silver, Ag/AgCl , and carbon inks cured for approximately 10 minutes each. No adverse effects were seen when the curing times were a few minutes longer or shorter, other than a slight increase in conductivity for the silver inks if not cured long enough. A glass slide was used for spreading the ink across the substrate, applying moderate pressure, and forming a relatively acute angle with respect to the substrate. A few passes of the glass slide blade were done until the pattern was fully reproduced by the ink.

3.3. PANI pH Sensors

In this section, PANI's unique conduction mechanism is first discussed. Next, the different methods reported in literature for its synthesis are reviewed along with efforts to improve processability through doping. Then, the methods used in this thesis for depositing PANI films onto the textile SPEs for characterizing its pH response will be discussed. Finally, the screen-printable PANI composite fabrication and optimization will be discussed.

3.3.1. PANI Background

Conduction Mechanism

Polyaniline (PANI) was first characterized in the 1960s [175], however, it was not until the late 1980s when its conductivity was discovered that it started garnering the attention of researchers [176]. Since then, PANI's semiconducting properties have been extensively reviewed for numerous applications [177-179]. Its unique conductivity mechanism is detailed in Figure 14. It has three distinctive oxidation states, namely: the fully reduced leucoemeraldine state, the semi-oxidized emeraldine state, and the fully oxidized pernigraniline state. The fully oxidized and fully reduced states are electrically insulating. The semi-oxidized emeraldine state is semi-conducting. When doped with protons, PANI is said to be in the conductive emeraldine salt (ES) state. When undoped, PANI is in the insulating emeraldine base (EB) state. It can exist in any number of states between these two extremes displaying a range of conductivities. When PANI-ES is pressed into a pellet, conductivities in the range of 2-10 S/cm have been reported [177].

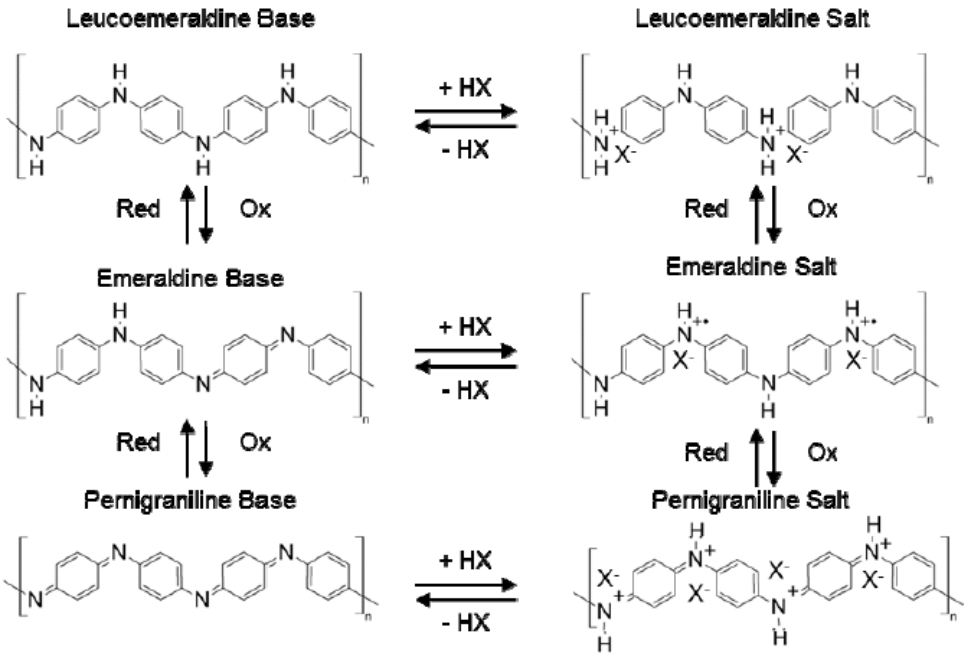

Figure 14. Polyaniline's electrochemical redox states (base) and corresponding doped states (salt) reproduced with permission from authors [177]

This change in conductivity represents an ideal sensing mechanism for monitoring pH levels of solutions, particularly as a conductimetric sensor [133]. The ability to act as a proton acceptor or donor also allows it to be used for potentiometric sensors [124] and ISFETs [180]. One group has also reported its use as an amperometric pH sensor based on the transition between oxidation states [125]. As was reported in section 3.2.4, PANI pH sensors generated some of the highest sensitivities for electrochemical sensors for potentiometric sensors. In addition to its favorable sensing characteristics, PANI is relatively inexpensive, has a simple synthesis procedure, good environmental stability, and good biocompatibility [127, 128]. Its processing has typically been a challenge mainly due to its insolubility in all but polar aprotic solvents. However, dopants can be added to help with its processability, which will be discussed in a subsequent section in this chapter. For these reasons, PANI was selected as the pH sensitive filler to add to a screen-printable polymer matrix.

Synthesis Methods

Various polymerization approaches have been reported to try to obtain PANI with different morphologies and properties [177]. These have included chemical, electrochemical, and interfacial polymerization.

In chemical polymerizations, an acidic solution of aniline monomer is prepared and a chemical oxidizer, typically ammonium persulfate (APS), is added to the stirred solution. Hydrochloric acid (HCl) is commonly used as the acidic media. Numerous other synthesis conditions and chemical additives such as surfactants have been added to the polymerization media to try to modify the polymer morphology [181-183]. After the completion of the reaction, PANI polymer particles are present in solution as well as adhered to all surfaces in contact with the solution in the form of a thin film.

Electrochemical polymerization uses a similar procedure; however, the chemical oxidizer is replaced by an oxidative electric potential. In these cases, the polymerization only occurs at the location of the WE and PANI takes the form of a film.

Interfacial polymerization is another chemical polymerization approach which uses an acidic aqueous solution with APS overtop of an organic phase containing the aniline monomer. At the interface where the two phases meet, polymerization is initiated. As the polymerization proceeds the growing PANI polymer chain which is insoluble in the organic phase extends into the aqueous phase. This procedure was used to try to grow long PANI nanofibers (NFs). However, similar results with greater quantities can be achieved using regular chemical polymerization by adding APS all at once [177].

Dopants and Processing

Despite the numerous synthesis approaches and reports of PANI as sensors, the processing of PANI has still been a challenge. PANI is only somewhat soluble in polar aprotic solvents such as N-methyl pyrrolidone (NMP), Dimethylformamide (DMF), and Dimethylsulfoxide (DMSO). However, these solvents typically present high boiling points, low vapor pressure, and high toxicity. As such, most groups fabricating PANI pH sensors for wearable applications use non-scalable methods such as electrochemical polymerization or drop-casting with a lengthy evaporation step to produce PANI films. As was highlighted in previous sections, there are still relatively few methods reported for processing PANI using a scalable approach. Furthermore, there are no scalable approaches to fabricating flexible PANI sensors on textiles known to the author at the time of writing.

Only a few groups have developed PANI pH sensors using scalable approaches. A few groups have incorporated PANI particles into an ink for inkjet printing [134-136] of

PANI films on SPE on various flexible substrates. Gill et al. [133] reported a novel composite for screen-printing PANI using polyvinyl butyral (PVB) as a binder and PS3 surfactant to disperse the PANI particles. They were able to screen-print this composite onto a set of interdigitated electrodes (IDE) on a rigid alumina substrate and demonstrated pH sensitivity between pH range of 2-11.

Another consideration in play is that pure PANI reportedly loses much of its intrinsic conductivity in solutions with a pH greater than 5 [177]. This inherently does not lend itself well to monitoring physiological pH levels. As such, much research has been published on the addition of dopants with sulfonate and phosphonate groups to extend PANI's linear range of operation up to levels as high as pH 10 [177, 184, 185]. The dopants become entrapped within the PANI matrix via hydrogen bonding between the anionic sulfonate or phosphonate group of the dopant and the amine group of the PANI. Meanwhile, the other end of the dopant acts as a plasticizer and allows PANI to be suspended in a variety of readily-processable solvents depending on its composition. Camphorsulfonic acid (CSA) has been used for polar protic like m-cresol and aprotic solvents like n-methyl pyrrolidone (NMP) and dimethylsulfoxide (DMSO) [186, 187]. Dodecylbenzensulfonic acid (DBSA) has been used to make PANI processable with many solvents including organic solvents [188] and aqueous solvents alike [189]. DBSA was selected based on its versatility for solvent compatibility meaning it could be used for both plastisol and water-based screen-printing inks. The structure of DBSA and CSA are shown in Figure 15. These dopants can be added during the polymerization or after their synthesis (post-doping).

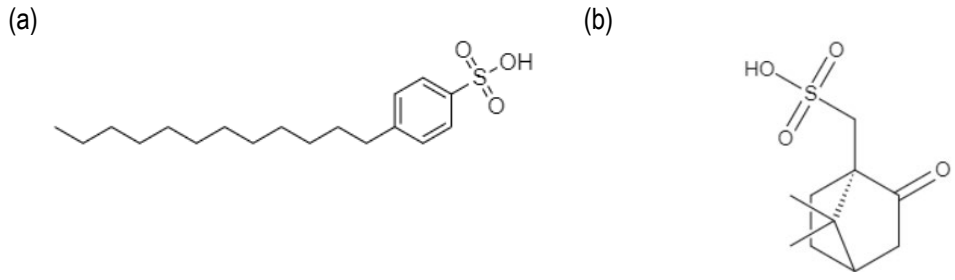

Figure 15. PANI Dopants: (a) DBSA; (b) CSA

3.3.2. PANI Chemical Polymerization

Prior to testing the PANI composites, PANI films were first synthesized onto the WE of textile SPEs and Pine Research SPEs to get an idea of the best possible sensor

response achievable for PANI. The Pine Research SPE is shown in Figure 16. The 2 mm diameter and 4 mm x 5 mm WE designs were used interchangeably.

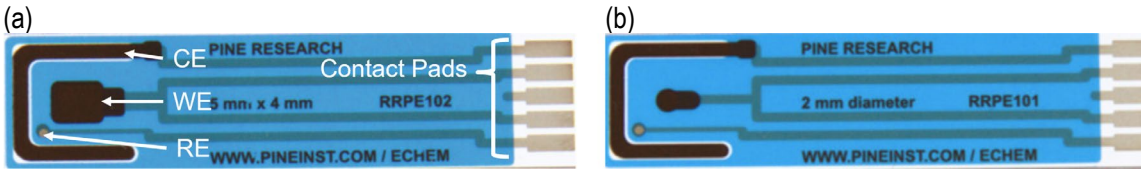

Figure 16. Pine Research SPEs with (a) 5 mm x 4 mm, and (b) 2 mm diameter WE [190]

Chemical oxidative polymerization was first performed according to the synthesis conditions listed in Table 3 and were based on [188] and [191].

Table 3. Synthesis conditions for the chemical oxidative polymerization of PANI

#	Aniline	APS	DBSA	Solvent
1	125 mM	50 mM	187.5 mM	DI water
2	55 mM	68.6 mM	55 mM	0.1 M HCl
3	125 mM	50 mM	187.5 mM	Hexane

Tests #1 and #2 were performed at room temperature whereas Test #3 was performed at 0°C by cooling in an ice bath. For tests #1 & #2, aniline and DBSA were mixed into half of the reaction volume of solvent whereas APS was added to the other half. The reactions were initiated by adding the two solutions together. The reaction was then allowed to proceed for 2 hours. For test #3, APS was mixed into 5 mL of solvent and injected slowly dropwise over 20 minutes using a Harvard syringe pump. The reaction was allowed to proceed for 2 hours after all the APS was added. It was expected that the PANI properties could be tailored based on synthesis conditions for optimizing the composite preparation and pH response.

For analysis, Pine SPEs, textile SPEs, and adhesive sheets were inserted into the reaction mixture and a polymer film was formed in situ. To try and constrain the area of the film formation, a patterned adhesive was applied to the SPEs. The synthesis setup is shown in Figure 17.

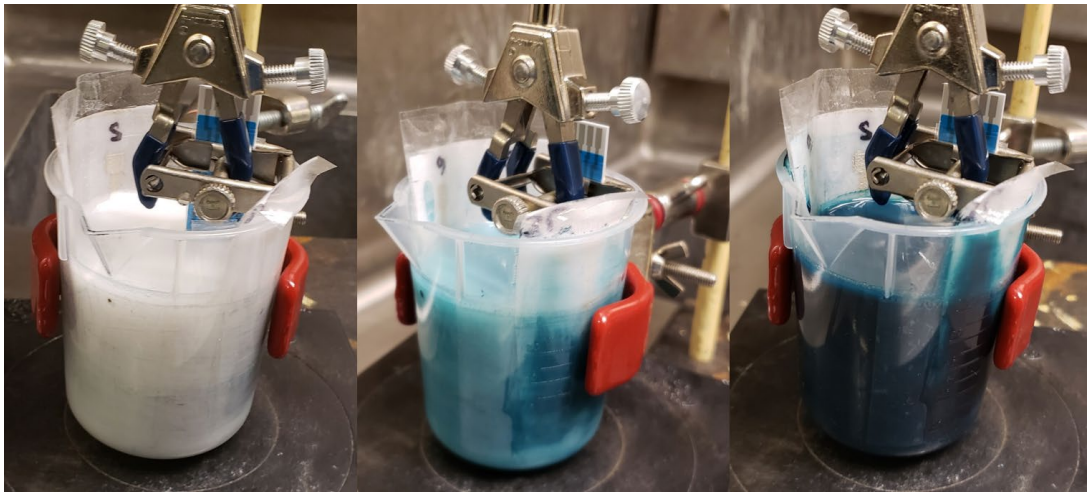

Figure 17. PANI chemical polymerization progression

The chemical oxidative polymerization progress proceeded similarly for all synthesis conditions. The solution was initially an opaque white colour and slightly foamy in texture because of the DBSA acting as a surfactant. Shortly after the APS was added, the reaction mixture started to change colour gradually into a dark blue.

After 2 hours of reaction time, the magnetic stir bar mixing was stopped, and 50 mL methanol was added to help precipitate the PANI. For synthesis conditions #3 which used hexane as a solvent, a clear phase separation and discoloration of the aqueous phase could be seen. This aqueous phase contained the newly added methanol as well as any unreacted monomer or reactants. The polymer was then present in the organic phase and was filtered out using a vacuum filtration setup. The phase separation after the addition of methanol in reaction #3, the vacuum test setup, and the collected polymer on filter papers are shown in Figure 18. The polymer collection was similar for all synthesis conditions tested. During filtration, the polymer residue was washed with 0.1 M HCl until the filtrate was clear, then thoroughly rinsed with water and acetone to assist with drying. The collected polymers were then placed in vacuum for over an hour for further drying.

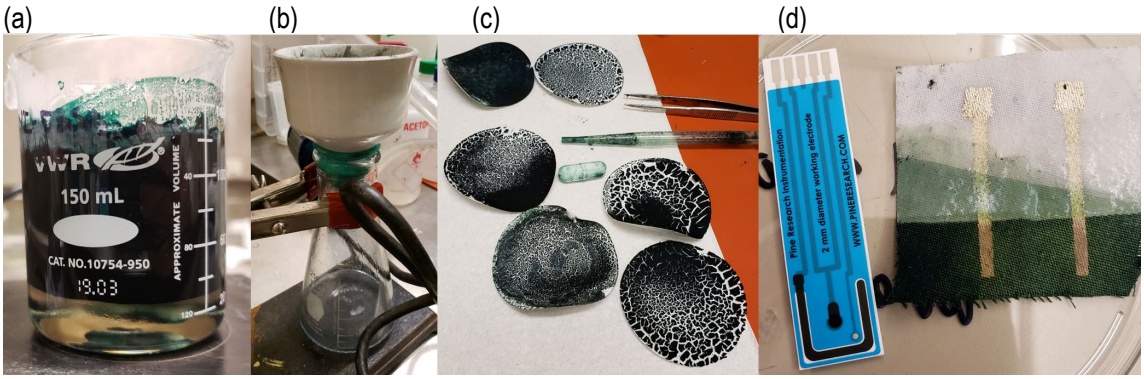

Figure 18. Chemically polymerized PANI post-processing: (a) PANI reaction media with hexane as a solvent (dark blue) after addition of methanol which collected any unreacted reactants (transparent yellowish); (b) PANI vacuum filtration setup; (c) PANI powders collected on Whatman filter papers; (d) Films formed on surfaces in contact with reaction media including textiles and Pine SPE

Given that a PANI film formed on all surfaces in contact with the reaction media, a challenge arose in selectively depositing a PANI film at the WE area of the SPEs. For this purpose, an adhesive sheet cover patterned with the laser cutter was designed to block certain regions of the SPE. However, this method did not protect the textile SPEs as a poor seal formed between the adhesive sheet and the textured textile substrate resulting in a PANI layer forming at undesired areas. For the Pine SPEs, removal of adhesive cover resulted in a peeling of the carbon layers. Thus, a plastic shield was designed in Corel Draw and cut out with the laser cutter to protect the carbon layer when the patterned adhesive was placed overtop. Despite this design, this method was still not very reliable and would still leak occasionally. The carbon layer peeling, the plastic shield, the PANI deposition at the WE, and the leaking of PANI solution over the Pine Research SPE are shown in Figure 19.

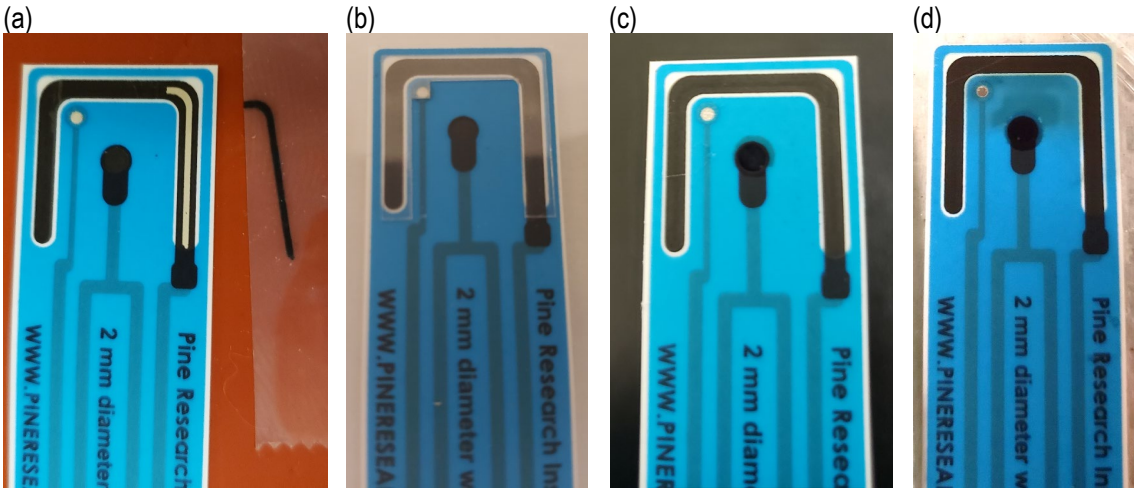

Figure 19. Pine Research SPE peeling of carbon layer from CE through tape adhesion and removal; plastic cover used to protect carbon layer from adhesive;

Additionally, the PANI powders collected using the chemical synthesis were not overly useful for polymer preparation as they aggregated into clumps that were too big and would not mix properly with other components. Attempts were made to break these down into smaller particles using a mortar and pestle, but they would still stick together somewhat, likely due to inadequate drying and purification on post-processing. Further purification would be required to make these powders workable.

Therefore, despite the simplicity of the chemical polymerization, it was deemed too labour intensive and time consuming, plus the collected PANI was not very refined and too small in quantity to be used for composite formulation. In the interest of time, convenience, and reproducibility, electropolymerized and drop-cast PANI were used for characterization of PANI's pH response instead. For the same reasons, commercial PANI powders purchased from Sigma-Aldrich were used for the composite preparation.

3.3.3. PANI Electro-Oxidative Polymerization

Given the challenges encountered with the chemical polymerization of PANI, PANI electropolymerization onto the WE of textile SPEs and Pine Research SPEs was tested for the purpose of characterizing PANI's pH response. The different synthesis conditions tested for electropolymerization are listed in Table 4. All reaction mixtures were prepared by mixing aniline and DBSA into 1 M HCl and stirring with a magnetic stir bar for over an hour until the solution was homogeneous. The electro-oxidative polymerizations were

performed by placing the SPE in about 15 mL of reaction mixture in a 20 mL beaker. Both the Pine Research SPEs and textile SPEs were tested to further confirm proper operation of the textile SPE. The potential would then be cycled between +1.0 V and -0.2 V at a scan rate of 40 mV/s for 20 cycles using a Parstat 4000 potentiostat with the VersaStudio software. Following, the potential cycling, the SPE would be rinsed off with DI water and air dried.

Table 4. Component concentrations for PANI electropolymerization

#	Aniline	DBSA	Molar Ratio Relative to Aniline
1	55 mM	0 mM	0
2	55 mM	55 mM	1
3	55 mM	68.75 mM	1.25
4	55 mM	82.5 mM	1.5

Visually, no change could be observed in the solution as the polymerization was occurring. However, after the potential cycling was completed, a subtle dark polymer film could be seen adhered to the WE of the Pine Research SPEs and textile SPEs as shown in Figure 20. These were particularly noticeable on the backside of the textile WE.

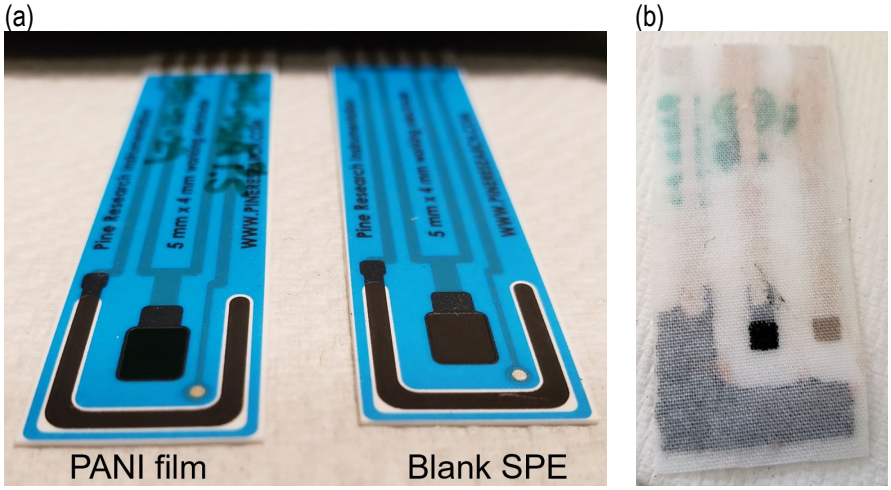

Figure 20. Electropolymerized PANI-DBSA film on (a) a Pine Research SPE (next to a blank Pine SPE next to a blank Pine Research SPE (right)

3.3.4. PANI Drop-Casting and Solution Processing

To confirm that DBSA enhanced the solubility of PANI in organic and aqueous solvents and that proper blending could be achieved with screen-printable inks, different states of doped and undoped PANI were added to 5 mL of various solvents at

concentrations of 5 mg/L. The solubilities of PANI-EB, PANI-ES, and PANI-EB + DBSA were compared in DMSO, Xylene, Heptane, and DI water. PANI-EB (MW ~10,000), PANI-ES (MW~15,000) and DBSA (95% mixture or isomers, ordered from Sigma Aldrich) were purchased from Sigma-Aldrich and used as is. The mixtures prepared are listed in Table 5. The purchased PANI-ES is doped with a proprietary sulfonic acid. For the PANI-EB + DBSA solutions, one molar equivalence of DBSA to aniline monomer was added. The solutions were shaken by hand for 1 minute before being allowed to settle. The solutions were then compared after 1 hour and 1 day without agitation.

Table 5. PANI solubility test

#	Solvent	PANI	DBSA
1	DMSO	EB	0
2	DMSO	EB	17.4 mg/mL
3	DMSO	ES	0
4	Xylene	EB	0
5	Xylene	EB	17.4 mg/mL
6	Xylene	ES	0
7	Heptane	EB	0
8	Heptane	EB	17.4 mg/mL
9	Heptane	ES	0
10	DI Water	EB	0
11	DI Water	EB	17.4 mg/mL
12	DI Water	ES	0

DMSO was selected as literature suggested that PANI was most soluble in polar aprotic solvents [186, 192]. DMSO is also water soluble and could potentially be mixed with the Speedball ink during composite preparation. Water was also evaluated as a solvent for PANI as it could also be mixed with Speedball inks, is non-toxic, and has a much lower boiling point (100°C) than DMSO (189°C) and the recommended curing temperature of the screen-printing inks (130°C). Xylene and heptane are both non-polar solvents having respective boiling points of 139°C and 98°C and relatively low vapour pressure. Heptane has been shown to mix with plastisol [16] and xylene is a non-polar solvent with a higher boiling point with similar molecular structure to the PANI monomer. The mixed solutions are shown in Figure 21 after 1 hour of settling.

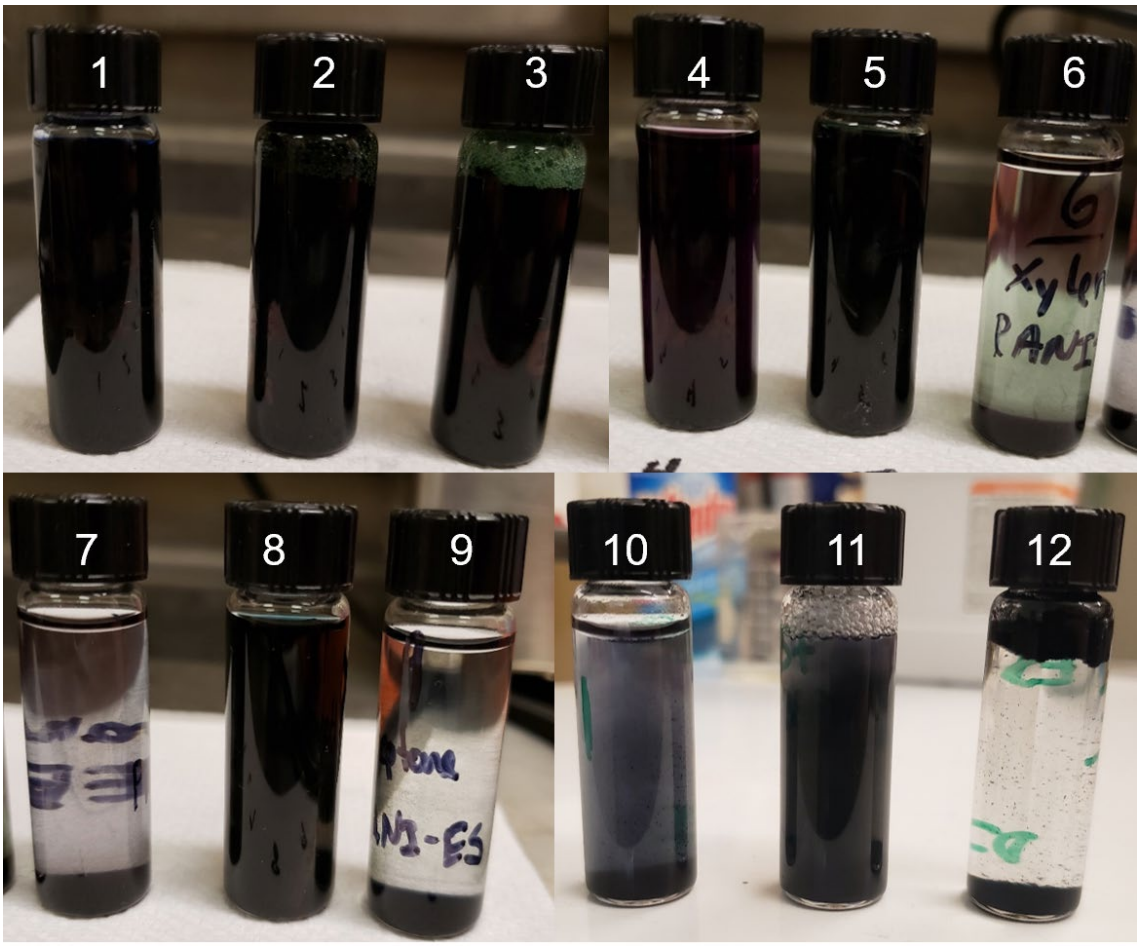

Figure 21. Mixtures of PANI in various solvents to evaluate solubility; vial #'s correspond to the solutions specified in Table 5

The solubility of the different forms of PANI in the various solvents could be observed qualitatively based on the transparency of the mixtures. Opaque solutions where the powders could not be distinguished from the solution indicated good mixing, whereas solutions where the PANI powders had precipitated out, leaving it transparent, indicated poor solubility.

All forms of PANI were soluble in DMSO. All but the PANI-ES were soluble in xylene. However, only the PANI-EB + DBSA was soluble in heptane. In DI water, the PANI-ES was not soluble, PANI-EB was slightly soluble, and PANI-EB + DBSA was more soluble. The PANI-ES was only soluble in DMSO, the polar aprotic solvent. In contrast, the PANI-EB + DBSA was mostly soluble in all solvents. These results were essentially as expected and demonstrated that the addition of DBSA greatly enhanced the solubility of PANI in polar protic and non-polar solvents. The only difference after 1 day came from

the water solutions where a greater amount of PANI had precipitated leaving the solution dyed, but more transparent. This longer-term instability indicates that PANI-EB is not fully soluble in water at these concentrations and that PANI-EB post-doped with DBSA is marginally soluble. A picture of the water solutions 1 day later without agitation are shown in Figure 22.

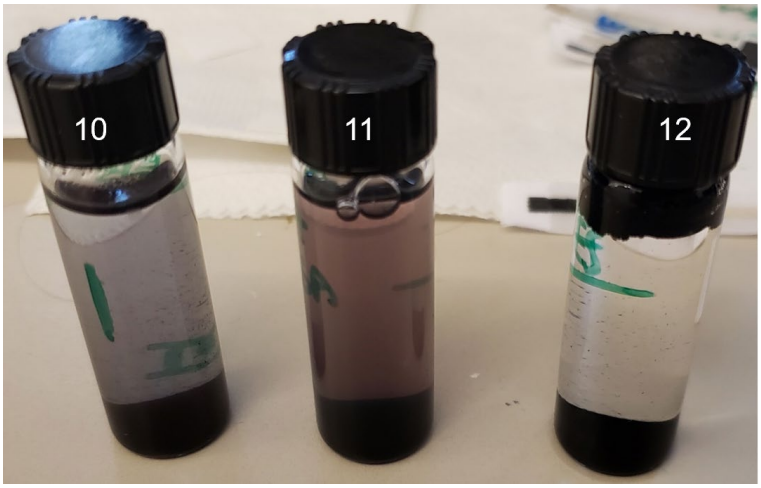

Figure 22. DI water solutions with PANI-EB (10), PANI-EB + DBSA (11), and PANI-ES (12)

Following this test, the unprecipitated solutions were filtered through a 0.2 µm syringe filter and used for drop-casting PANI onto textile WEs for electrochemical characterization. The DI water solutions mixing was characterized at a later stage of the project after the response from the electropolymerized and drop-cast PANI had already been characterized, so no textile WEs were drop-cast with the water solutions. For the other solvents, several droplets would be added and evaporated until a colour was observable on the surrounding fabric as shown in Figure 23. An increasing number of droplets was added to successive samples to determine how many would be required to form a proper film. The DMSO and xylene solutions were heated up on a hotplate at 130°C to accelerate the solvent removal.

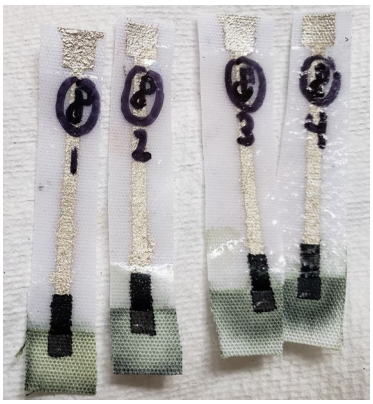

Figure 23. Drop-cast PANI onto textile WE

3.3.5. Screen-Printable PANI Composite Preparation

Conductive polymer composites are generally created by dispersing conductive filler particles in an insulating polymer matrix. As the fraction of conductive filler increases in the insulating matrix, the proximity between successive conductive particles shortens and electron tunneling pathways are created throughout the composite. Beyond a certain fraction of conductive filler known as the percolation threshold, the bulk composite becomes conductive.

In this work, the conductive filler was PANI-EB or PANI-ES and the polymer matrix was either the plastisol P-5011 or Speedball screen-printing ink. DBSA is added as a dopant and plasticizer. Several droplets of solvent were added dropwise to the mixture to facilitate mixing and adjust the composite's viscosity. For the plastisol, the solvent selected was heptane as it had previously been shown to mix well with plastisol [16] and showed good mixing with PANI when DBSA was added. For the Speedball composites, water was selected due to its non-toxicity and mixing with Speedball inks and partial solubility for PANI when DBSA was added.

The screen-printable PANI composites were prepared by weighing out the components in a small polyethylene weigh boat on a Baoshishan precision balance and mixing them with a metal spatula. Once the optimization of the PANI composite formulation was completed, the composite would be screen-printed as the WE material of the textile SPEs in place of the carbon paste used for the textile SPE design validation.

3.4. PAPBA Lactate Sensors

In this section, boronic acids as binding elements will be discussed in the context lactate sensors using PAPBA. Synthesis methods from the literature will be reviewed as was done for PANI in the previous section. This section will then be concluded by the methods used to deposit PAPBA onto textile SPEs for characterizing the potentiometric response to changes in lactate concentration.

3.4.1. PAPBA Background

Boronic Acid Binding Mechanism and PAPBA Sensors

Boronic acids (BAs) have earnt some attention in recent studies as they have been shown to form a reversible covalent bond with diols [193-198]. Upon addition of a molecule with a diol group, BAs can form a cyclic diester compound which results in a measurable shift in the electron density on the boron atom. These boronic acid groups can be included as functional side groups of conductive polymers to create self-doping polymers. This is typically done through use of a modified monomer unit. This has been shown with PPY and PEDOT:PSS as the polymer backbones for the detection of saccharides such as glucose [199, 200]. Similarly, aniline can be functionalized with BAs and polymerized to generate a BA-PANI known as PAPBA [193].

In sweat, lactate and glucose are the only diols present in significant quantities. From Table 1 in Chapter 2, the typical concentrations of lactate and glucose lie in the range of 5-40 mM and 0.01-0.2mM, respectively. Additionally, Zaryanov et al. [160] reports that the respective binding constants of lactate and glucose at physiologically relevant pH values further favours the binding of lactate. Given this information, glucose interference is essentially negligible. As such, PAPBA presents a viable option for the binding and signalling of lactate. Additionally, given its PANI backbone, it shares many of the same favourable properties as PANI including simple synthesis, good environmental stability, and biocompatibility.

Zaryanov et. al. demonstrated PAPBA sensors relying on EIS. This approach uses the binding of the analyte to a boronic acid layer fixed at the sensing electrode which impedes the electron transfer of a redox probe. At greater concentration of analyte, the impedance is increased. Although this method provides good sensitivity, it is not amenable

to wearable applications due to the need for a redox probe such as ferrocyanide or ferrocene which must be present in the solution of interest. Other groups have thus implemented this approach as a potentiometric sensor where this redox probe is not required and the implementation to wearables is more favorable. Yet, no studies have been conducted on the response to lactate at physiologically relevant concentrations. The structure of 3-aminophenylboronic acid (3-APBA) is shown in Figure 24 along with the binding of a diol species to a phenylboronic acid group.

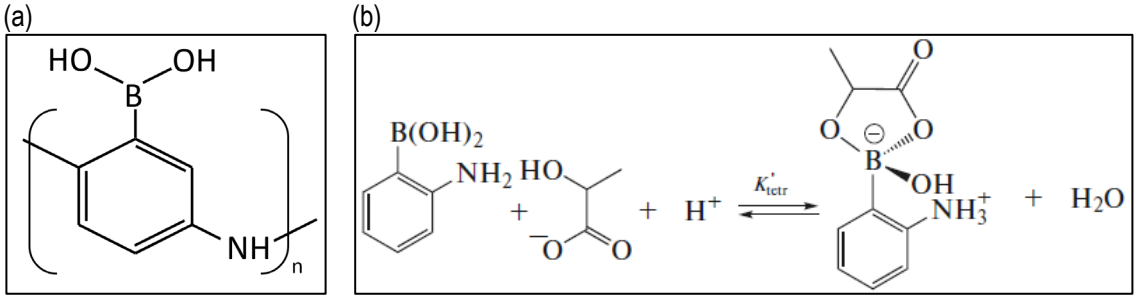

Figure 24. (a) PAPBA chemical tructure; (b) 3-APBA binding reaction with lactate reprinted with permission from Springer Nature [200]

Synthesis

Like the synthesis of PANI, the synthesis of PAPBA can be performed through chemical polymerization or electropolymerization and many different morphologies can be obtained by modifying the reactant concentrations and synthesis parameters [202-205]. The main difference for the PAPBA polymerization compared to that of PANI is that the aniline monomer is replaced by 3-APBA. 3-APBA is essentially aniline with an added boronic acid functional group. Fluoride ions must also be added to the reaction media for the polymerization to proceed. The fluorine atom hybridizes with the boron atom converting it from sp^2 to sp^3, pulling the electron cloud density away from the aromatic ring, thus making the monomer more reactive. Some have reported that the fluoride can instead be replaced by a diol such as lactate to imprint the polymer during polymerization, or by using ionic liquids [160, 205].

3.4.2. PAPBA Synthesis

PAPBA Chemical Polymerization

As was done for PANI, PAPBA was chemically synthesized. In one beaker, 20 mM 3-APBA and 100 mM NaF were dissolved in 50 mL 0.1M HCl. In a second beaker, 20 mM

APS was dissolved in 0.1 +M HCl. The reaction was initiated by mixing the content of the two beakers. The reaction proceeded for 2 hours at room temperature and was stirred using a magnetic stir bar. The reaction progression is shown in Figure 25. The polymer would then be filtered out using the same vacuum filtration setup used for PANI and the collected powders were dried in a vacuum oven for over an hour.

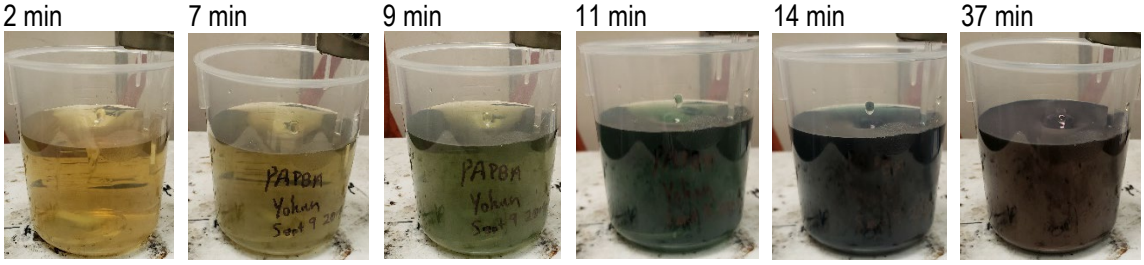

Figure 25. PAPBA chemical polymerization progression

For the same reasons chemical polymerization was abandoned for PANI synthesis, chemical polymerization was abandoned for PAPBA in place of electropolymerization. Namely, this synthesis approach was much more time-consuming and labour intensive than the electrochemical polymerization for rapid prototyping.

PAPBA Electropolymerization

The setup used for synthesizing PAPBA was essentially the same to that used for the PANI electropolymerization. The reaction mixtures and potential cycling parameters tested are listed in Table 6. These conditions are based on the approaches reported by [160] and [194]. The electropolymerization reactions were done at room temperature and were cycled between 10 and 15 times.

Table 6. Chemical concentrations for PAPBA electropolymeriation

#	[3-APBA]	[NaF]	[L-Lactate]	Solution	Potential Cycling Range	Scan Rate
1	150 mM	-	900 mM	0.3 M H_2SO_4	0.9 V to 0 V	40 mV/s
2	150 mM	900 mM	-	0.3 M H_2SO_4	0.9 V to 0 V	40 mV/s
3	20 mM	-	200 mM	0.5 M HCl	1.1 V to -0.1 V	20 mV/s
4	20 mM	200 mM	-	0.5 M HCl	1.1 V to -0.1 V	20 mV/s

Chapter 4. Experimental Methods

This chapter discusses the methods used for testing both the devices and the polymers elaborated in Chapter 3. The test setups and parameters for confirming the PANI electropolymerization, drop-casting, and PAPBA electropolymerization are explained. Additionally, the tests used for optimizing the PANI composite formulation are defined.

4.1. Textile Screen-Printed Electrodes Design Validation

To confirm that the textile SPE was performing as intended, commercial carbon SPEs were purchased from Pine Research as a comparison. The Pine Research SPEs are printed on PET substrates and have a carbon WE and CE, along with a Ag/AgCl RE. The Pine SPE was connected to a Parstat 4000 potentiostat from Ametek using an adaptor designed for Pine Research SPEs purchased from IORodeo. The textile SPE was attached directly to the alligator clips of the potentiostat cable.

Both textile SPEs and Pine Research SPEs were tested using CV and CA using the Versa Studio software. It was initially believed that CA could be used for measuring the pH response of the redox-active PANI electrodes based on previous literature [125]. Consequently, this method was first tested using $K_3Fe(CN)_6$ as a test redox mediator. This also served to confirm the proper operation of the three-electrode textile SPE design. Each electrode of the textile SPE (i.e., WE, CE, and RE) was individually validated in combination with the two electrodes from the Pine SPE before being tested as a full system. The various WE designs were tested using a CE and RE confirmed to be working as expected (either from the Pine Research SPE, or a combination of a square 15 mm x 15 mm screen-printed carbon electrode on a textile substrate as the CE and a standard Ag/AgCl RE from Cole Parmer). The test setup is shown in Figure 26.

(a)

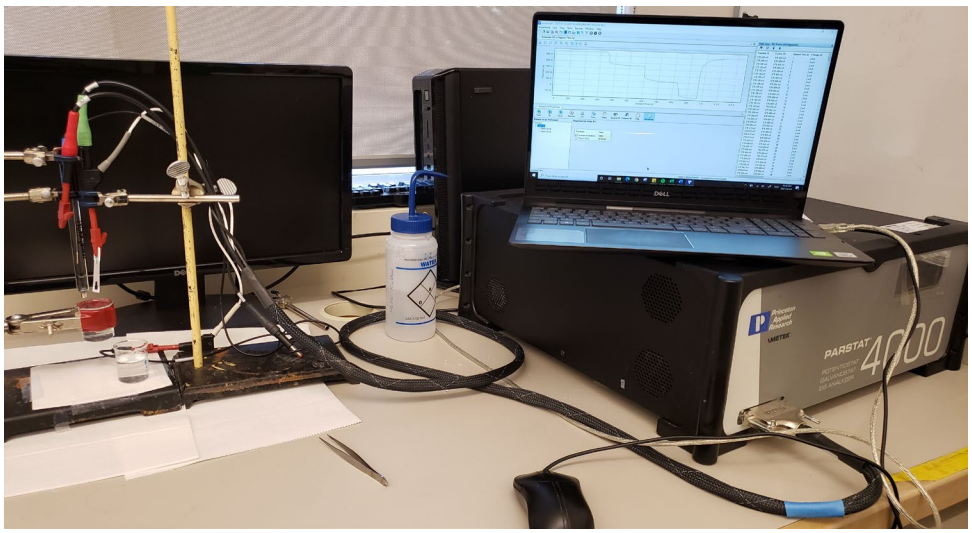

(b)

(c)

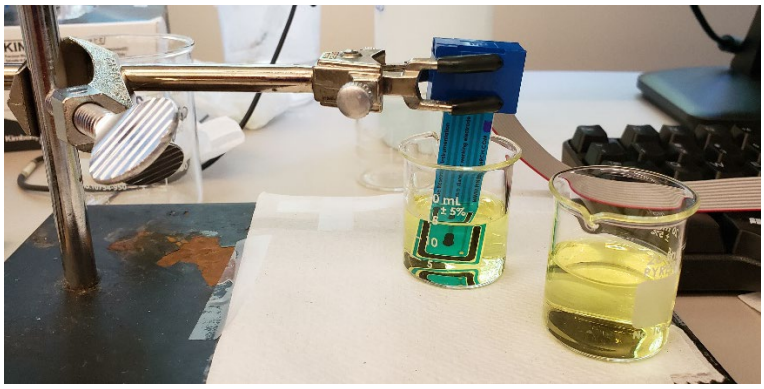

Figure 26. (a) Potentiostat and Electrochemical Characterization Test Setup (b) Textile electrodes printed on separate substrates in 0.5 M KCl solution of $K_3Fe(CN)_6$; (c)Pine Research SPE with IO Rodeo attachment in 0.5 M KCl solution of $K_3Fe(CN)_6$

To determine the optimal potential at which to operate the CA study, a CV analysis was initially performed. CV is an electrochemical technique which is typically used to examine the redox characteristics of analytes in solution or fixed to the working electrode. This is done by cycling between established potential limits in a linear fashion with respect to time, and plotting the resulting current on a cyclic voltammogram. During a CV scan, increasing the potential results in electron loss at the WE and is referred to as moving in the forward direction, or the anodic scan, or also the oxidative scan. Decreasing the potential corresponds to electron gain at the WE and is referred to as moving in the reverse direction, or the cathodic scan, or also the reductive scan. By convention, CV scans start at the upper potential limit and proceed in the reverse direction, decreasing until the lower limit is reached, at which point the scan direction is reversed and then proceeds in the

forward direction. At redox potentials where a chemical species can gain or lose an electron, a peak in the current can be seen on the resulting cyclic voltammogram. Analogous electrical behavior is expected when scanning in opposite directions, albeit inverted in sign. CV typically uses a non-stirred, still solution as it relies on the diffusion properties of the species in solution to measure electron transfer properties [206].

The CV analysis for the textile SPEs was performed with 50 mM KCl electrolyte solutions with $K_3Fe(CN)_6$ concentrations of 10, 5, 3, 2, 1, and 0 mM. Both chemicals were purchased from Sigma-Aldrich. Next, sensitivity curves are created by extracting the current at the same potential level for all cyclic voltammograms at the different concentrations of $K_3Fe(CN)_6$. Then, a linear model would be fit relating the analyte concentration to the extracted current level measured through CV. The model with the highest slope would display the theoretical highest level of sensitivity and be used for all subsequent CA experiments. For CV and CA, Pine Research SPEs and three-electrode textile SPEs were used and placed in an electrochemical cell consisting of a 20 mL glass beaker with approximately 15 mL of test solution. The theoretical CV curves and sensitivity curve for Pine Research SPEs $K_3Fe(CN)_6$ are shown in Figure 27.

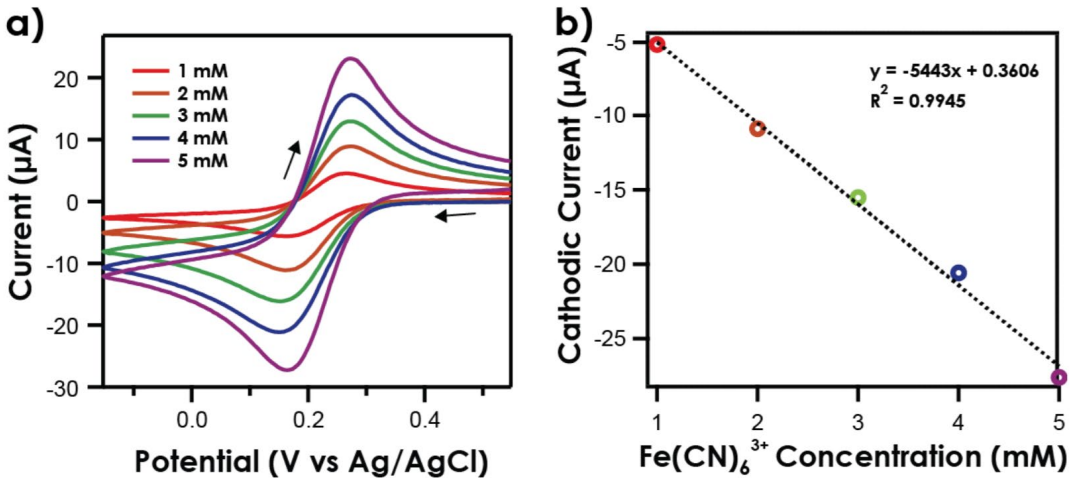

Figure 27. $K_3Fe(CN)_6$ solution electrochemistry on a gold SPE: a) CV of varying concentration and b) cathodic current as a function of concentration [190]

4.2. PANI and PAPBA Film Deposition Validation

To confirm the deposition of PANI and PAPBA films on the Pine SPEs and textile SPEs, similar procedures were used so these sections have been lumped together.

PANI and PAPBA have well established redox potentials and thus it is possible to confirm their successful synthesis based on their corresponding cyclic voltammograms and comparing these to characteristic cyclic voltammograms. This was done for the electropolymerized PAPBA, electropolymerized PANI, chemically polymerized PANI, and drop-cast PANI on either Pine Research SPEs or textile SPEs.

The CVs were recorded in a 1 M HCl solution using the Parstat 4000 potentiostat controlled via the Versa Studio software. The ideal CV curves from literature are shown in Figure 28 for PANI and PAPBA. The two oxidation peaks for PANI occurs at a potential of about 0.2 V and 0.8 V. For PAPBA, peaks are seen at 0.18 V and 0.5 V.

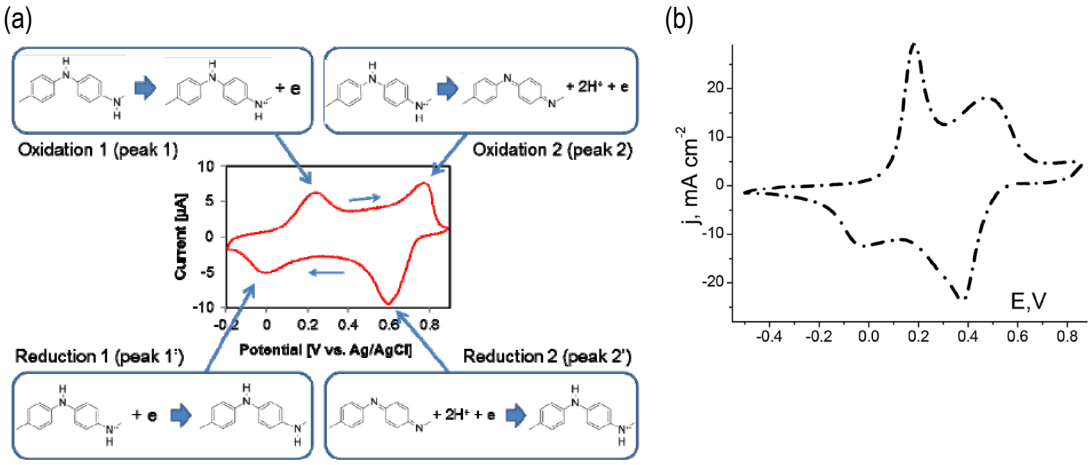

Figure 28. Characteristic CV curves in 1M HCl of (a) PANI reprinted with permission from [177]; and (b) PAPBA figure modified and reprinted with permission from [160]

4.3. PANI pH Response

All pH responses were determined using the Parstat 4000 potentiostat with the Versa Studio software. A set of standard buffers from pH 3 to 10 were purchased from Sigma-Aldrich were used to create the pH solutions. KCl was added to the solution to reach a concentration of 50 mM to simulate the electrolyte content in human sweat.

The pH response of PANI was first characterized by performing a set of CV scans at different pH levels for the drop-cast PANI sensors. These were then plotted with the intention of performing a set of sensitivity curves for finding the optimal operating potential for CA as was done for the $K_3Fe(CN)_6$ study with just the carbon WEs. The CV scans were performed from +1.0 V to -0.2 V for three cycles at each pH level with a 45 second break

in between to allow for the solution to be manually switched. The last CV cycle of each is then shown. However, the CV curves revealed that the PANI films were not recovering in the buffer solutions, and so this method along with CA were abandoned in place of OCP. A set of CV curves was also recorded for the screen-printed PANI + DBSA + Speedball composite but the results of these were not indicative of any response using CA.

As discussed in Chapter 3, OCP measures the potential between a RE and a WE whose potential is dependent on the analyte concentration. In this work, the OCP measurement scheme followed an indefinite loop where a data point was collected every second for 45 seconds, followed by a 15 second break to allow for the solution to be changed. The solution would only be changed once the OCP had reached an approximate steady state. Without a break, the potential readings tended to be unstable while the solution was being changed, especially when the standard Ag/AgCl RE was being used. In some cases, the first data point after switching solutions would jump to an extreme value before settling back to a value in line with that before the change. These extreme values were removed from plots in the results section. The last data point prior to switching the analyte solution to a different lactate concentration or pH was used to create the sensitivity curves. The sensor response time was determined by looking at the time it took for the sensor to reach its steady state potential from the time it was switched. For the PANI pH sensors, this was done whenever the solution was changed from pH 9 to pH 3. Given that the steady-state potential criterion was selected somewhat subjectively during the measurement recording, the time for reaching 75% and 90% of the steady state potential was also calculated for a more objective representation of response time. Additionally, any time the change from pH 9 to pH 3 was done more than once, these values were averaged.

4.4. Screen-Printable PANI Composite Formulation Optimization

For the purpose of this thesis, the optimization was done based on three key parameters and through four main sequences of experiments. The three parameters and the methods for characterizing these will be discussed in this section. The experiment sequences will be briefly outlined here to explain the thought process used for the formulation optimization. But the experiment sequences will be discussed in greater detail

in the following chapter, along with the specific formulations tested, as the results are needed to better explain the progression between these.

4.4.1. Optimization Methods

The three key parameters used for optimizing the PANI composites were: (1) pH response; (2) print quality; and (3) resistivity. The means to manipulating these three metrics came from the modification of the formulation of the composite. As was discussed in Section 2.3.2, polymer composites are typically created to achieve bulk materials which blend the properties of their various constituents. For the PANI composites developed in this thesis, the goal was to retain the conductivity and pH sensing properties of the PANI while allowing it to be patterned via screen-printing onto textile substrates through the blending with commercial screen-printable textile inks. To aid with this, DBSA was added as a plasticizer to assist in creating a compatible blend.

The pH response was the most important requirement for the optimization and was addressed in the previous section, Section 4.3, using the OCP method and the textile SPE design. However, initially, various implementations for conductimetric, amperometric, and potentiometric sensing were still being explored simultaneously to the development of the composite. As such, the print quality and conductivity were the main metrics used for optimization for the first sequence of experiments. In terms of sensor response, the sensitivity, linearity, response time, and reproducibility were considered.

The print quality, or mechanical properties, of the PANI composite needed to be sufficient that it could be formed into the desired shape and maintain its form long enough to be tested. This property was assessed visually by determining whether the print formed a continuous print. It could also be seen during printing if the composite did not adhere to the textile or cracked immediately upon handling. Additional inspection using an optical microscope was also performed.

Although the print quality criteria were mostly qualitative, the print's resistance could be quantitatively measured and used as a metric for optimizing the PANI composite formulation. Ultimately, the PANI composite needed to be sufficiently conductive to be used as an electrode, so lower resistivity values were preferred. As such, a range of formulations were printed generally with increasing PANI content, and their resistances

measured. In this way, a percolation threshold could be found with PANI acting as the conductive filler.

Test Line Design

To test the print quality and conductivity of various formulations prepared during the composite optimization, 8 to 14 test lines with a length of 1 cm and a width of 1 mm were printed for statistical purposes. The test line structures are shown in Figure 29. The substrate used was a 100% polyester textile purchased from Fabricana (Barcode # 17166). The mask used for the screen-printed test lines was prepared by laser cutting the pattern designed in Corel Draw on an adhesive sheet using a Universal Laser Systems CO_2 laser cutter.

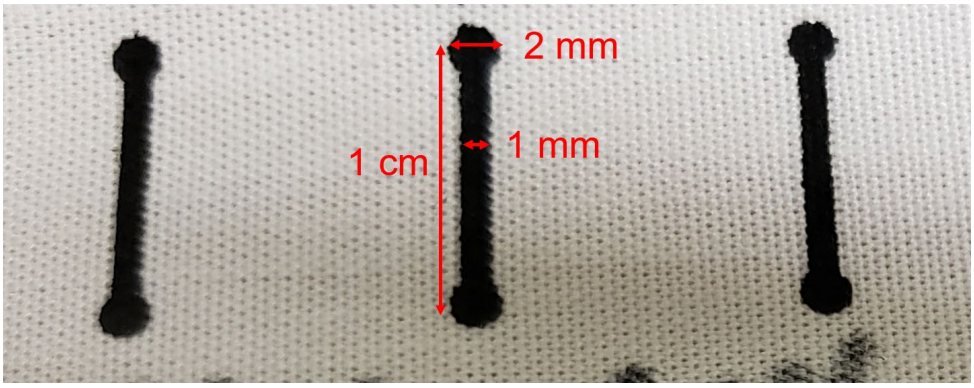

Figure 29. Test lines for PANI composite optimization

Adhesion Test

To further quantify the print quality and the adhesion properties of the PANI composites to the textile substrate, a test referred to hereon as the adhesion test. In this test, a layer of tape (Scotch Magic Tape™) is manually pressed overtop of the entire screen-printed composite test line pattern and peeled away by hand. The number of peels required before there is electrical discontinuity (unmeasurable resistance on the DMM, >300 MΩ) in the conductive pathway between the two touchpads of the test line is recorded and compared.

Flexibility Test

The flexibility of the PANI composite was the last property tested and related to both its print quality, and its pH response. These tests were done by recording the OCP of two-electrode textile SPEs with the PANI composite as the WE in the initial unbent state,

again in a bent state, and a third time after straightening out again. For the bent state, the textile SPEs were wrapped around a cross-section of a disposable 5 mL plastic pipette with a radius of curvature of 4 mm and stapling the fabric to itself to fix them in place. The sensor was then immersed in solutions and the pH response was measured as before using OCP. To straighten the SPE out again, the staple was carefully removed by hand. The staple was carefully positioned as to avoid contacting the conductive silver traces of the textile SPE. The plastic piece along with the textile SPE are shown in Figure 30.

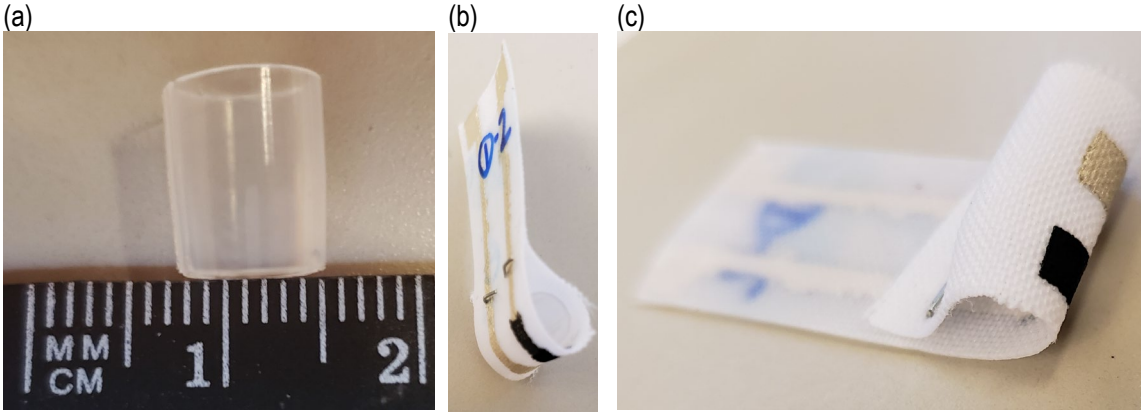

Figure 30. **(a) Cross-section of disposable 5 mL plastic pipette used for setting radius of curvature of textile SPEs for flexibility testing; (b) and (c) Bent textile SPE with PANI +DBSA + Speedball composite WE and screen-printed Ag/AgCl RE**

As a second test for flexibility, the pH responses of the PANI composites were tested with multiple bend cycles using the test setup shown in Figure 31. A servomotor was programmed to rotate a hand 180°, pulling the textile substrate attached via a thread and a binder clip. This rotation would create over a 90° bend on the screen-printed composite which was fixed to the apparatus via duct tape. A set of glass slides affixed to a piece of polycarbonate are used to secure the textile sample and force the substrate to be bent in the direction of the motor. The weight of the binder clip ensures that the textile regained its original position after being bent. The servomotor was programmed using an Arduino. The sample was bent and released a total of 100 times, with a 3 second hold before changing position.

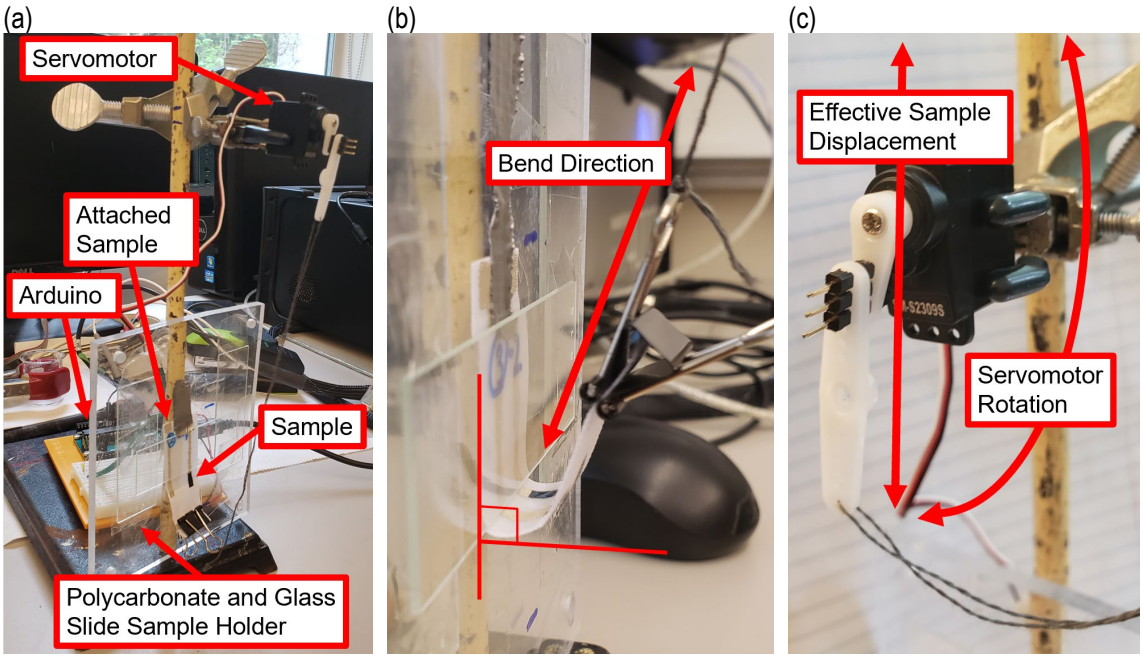

Figure 31. **(a) Apparatus for effecting multiple bend cycles; (b) Sample attached to servomotor with binder clip bent to over 90° angle; (c) Servomotor programmed via an Arduino to rotate 180° to bend sample**

4.4.2. Experiment Sequences

At the time of the first sequence of experiments, only the PANI-EB and the plastisol LFP-1070 had been purchased and the methods for measuring the pH response were still being developed. This first sequence was thus only characterized using print quality and resistivity. This sequence resulted in poor quality prints with high resistivities.

As a result, the second sequence of experiments sought to improve the print quality through the addition of DBSA and the replacement of PANI-EB with PANI-ES. At this stage, PANI's pH response had been confirmed via OCP with the electropolymerized and drop-cast textile sensors. However, a very slow response was observed with the plastisol composites. No adhesion testing or conductivity measurements were performed for the second sequence given the lack of pH response.

Therefore, the third sequence of experiments replaced the plastisol polymer matrix with the water-based, Speedball screen-printing ink. The PANI-ES was again switched back to the PANI-EB form. These generated consistent, linear responses, good print quality based on adhesion testing, and acceptable resistivities.

The fourth and final sequence of experiments was done to try and further optimize the PANI + DBSA + Speedball composites and to prepare samples for flexibility testing. PANI-EB and PANI-ES were both tested. This was the only sequence in which the flexibility testing was performed. Adhesion testing was also performed.

4.5. PAPBA Lactate Response

PAPBA was tested via OCP as was done for the PANI pH response. But instead of using solutions with different pH levels, the solutions for lactate testing all had the same pH but differing concentrations of lactate. Solutions of phosphate buffered saline (PBS) at pH 7.4 were prepared with different concentrations of lactate (0, 0.1, 0.5, 1, 5, 10, 50, 100 mM). The pH was adjusted to 7.4 by adding NaOH and verified by an Apera pH meter. The lactate (70% L-(+)-lactic acid) and PBS tablets were purchased from Sigma-Aldrich. The response times were also calculated for 75%, 90%, and 100% of the steady state potential. These were calculated whenever the lactate concentration was switched from 0 mM to 100 mM and averaged if recorded more than once.

Chapter 5. Results and Discussion

5.1.1. Textile SPE Design

The Pine Research SPEs were used to determine the expected CV curve behaviour for $K_3Fe(CN)_6$ and for confirming the proper operation of the textile SPEs. The CV curves obtained from the Pine Research SPE in 0.5 M KCl solutions with varying concentrations of $K_3Fe(CN)_6$ (0, 1, 2, 5 mM) are shown in Figure 32. We can observe a redox peak centered at 178 mV with a peak-to-peak separation of 149 mV.

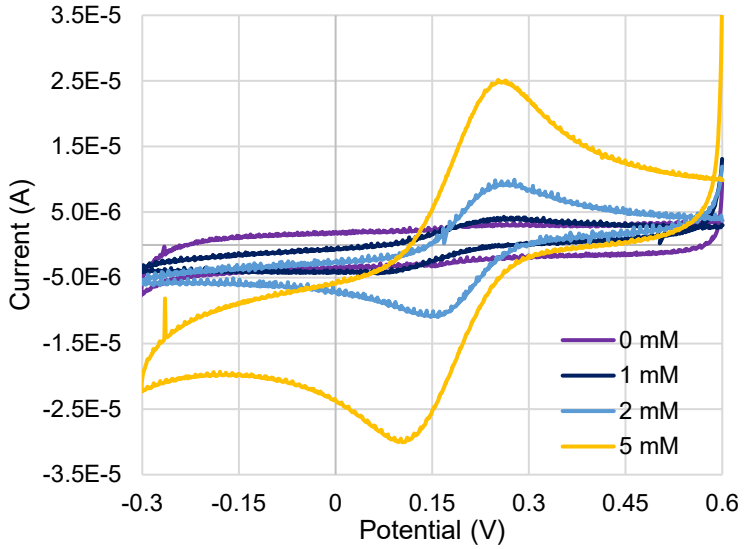

Figure 32. CV curves of Pine Research SPEs at various concentrations of $K_3Fe(CN)_6$

Next, the CV curves for the two designs of the textile SPEs discussed in Section 3.2.1 were recorded in $K_3Fe(CN)_6$ and are shown in Figure 33. Comparing the CV curves from the textile SPEs with Design 1 (silver extension) and Design 2 (WE extension) shown in Figure 32, an obvious distinction can be made, making it apparent which design was more favorable.

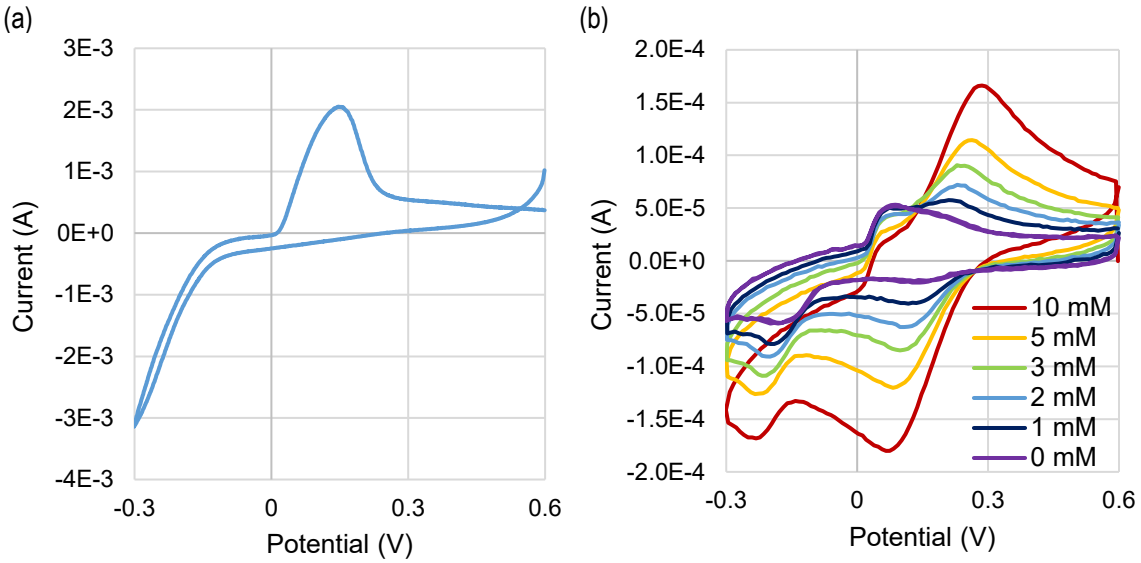

Figure 33. CV curves with $K_3Fe(CN)_6$ as a redox mediator for (a) Design 1, 2 mM $K_3Fe(CN)_6$ scan shown; and (b) Design 2 at various concentrations of $K_3Fe(CN)_6$

The CV curve obtained for the textile SPE with Design 1 does not show the expected characteristic redox peak. Instead, only a single peak is shown in the oxidative scan direction suspected to correspond to the oxidation of silver. Theoretically, this design would work if the carbon paste screen-printed overtop formed a pristine layer. However, due to a combination of the textured textile substrate and the carbon paste properties, a pristine layer is not formed. As can be seen in the microscope image in Figure 34, the carbon paste is slightly porous leaving the conductive silver trace exposed and able to contact the solution and interfere with the measurement.

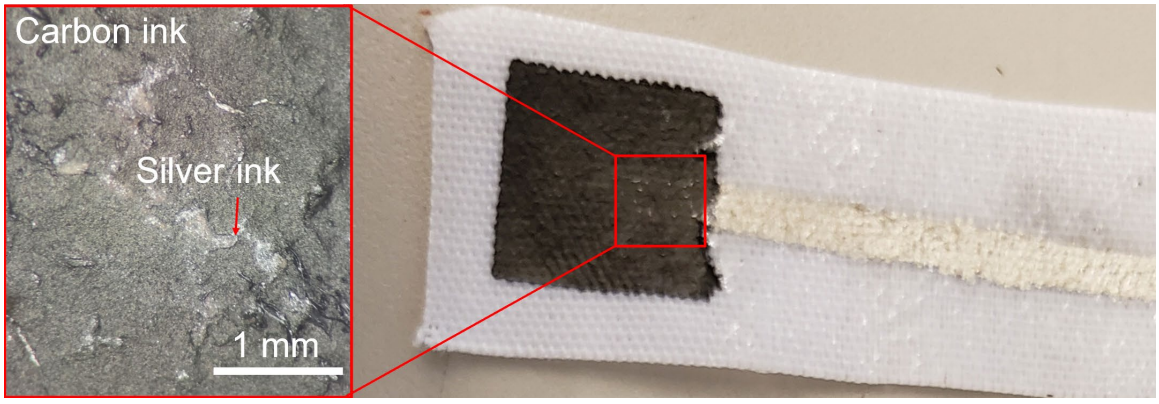

Figure 34. Textile SPE design with silver conductive trace extending past plastisol cover and under the carbon trace; and close up of exposed silver ink under carbon in

For the textile SPE with Design 2, a very similar behaviour to that of the Pine Research SPE with a notable redox peak centered at almost the same potential (180 mV) and a peak separation of 211 mV. The increase in peak separation indicates slightly slower electron transfer kinetics, but the proper peak positioning indicated that the textile SPE was responding properly and suitable for performing electrochemical measurements. smaller redox peak centered at -47 mV was observable with the textile SPE at all concentrations of $K_3Fe(CN)_6$ where no redox active species should be present. This peak was attributed to some component of the carbon/graphite screen-printable paste but had no other effect on measurement given its inferior magnitude.

All textile SPEs used for the remaining analyses were fabricated using the extended WE design where the conductive silver trace is solely under the plastisol cover. The textile SPE design where the electrodes were fully covered by the plastisol cover and the solution only contacted the electrodes through the textile backside showed comparable results to that of the uncovered textile SPE design.

5.1.2. CA Analysis

From the data in Figure 35, it was possible to obtain sensitivity curves to determine the potential with the highest sensitivity towards a change in concentration of $K_3Fe(CN)_6$. Sensitivity curves were created at 100 mV intervals in both oxidative and reductive scan directions. The potential which displayed the highest sensitivity would then be selected for chronoamperometry (CA). This corresponded to 0 V in the reductive direction (negative slope), and 400 mV in the oxidative direction (positive slope).

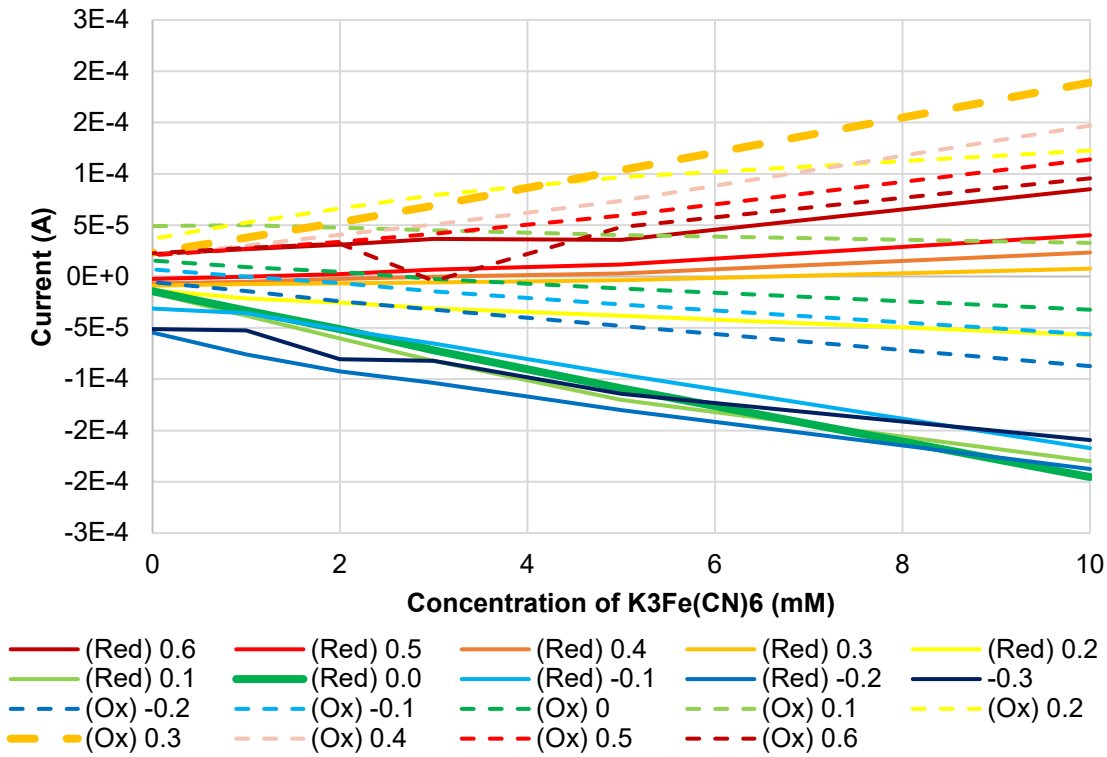

Figure 35. Sensitivity curves obtained from CV curves of textile SPE at 0.1 V intervals

A range of different potentials were then tested to confirm the measurements of the CV sensitivity curves. The optimal potential was found to be -100 mV which was relatively close to the 0 V found using the CV curves. The CA study with the greatest sensitivity is shown in Figure 36 along with the sensitivity curves obtained for a few potentials tested.

These successful results served to validate the real time sensing capabilities of the textile SPE design. With modifications to the WE material, this design could then be used to detect numerous other analytes in solution using this method. With this in mind, the pH and lactate sensors could now be reliably tested with the textile SPE design.

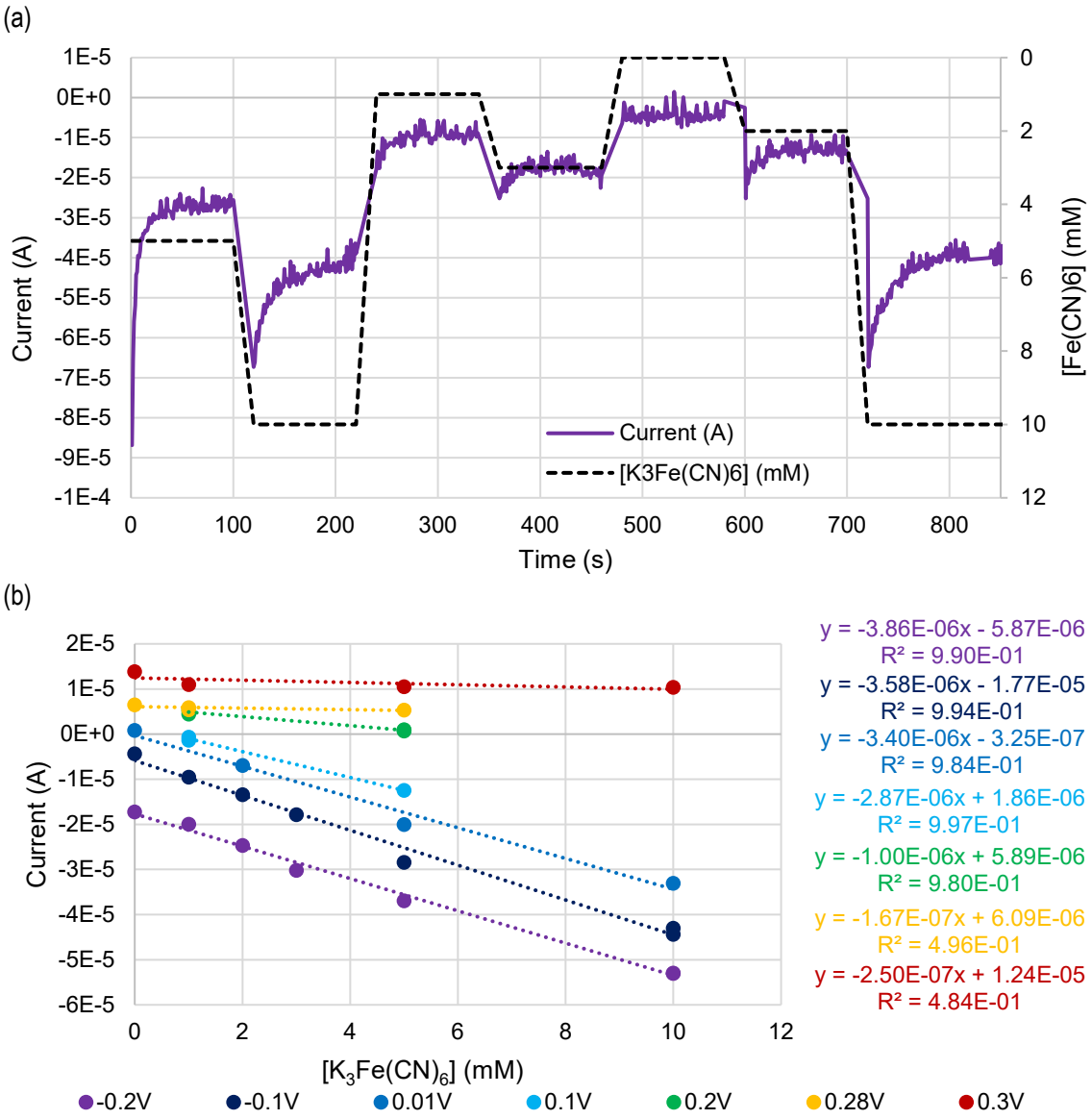

Figure 36. (a) CA study using textile SPEs at -0.1 V; (b) Sensitivity curves of various CA studies tested with textile SPEs

5.2. Chemically Polymerized PANI

The chemical polymerization of PANI was confirmed by comparing the CV curves of the deposited film to that of literature values. Figure 37 shows the characteristic curve shape of PANI with oxidation peaks at around 330 mV and 920 mV corresponding the transitions from leucoemeraldine to emeraldine and on to pernigraniline.

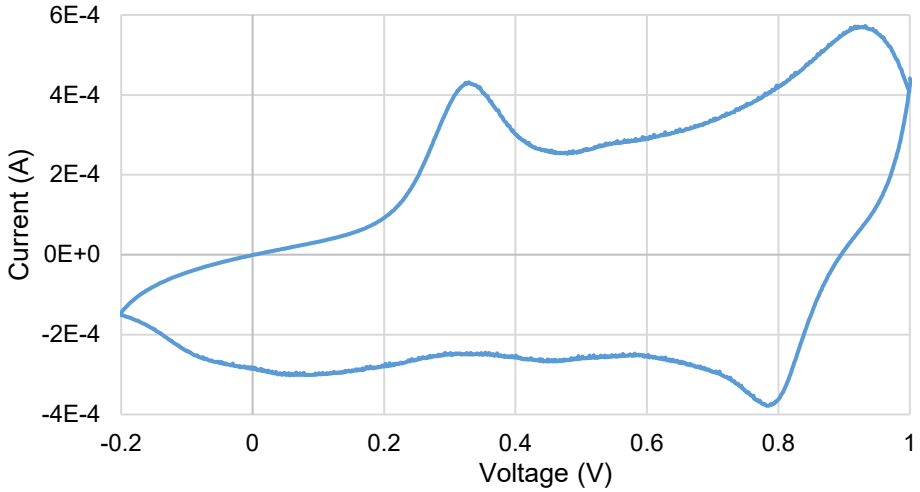

Figure 37. CV curve of chemically polymerized PANI

As was discussed earlier, the synthesis and characterization of PANI via chemical oxidative polymerization was not pursued given that it was much more time consuming, labour intensive, less reliable for selective patterning of WEs, and produced a small quantity of PANI which would require further process optimization to be useful. Instead, PANI powders were purchased and PANI films were electropolymerized and drop-cast to validate PANI's pH response.

5.3. Electropolymerized PANI

5.3.1. PANI Electropolymerization

The progression of the electropolymerization reaction could be monitored is situ by observing the increase in current with each potential cycle. Figure 38 shows an example of the progression of the electropolymerization reactions. As the number of cycles increases, an increase in current is observed indicating additional deposition of PANI onto the WE.

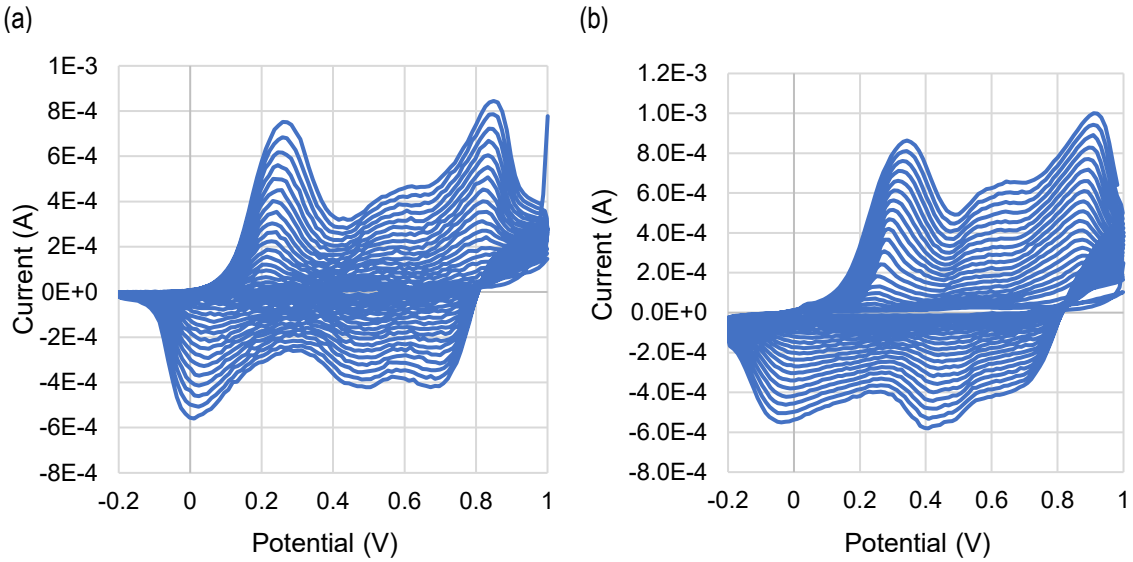

Figure 38. Electropolymerization progression of (a) PANI-HCl on a Pine Research SPE; and (b) PANI-DBSA (1 molar equivalence) on a textile SPE

The polymer synthesis could then be further confirmed by comparing the CV curve after electropolymerization in 1M HCl to that of literature similarly to that of the chemically polymerized PANI. In Figure 39, we can see that all CV curves show the two characteristic redox peaks associated with PANI. For the textile SPE, some of these peaks are slightly shifted or of different prominence, but they still demonstrate successful polymerization.

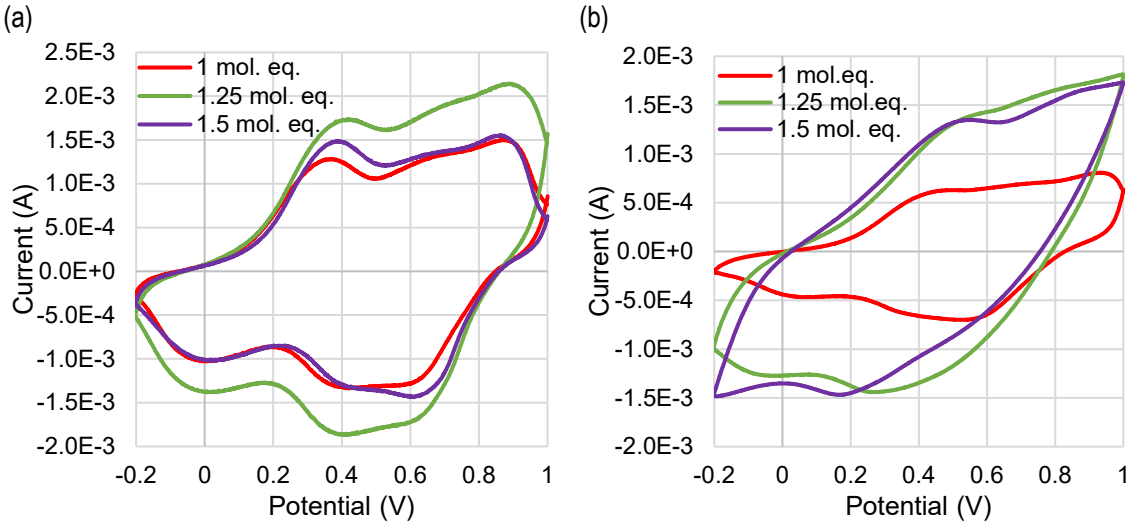

Figure 39. Electropolymerized PANI on (a) Pine and (b) Textile SPEs

5.3.2. Electropolymerized PANI pH Response via CV

As was mentioned in Chapter 4, the PANI films were first characterized through a set of CV analyses for the purpose of testing with CA as was done for the blank carbon SPEs and $K_3Fe(CN)_6$. CV curves were recorded in 0.5 M KCl solutions of various pH levels, beginning at pH 3 and decreasing to pH 10. However, these did not show strong responses and did not recover back to their original levels when the solution pH was increased back up to pH 3, as shown in Figure 40. The CV curves in 1M HCl were compared before and after this parametric CV analysis and for these, the CV curves showed similar shapes, although with some slight broadening and weakening current level. Overall, this analysis demonstrated that CA would not be a feasible sensing method for pH monitoring with PANI.

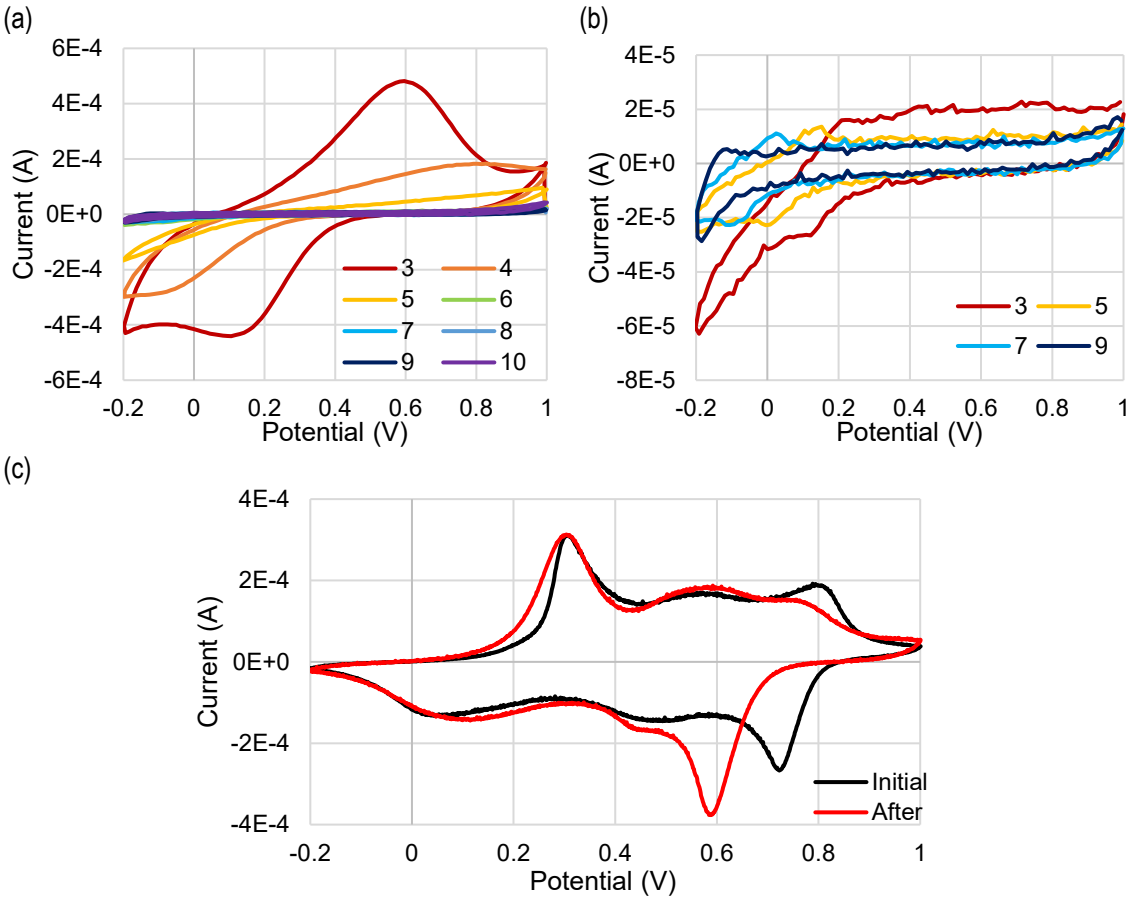

Figure 40. CV curves at different pH levels for eElectropolymerized PANI-DBSA (1 molar equivalence) on textile SPEs through (a) decreasing from pH 3 to 10 in unit increments; (b) increasing from pH 9 to to 3. (c) CV curves before (Initial) and after (After) conducting set of scans in (a) and (b).

It is suspected that a strong oxidizing agent such as 1 M HCl is required to restore PANI back to its original state. For buffer solutions with a lower pH value, the PANI does not recover enough for the response to be measured using CV or CA studies.

5.3.3. Electropolymerized PANI pH Sensor Response via OCP

Given the lack of response with the CV analysis, OCP was instead used for measuring the pH response with the electropolymerized PANI films. The OCP for the electropolymerized PANI under various conditions on Pine Research SPEs is shown in Figure 41 along with the response of a blank Pine Research SPE and the sensitivity curves.

From the sensitivity curves, we can see that the electropolymerized PANI sensors demonstrate a strong pH dependent OCP. The PANI-HCl demonstrated a super-Nernstian sensitivity of -62.9 mV/pH. The PANI electropolymerized in the presence of 1 to 1.5 molar equivalence of DBSA to monomer showed roughly Nernstian/sub-Nernstian behaviour with similar sensitivities ranging between -59.3 to -54.2 mV/pH. It is suspected that the DBSA may slightly limit the ability of the PANI to adsorb as many protons as the pure PANI-HCl by counteracting some of the negative charge thus decreasing the sensitivity. PANI-HCl may also be able to form a denser more pristine film without the presence of the bulky DBSA group. It is worth noting that the blank carbon-based Pine Research SPE also showed a pH response albeit at a much lower sensitivity of -21.6 mV/pH. As discussed earlier, carbon oxides can also act as proton acceptors or donors, meaning they can act as pH dependent electrodes, although evidently with a lower sensitivity.

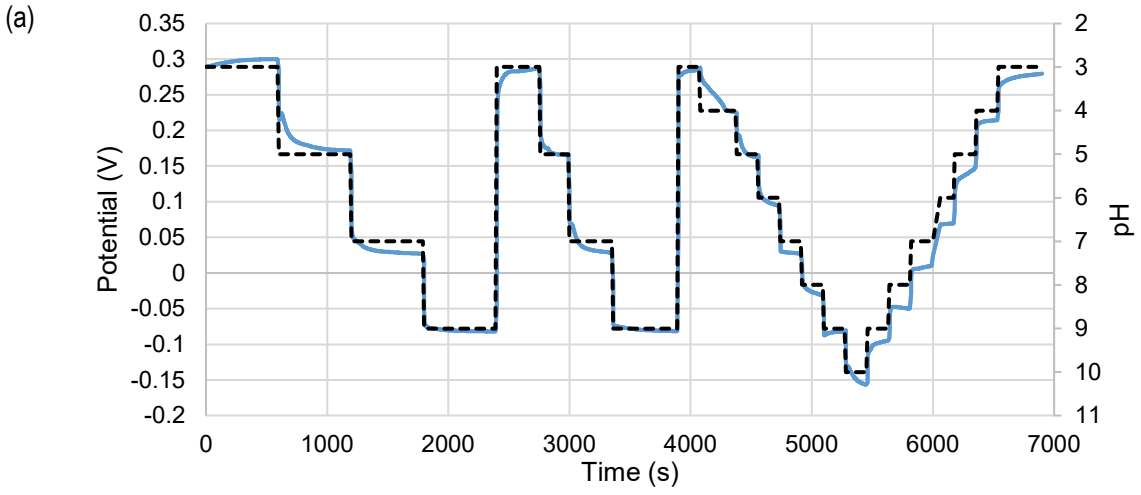

(b)

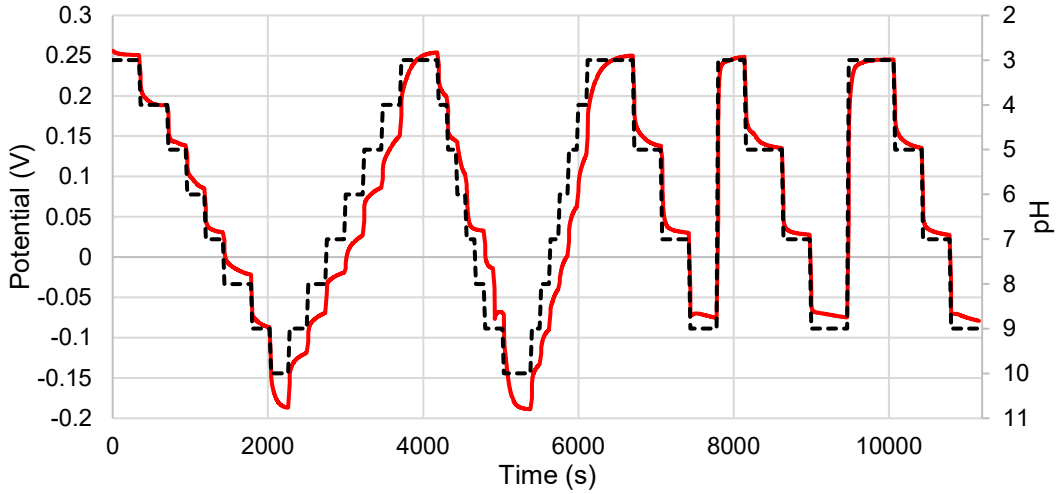
Potential (V)
pH
Time (s)
0.3
0.25
0.2
0.15
0.1
0.05
0
-0.05
-0.1
-0.15
-0.2
2
3
4
5
6
7
8
9
10
11
0
2000
4000
6000
8000
10000

(c)

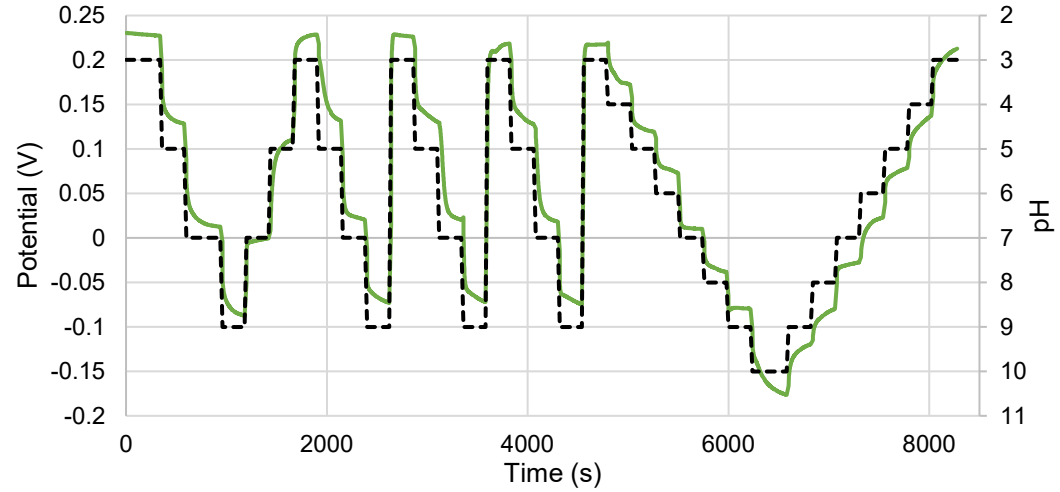
Potential (V)
pH
Time (s)
0.25
0.2
0.15
0.1
0.05
0
-0.05
-0.1
-0.15
-0.2
2
3
4
5
6
7
8
9
10
11
0
2000
4000
6000
8000

(d)

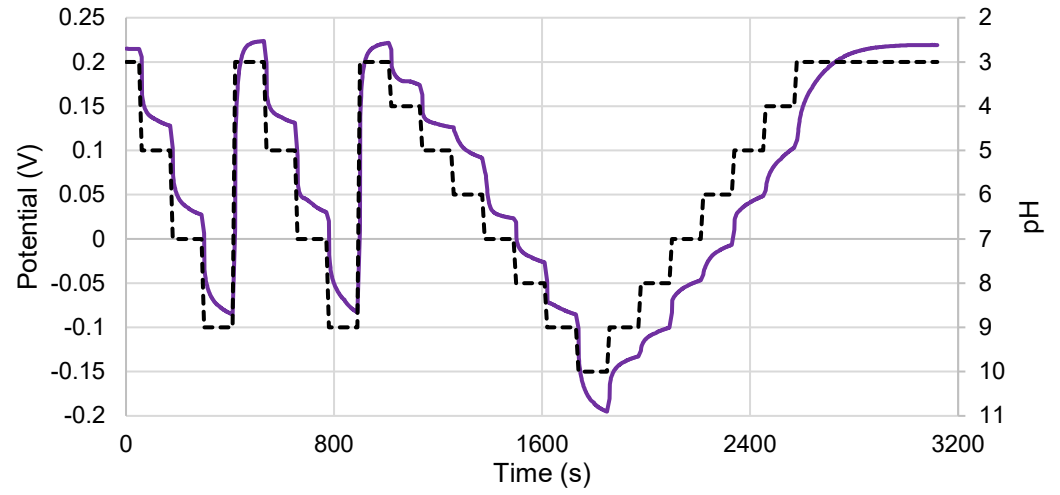
Potential (V)
pH
Time (s)
0.25
0.2
0.15
0.1
0.05
0
-0.05
-0.1
-0.15
-0.2
2
3
4
5
6
7
8
9
10
11
0
800
1600
2400
3200

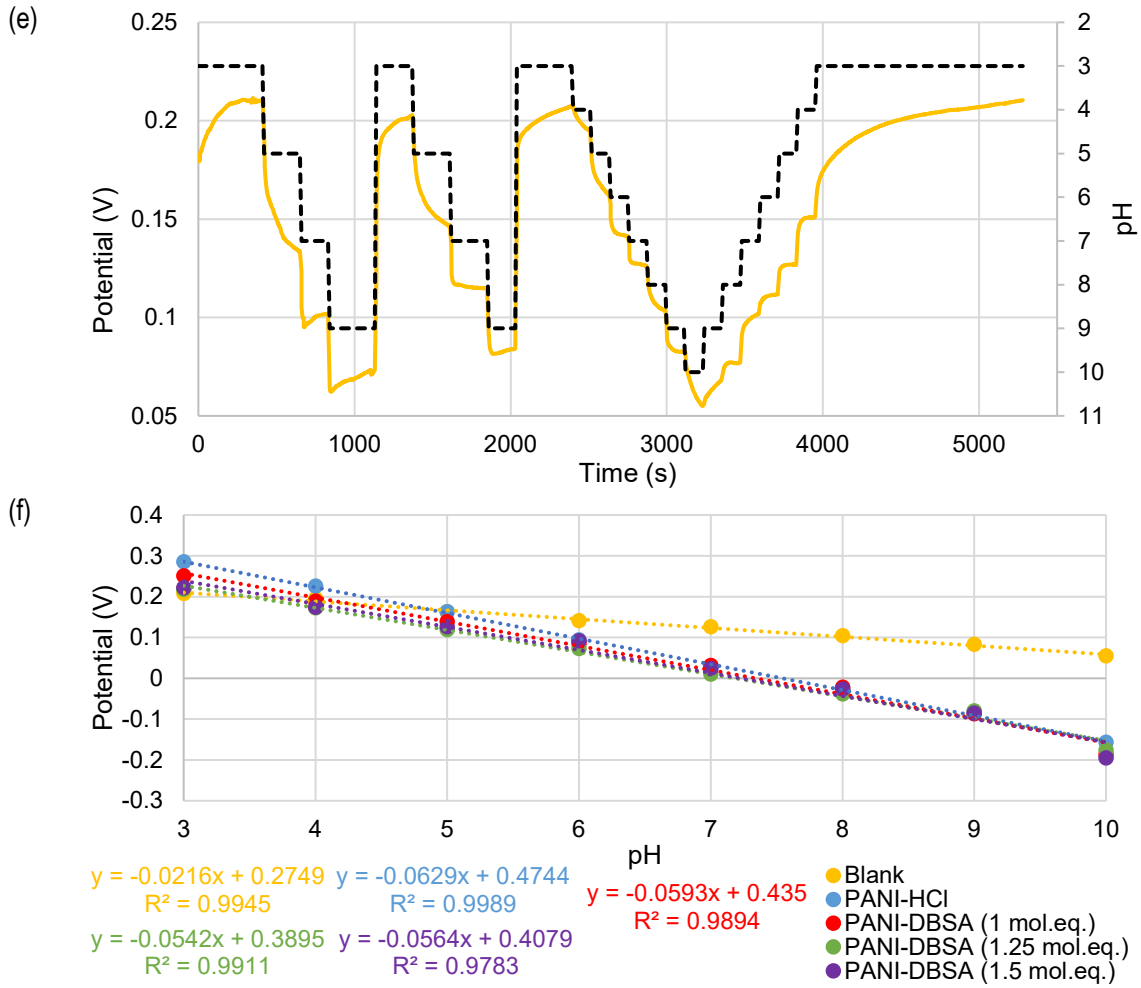

Figure 41. pH response of electropolymerized PANI on Pine Research SPEs with (a) 1M HCl, (b) 1 molar equivalent DBSA, (c) 1.25 molar equivalent DBSA, (d) 1.5 molar equivalent DBSA, (e) blank carbon; and the corresponding sensitivity curves (f)

In terms of response time, Table 7 highlights the response times of the electropolymerized PANI on the Pine SPEs.

Table 7. Summary of response times for electropolymerized PANI on Pine Research SPEs

Sample	Response Time to 75% steady state OCP	Response Time to 90% steady state OCP	Response Time to steady state OCP	Measurements Averaged
PANI-HCl	122.5 s	219.5 s	553 s	2
PANI-DBSA 1 m.e.	4.5 s	23 s	460 s	2
PANI-DBSA 1.25 m.e.	0.3 s	6.7 s	220 s	3
PANI-DBSA 1.5 m.e.	3.5 s	15 s	110 s	2
Carbon Blank	3 s	75 s	290 s	2

The textile SPEs showed similar trends to that of the Pine Research SPEs with the PANI-HCl showing the highest sensitivity and PANI-DBSA showing a slightly inferior sensitivity. Given the similar sensitivities obtained for PANI-DBSA at different DBSA concentrations on the Pine Research SPEs, only the 1 molar equivalent case was tested for OCP on the textile SPEs. The blank textile SPE with a carbon paste WE also showed a very faint pH response but the OCP scan seemed much less reliable. These responses are shown in Figure 42. The blank carbon WE for the textile SPE showed a faint pH response like the Pine Research SPE, albeit with a much lower sensitivity and linearity based on the OCP and resulting sensitivity curve.

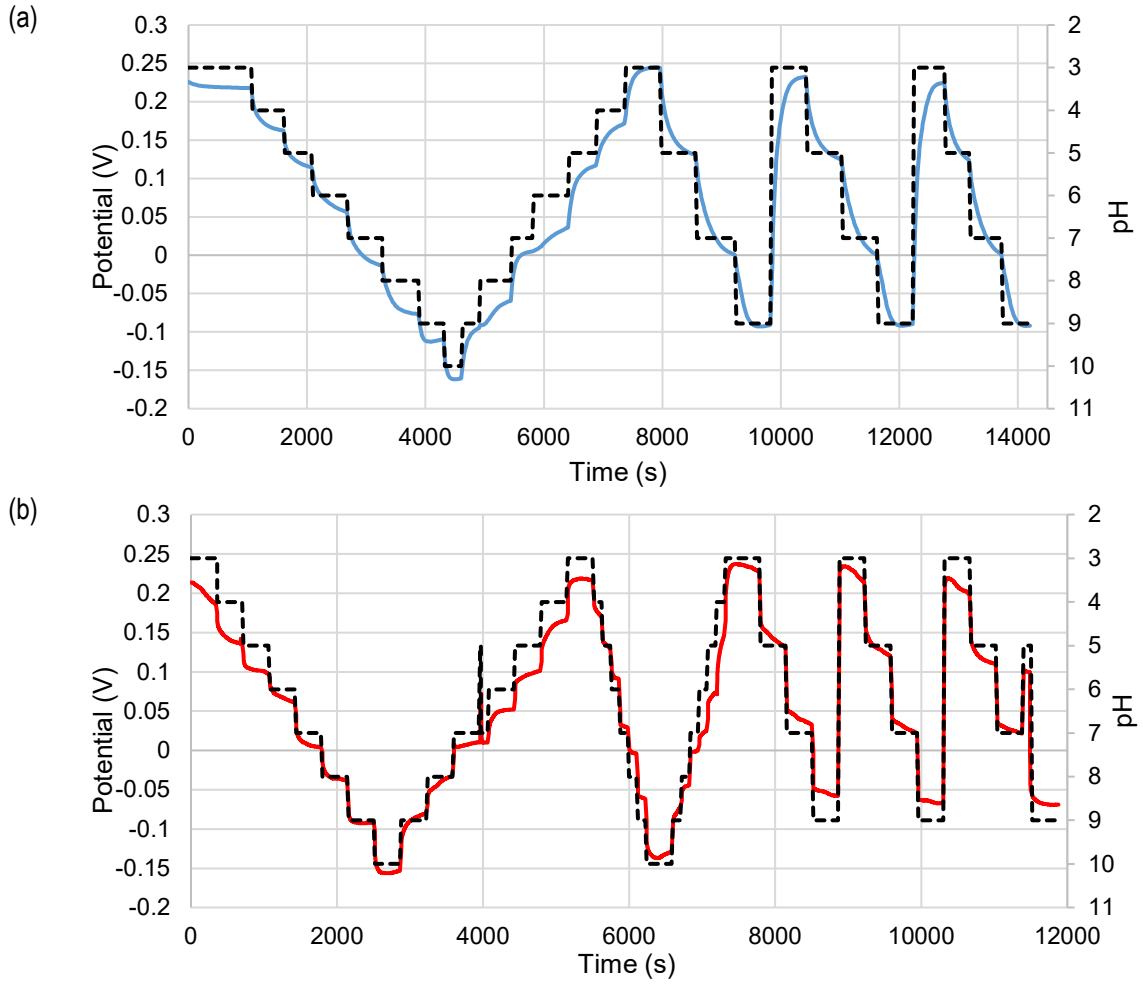

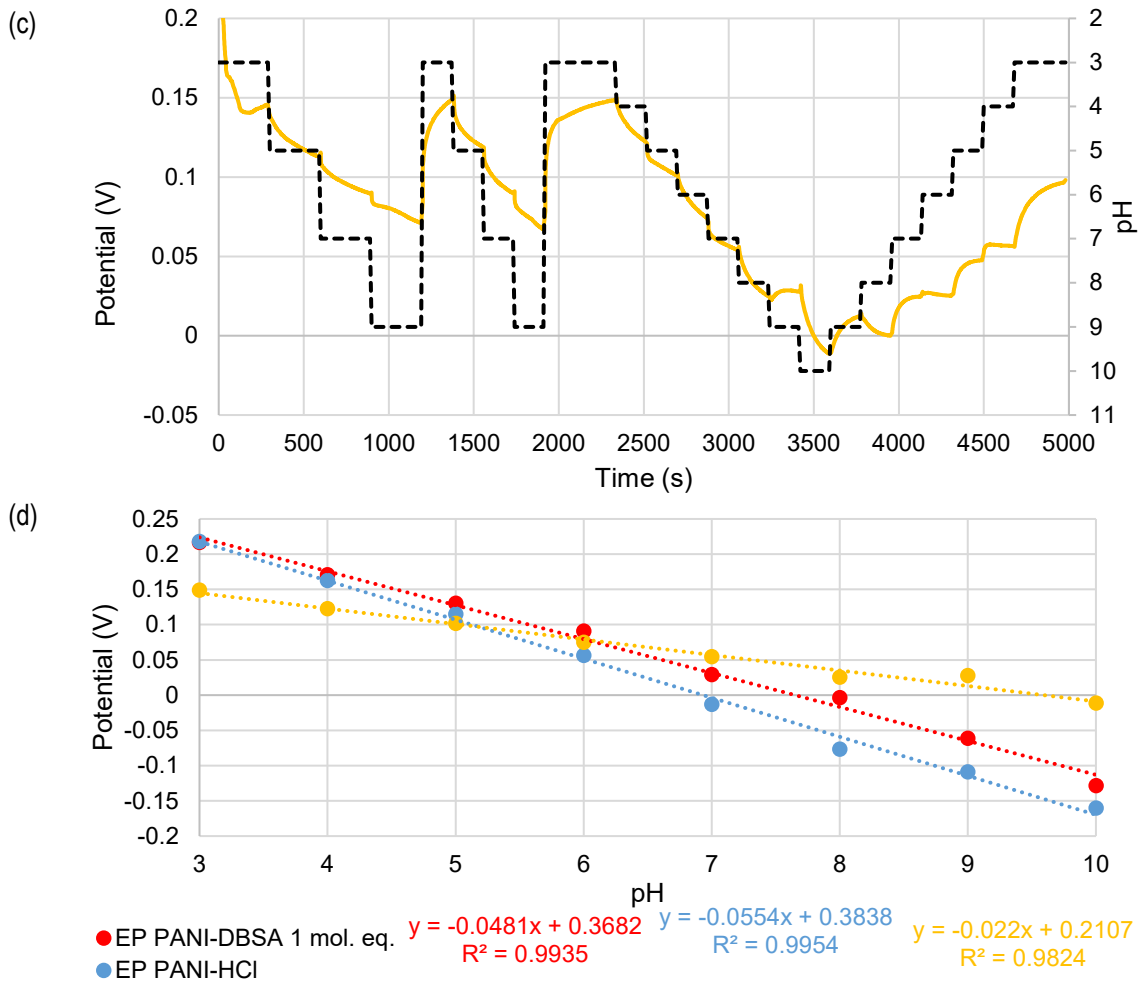

Figure 42. pH response of electropolymerized PANI on textile SPEs with (a) 1 M HCl, (b) 1 molar equivalent DBSA, (c) 1.25 molar equivalent DBSA, (d) 1.5 molar equivalent DBSA, (e) blank carbon; and the corresponding sensitivity curves (f)

The response times for the electropolymerized PANI on the textile SPEs are listed in Table 8. The response times for the textile SPEs were largely equivalent to that of the Pine Research SPEs, showing an almost instantaneous response for the PANI-DBSA and a slightly slower response for the PANI-HCl. Again, this likely has to do with the stronger binding of the protons for the PANI-HCl film.

Table 8. Summary of response times for electropolymerized PANI on Textile SPEs

Sample	Response Time to 75% steady state OCP	Response Time to 90% steady state OCP	Response Time to steady state OCP	Measurements Averaged
PANI-HCl	115 s	215.5 s	553 s	2
PANI-DBSA 1 m.e.	0 s	0.5 s	340 s	2
Carbon Blank	34 s	130 s	290 s	2

5.4. PANI Solution Processing and Drop-Casting

5.4.1. PANI Drop-Casting

The drop-casting of the PANI solutions was done with an increasing number of droplets as it was unknown how much volume would be required to create a proper film. However, the PANI drop-cast from DMSO would clog the nozzle of the dispensing needle and so the number of droplets were not counted. The drop-cast PANI solutions on the textile WEs were then characterized via CV to see whether an adequate film had been produced. Representative CV curves are shown in Figure 43. Generally, increasing the number of droplets increased the measured current, providing more defined redox peaks.

The various PANI forms drop-cast from DMSO produced variable quality of films as a result of the clogged dispensing nozzle which would rapidly eject droplets. A few samples still managed to produce adequate films based on their resulting CV curves shown in Figure 43 (a). The PANI drop-cast from the xylene or heptane solutions generated CV curves with relatively well-defined peaks. However, the PANI drop-cast from heptane would evaporate momentarily after addition without any heating, which allowed for samples to be prepared quickly. Given that no other significant difference existed, heptane was the solvent of choice for the PANI-EB doped with DBSA to be tested as a pH sensor using OCP and CA.

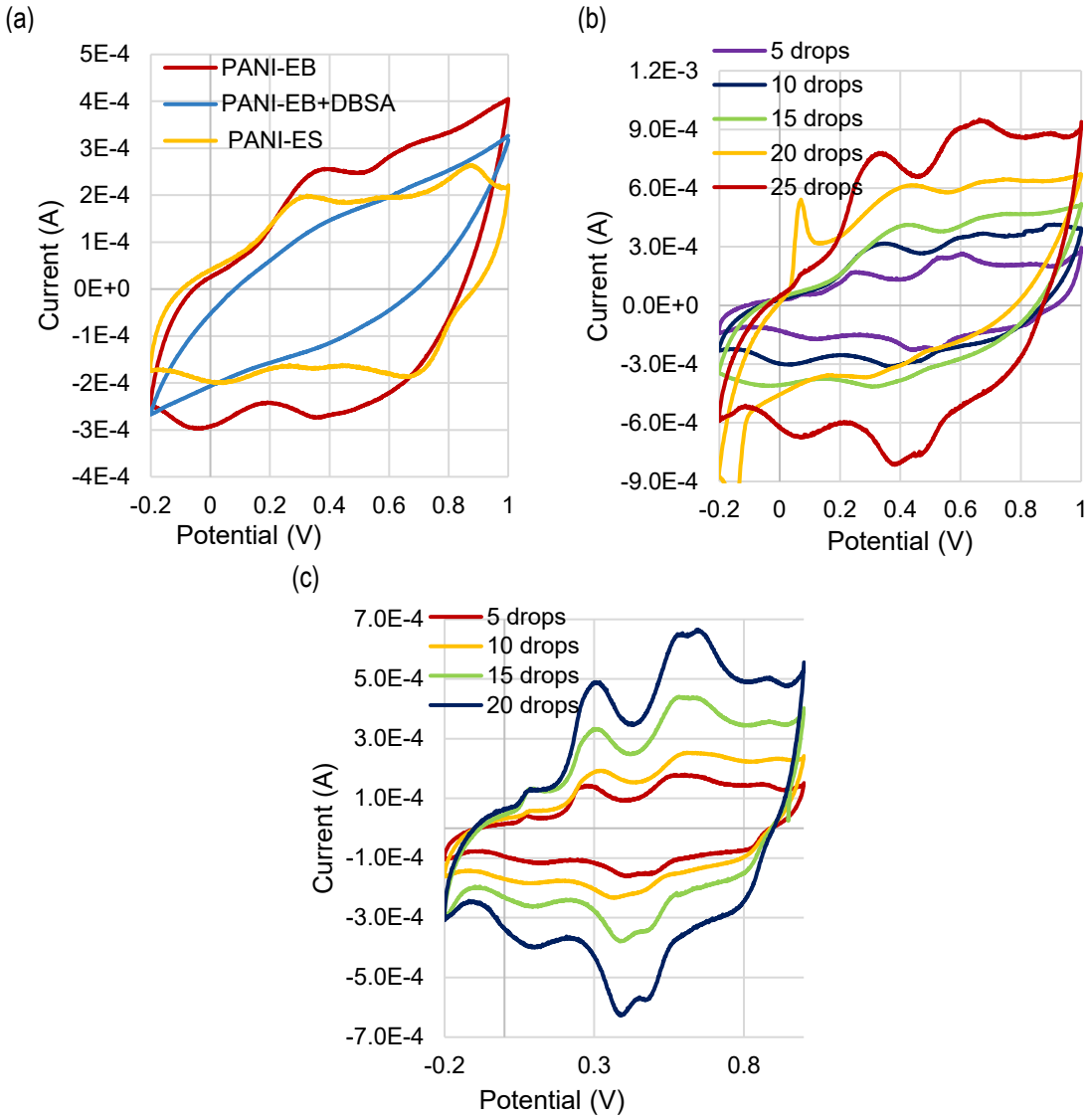

Figure 43. CV curves drop-cast from solution of (a) DMSO, (b) xylene, and (c) heptane

5.4.2. Drop-Cast PANI pH Response via CA

As was done with the textile SPEs with $K_3Fe(CN)_6$ and the electropolymerized PANI, a CV analysis was executed for the drop-cast PANI in anticipation of performing a CA study. CV scans were recorded from pH 3 to 10 and then back in the reverse order. A clear pH response was observed throughout this range, unlike the electropolymerized PANI. However, as with the electropolymerized PANI, when CV scans were performed successively scanning in the reverse direction from pH 10 to pH 3, the sensor did not

seem to recover back to its initial current levels. Figure 44 below shows the CVs obtained at different pH levels scanning from pH 3 to 10 and then back from pH 10 to 3.

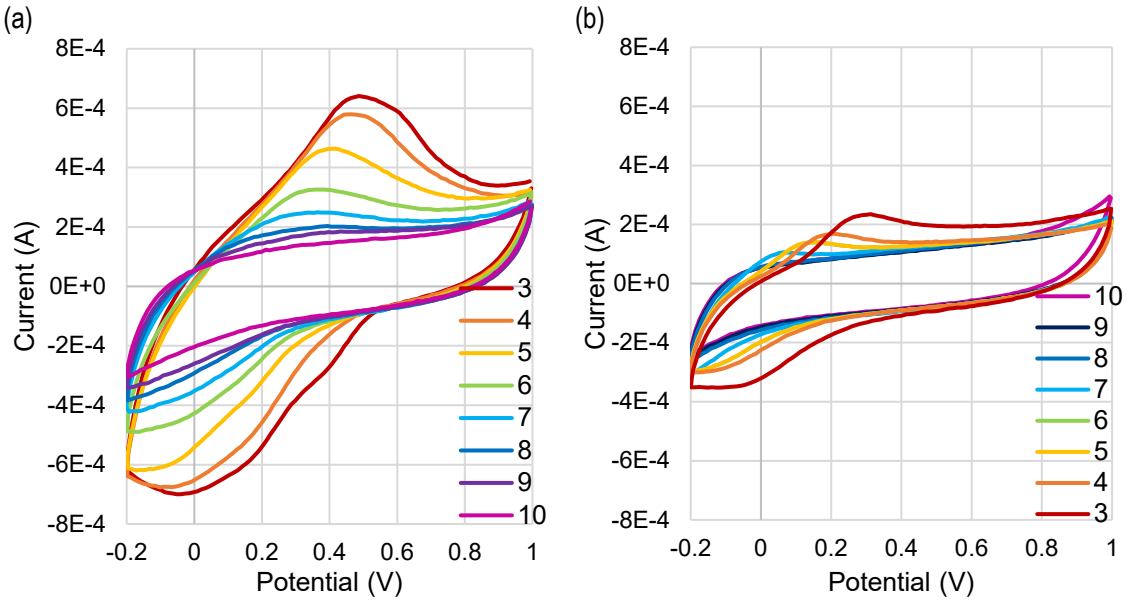

Figure 44. CV of drop-cast textile SPE at various pH levels scanning from (a) pH 3 to 10, and then (b) back from pH 10 to 3

As a result, it was expected that the drop-cast PANI textile sensors would not respond appropriately during CA given their lack of recovery during CV. Additional spectroscopic characterization would be required for confirming the exact mechanism for why this is occurring. Therefore, given that OCP more produced favourable results, CA was not pursued.

5.4.3. Drop-Cast PANI pH Response via OCP

The OCP recording for the drop-cast PANI from heptane onto a textile WE is shown in Figure 45 (a). A potential drift was observed over the course of the OCP recording and was recorded in a subsequent scan while not changing the solutions or test conditions. The drift is shown in Figure 45 (b). In this way, the drift could be accounted for and corrected on the original OCP recording such that the potential at a designated potential level could be repeated.

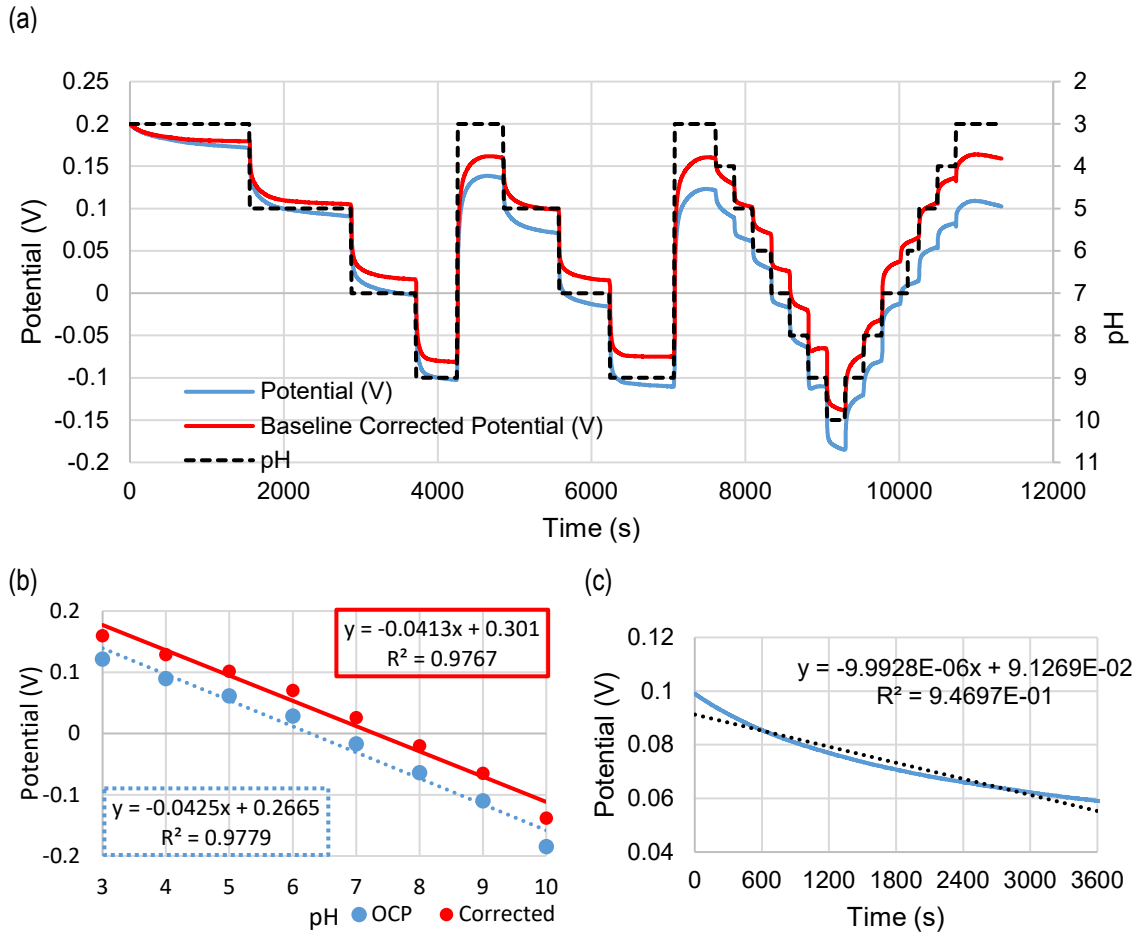

Figure 45. (a) OCP response from drop-cast PANI from heptane on Textile SPE; (b) Corresponding sensitivity plot; (c) RE drift

The response times to 75%, 90%, and 100% steady state OCP for the drop-cast PANI from the PANI-EB + DBSA on textile SPEs were 21 s, 73.5 s, and 560 s, respectively. These were taken over 2 measurements.

This scan serves to emphasize the importance of the RE in obtaining reliable measurements over extended periods of time. Although the drift can be accounted for in this way via post-processing, improvements in the RE stability are required. Again, the development of this RE exceeded the scope of this thesis and will be addressed in the Chapter 6 in discussing the future work.

5.5. PANI Composites

With the pH response of PANI now confirmed via OCP, the focus was moved on to the development of the screen-printable PANI composite. As was outlined in Chapter

4, the optimization of the PANI composite was done based on three key properties completed over four main sequences of experiments. The key properties in order of importance were sensor response, print quality, and conductivity. These were primarily addressed in Chapter 4. The results of the four experiment sequences will be discussed in the following subsections.

5.5.1. First Sequence: PANI-EB + Plastisol Composites

To begin with, only the PANI-EB and the plastisol LFP-1070 had been purchased and the methods for reliably measuring the PANI pH response were still being developed simultaneously to the composite optimization. Despite the different principles of operation behind the measurement methods, a couple of key properties for the ideal pH responsive PANI composite would be shared among them, namely: print quality and conductivity.

The results of this first sequence of tests are summarized in Table 9. A total of 10 test lines were used for all measurements, although some were excluded from measurements as they were not properly screen-printed, and their resistance were too high to be measured with the DMM (>300 MΩ). The number of successful prints also serves as a metric to helps illustrate the print quality for this first sequence.

Table 9. Summary of results from first sequence of formulations for PANI-EB + plastisol composite optimization

PANI wt%	# Conductive Samples out of 10	Average Resistivity (Ω.m)	Standard Deviation (Ω.m)	Average Thickness (µm)	Average # Peels to discontinuity
24	7	1.20E-03	9.15E-04	52.7	Not measured
26	9	4.70E-04	4.96E-04	58.5	10.7
28	9	4.23E-04	5.24E-04	73.1	2.9
30	9	1.28E-04	1.51E-04	72	2.5
32	10	3.50E-05	2.28E-05	95.3	2.1
34	9	3.96E-05	4.76E-05	100	1.3
36	7	1.31E-04	1.16E-04	87.2	Not measured
38	6	1.86E-05	8.21E-06	124.1	Not measured
40	7	9.28E-05	6.56E-05	62.4	Not measured

For quantifying the print quality, the adhesion test recording the number of tape peelings before discontinuity in the electrical pathway was performed. Above 26 wt% PANI, the number of tape peelings required decreased significantly and a large amount of residue was seen at each peel. A noticeable difference in texture could be seen between

the 28 wt% PANI-EB + plastisol composite and the 26 wt% PANI-EB + plastisol composite after mixing and letting the solvent evaporate, with the latter having a paste like consistency and the former being more granular. This is shown in Figure 46 along with the residue stripped from the prints during adhesion testing, and the overall results of the adhesion test for this first sequence of tests.

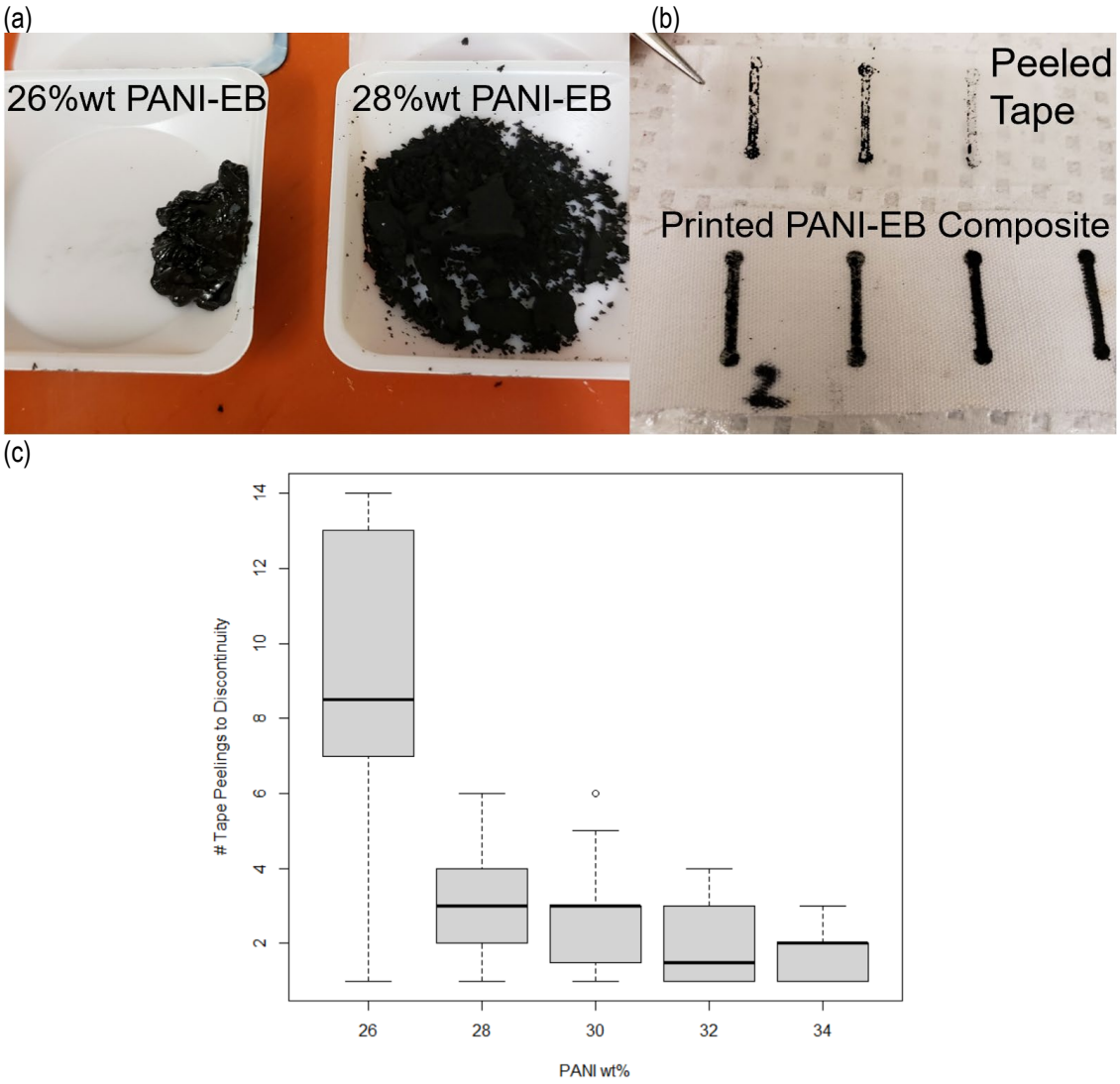

Figure 46. Adhesion testing results for PANI-EB + plastisol composite

The resulting resistivities are shown in Figure 47. Below 24 wt% the resistances were too large to measure with the DMM (>300 MΩ). Above about 32 wt%, a greater variability was noticed, and the resistance was less predictable mainly due to cracking and peeling of the grainier PANI-plastisol composites. These either failed to adhere to the substrate or would peel off in regular manipulation of the textile substrate.

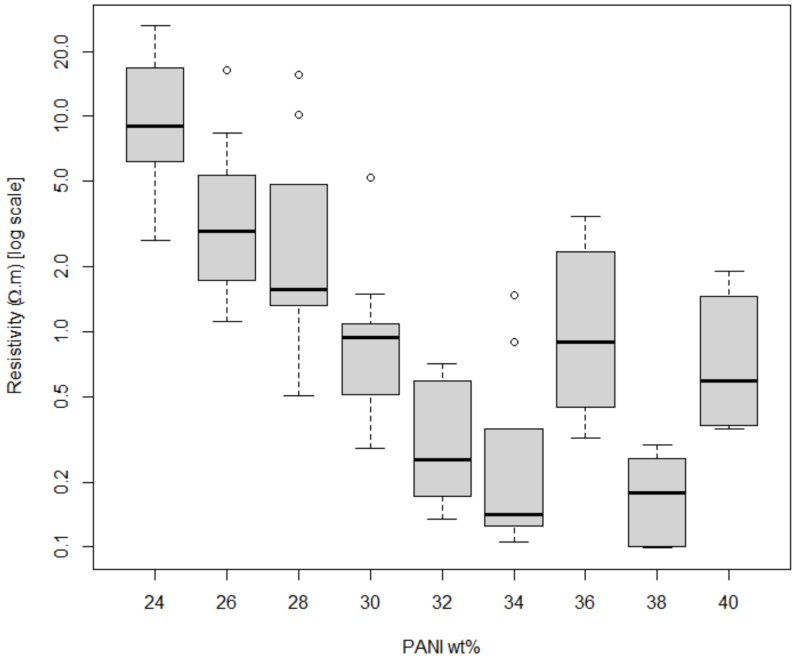

Figure 47. PANI-EB + plastisol composite optimization

Overall, this first sequence of formulations had unacceptably poor print quality, suffering from poor adhesion to the substrate, high resistances, and a relatively brittle composition.

5.5.2. Second Sequence: PANI-ES + DBSA + Plastisol Composites

The next sequence of PANI composites tested added DBSA which acted as both a plasticizer and a dopant. PANI-EB was at times also substituted with PANI-ES particles. These dramatically decreased the resistivity of the composites even at much lower concentrations of PANI. PANI-ES also had some noticeable differences in terms of particle size which made mixing with plastisol relatively easier despite the solvent mixing properties. From Figure 48, PANI-ES particles all appear smaller than 20 µm, likely on the 100s of nm to um size, whereas some of the PANI-EB particles could be as large as 150 µm.

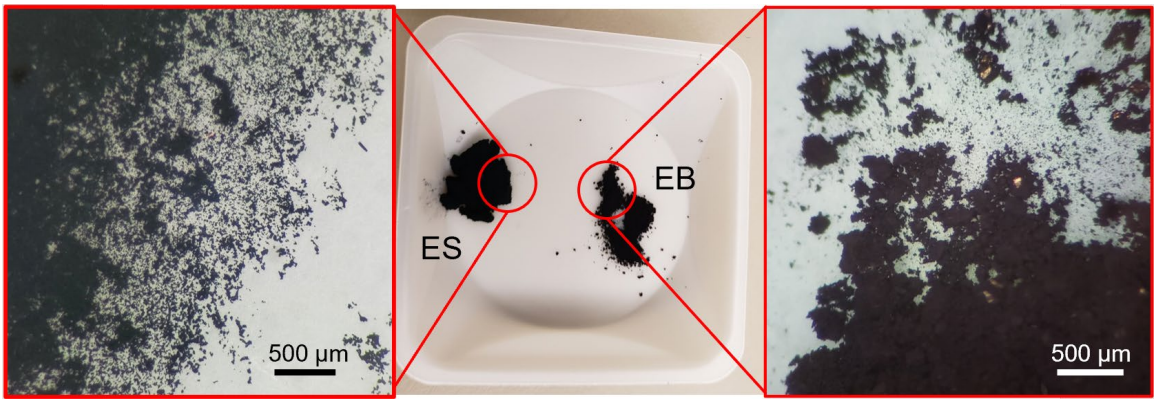

Figure 48. Comparison of PANI-ES and PANI-EB both purchased from Sigma-Aldrich

It was approximately at this stage of the composite formulation optimization that the textile SPE design had been validated and the pH response of the electropolymerized PANI and drop-cast PANI on the textile SPEs had been measured via OCP. Consequently, the order of priority for the PANI composite optimization shifted such that beyond basic printability and conductivity, the PANI composite must be pH responsive. For without a pH response, there was no point in further optimizing the composite formulation to improve conductivity and printability. The summarized formulations list tested for the PANI-ES/EB + DBSA + plastisol composites is given in Table 10.

Table 10. Summary of formulations prepared from second sequence of experiments for PANI-ES/EB + DBSA + plastisol composites

#	PANI wt%	DBSA wt%	Plastisol wt%	PANI type
1	40	10	50	EB
2	40	50	10	EB
3	30	52.4	17.6	ES
4	40	10	50	ES
5	40	50	10	ES

The OCP measurements for the PANI-ES + DBSA + plastisol composites were highly inconsistent. Many samples showed no response whereas select few showed a pH dependence. However, this response was typically relatively slow as can be seen in the example provided in Figure 49. The response times for the 75%. 90% and 100% steady state open-circuit potential were 554 seconds, 838 seconds, and 2724 seconds. Even at concentrations of PANI as high as 40-50 wt% PANI, which were qualitatively determined to be the approximate limit of printability for PANI-ES + DBSA + plastisol composites, the responses were no more favourable.

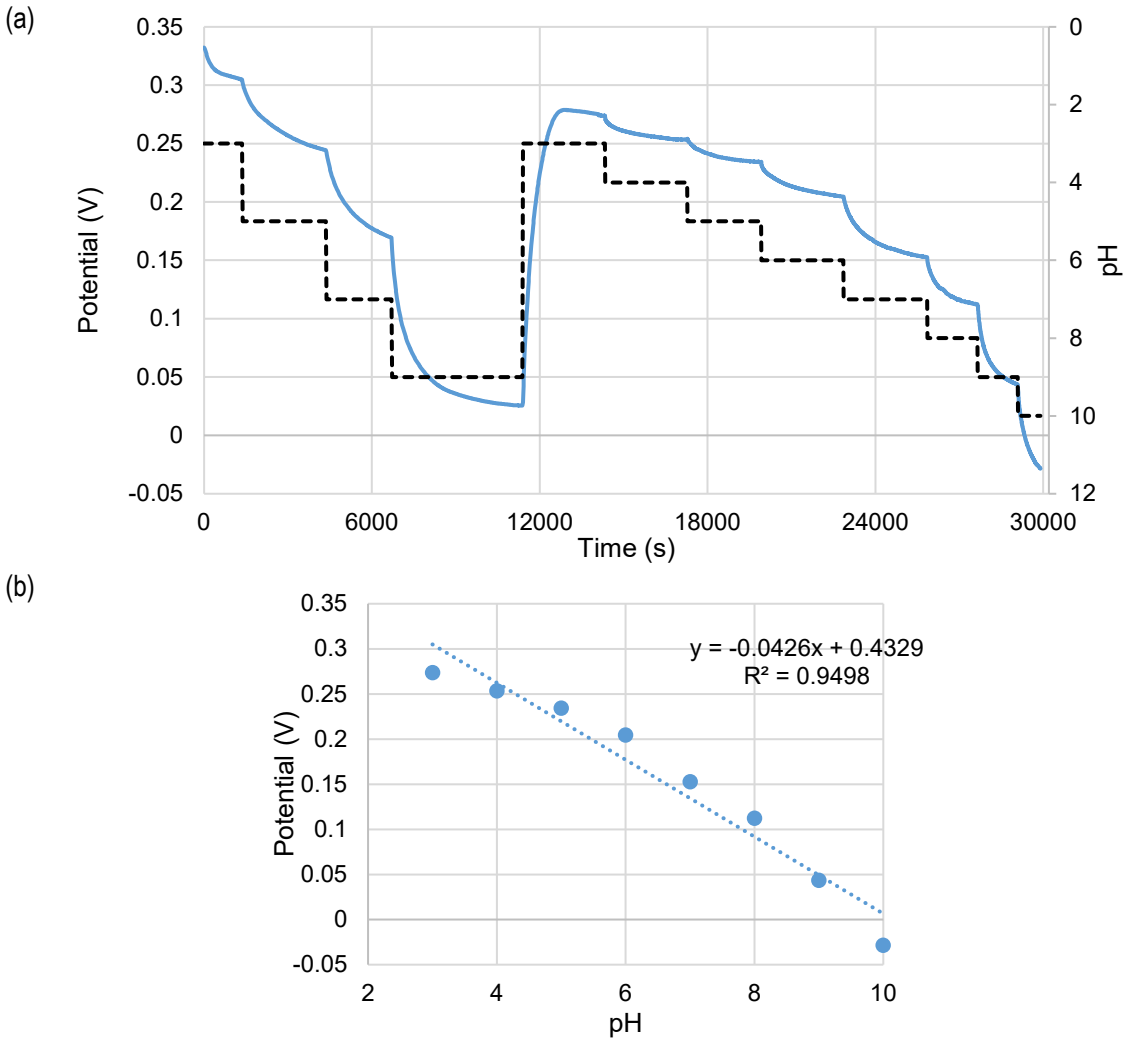

Figure 49. OCP pH Response of PANI-ES + DBSA + Plastisol Composite (30/52.4/17.6)

From Figure 49, the overall sensitivity of the screen-printed PANI-ES + DBSA + plastisol composite was quite high at 42.6 mV/pH. However, the response showed some non-linearity as the potential differences between pH steps increased with decreasing pH as seen in Table 11.

Table 11. Potential differences between pH steps of PANI-ES + DBSA + Plastisol composite

pH	Potential Difference (mV)
3 to 4	21.9
4 to 5	19.1
5 to 6	29.7
6 to 7	51.8
7 to 8	40.3
8 to 9	68.9
9 to 10	72.0

The PANI-EB + DBSA + plastisol composites also showed inconsistent results. The PANI loading percentage could be increased to about 30 wt% successfully through the addition of DBSA. At 40 wt% and above the composite again became granular and less favourable.

In terms of print quality, the PANI-ES composites could be loaded to concentrations as high as 50 wt% with no peeling after 10 series of peels from adhesion testing. The PANI-EB composites could only be loaded as high as about 30 wt% while still producing negligible amounts of peeling. The resistivity of the PANI-ES was measured to be between $3x10^{-4}$ and 10^{-3} Ω·m depending on the formulation, which was also significantly lower than that of the PANI-EB which ranged from $4x10^{-2}$ to $1.2x10^{-1}$ Ω·m. This was expected as the ES is the conductive form of PANI.

Overall, the general inconsistency in measurements, non-linear response, and slow response time meant these composites were not ideal. It was theorized that the slow response times were attributable to the hydrophobic nature of the plastisol. As such, the interface between the plastisol-based composite prevents proper diffusion of species in solution to reach the surface. Given the slow pH response, no further adhesion testing or resistance measurements were performed for this sequence of experiments.

Of note, it was discovered that PANI + DBSA could be screen-printed without the addition of any screen-printing ink with the proper formulation and the addition of solvent. However, given the absence of screen-printing ink, these did not cure very well and were slightly tacky. They also showed large inconsistencies in response.

5.5.3. Third Sequence: PANI-EB + DBSA + Speedball Composites

Given the inconsistent response of the plastisol composites, the choice was made to explore alternative screen-printing inks to plastisol as a polymer matrix for the PANI. A return to the PANI-EB was also made based on the non-linear response observed for the preliminary tests done with the PANI-ES. The water-based Speedball screen-printing was then selected and various formulations of PANI-EB + DBSA + Speedball were prepared. These formulations are listed in Table 12 along with a summary of results.

Table 12. Summary of results from third sequence of formulations for PANI-EB + DBSA + Speedball composites

PANI wt%	DBSA wt%	Speedball ink wt%	Average Resistivity (Ω·m)	Standard Deviation (Ω·m)	Average Thickness (µm)
5	5	90	Not measurable	-	48.3
10	10	80	9.713	6.712	54.5
15	15	70	5.029	6.661	67.4
17.5	17.5	65	4.019	1.934	56.6
20	20	60	0.103	0.037	59.8
25	25	50	0.160	0.103	62.5
30	30	40	0.124	0.084	57.1
35	35	30	0.138	0.111	51.8
40	40	20	0.330	0.226	79.8
50	50	0	0.209	0.159	44.6

Like the plastisol composites, as the amount of PANI increases, the composite ink becomes more granular, and the print quality degrades. The dropwise addition of water permits the composite to have a viscosity suitable for screen-printing, but an over dilution results in a loss of resolution of printed features, conductivity, and sensor functionality. A threshold concentration of PANI was required to obtain a composite with sufficient conductivity and sensor response. The percolation threshold was again found by increasing the amount of PANI and DBSA in the printed samples while decreasing the amount of Speedball® screen-printing ink. The average resistivity of 14 test lines is shown in Figure 50.

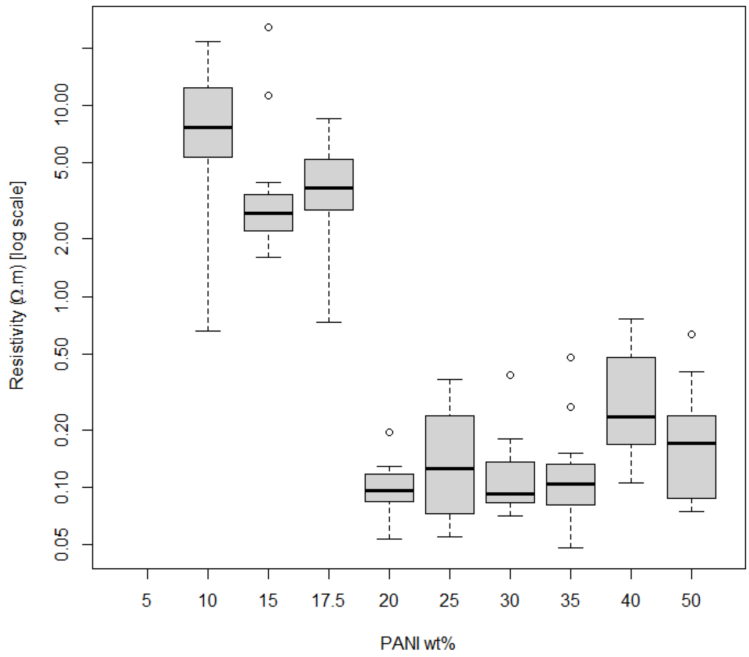

Figure 50. Average resistivity of PANI-EB + DBSA + Speedball composites

The OCP pH response for these was much more successful and repeatable. The OCP response for one of these is shown in Figure 51. A sensitivity of -27.9 mV/pH was obtained.

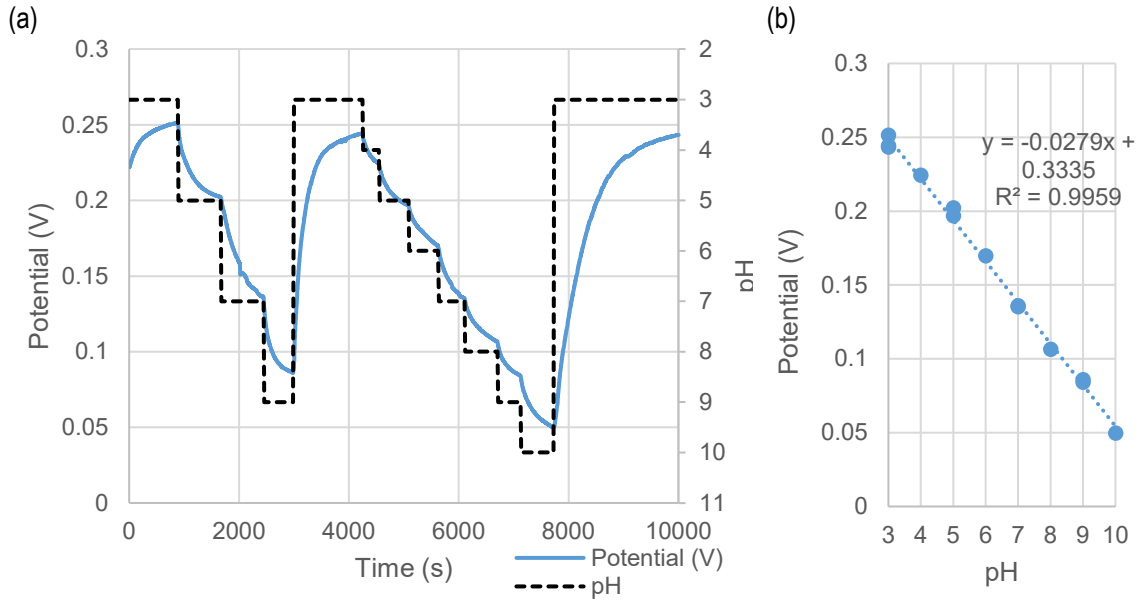

Figure 51. OCP pH response for PANI-EB + DBSA + Speedball composite with 30/30/40 formulation

Given these encouraging results, further characterization of the PANI-EB + DBSA + Speedball composites was performed, including adhesion testing. At concentrations at

40 wt% PANI and higher, the print quality started decreasing as an increasing amount of residue would be peeled off during adhesion testing. However, conductive pathways were still maintained even after 10 peels. At 30 wt% and below, the amount of residue being peeled off was negligible, and so this was selected as the optimal concentration of PANI.

5.5.4. Fourth Sequence: PANI + DBSA + Speedball Composites

From the previous sequence of experiments, 30 wt% PANI was identified as the optimal concentration for the composite formulation. Further optimization was thus performed by changing the concentrations of DBSA and Speedball and trying both the PANI-EB and PANI-ES. The summarized results of the formulations tested in the fourth sequences are listed in Table 13. The pH response of the optimized PANI-EB + DBSA + Speedball composite is shown in Figure 52.

Table 13. Summary of results from fourth sequence of formulations for PANI + DBSA + Speedball composites

PANI type used	PANI wt%	DBSA wt%	Speedball wt%
PANI-EB	30	40	30
PANI-EB	30	50	20
PANI-ES	30	40	30
PANI-ES	30	50	20

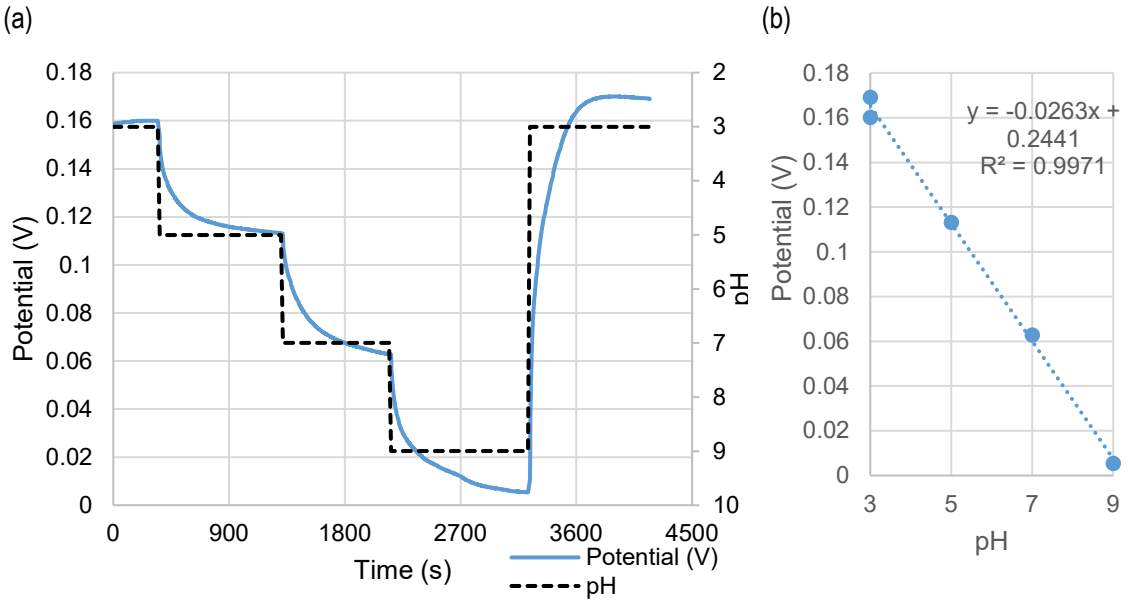

Figure 52. OCP pH response of PANI-EB + DBSA + Speedball composite with PANI-EB/DBSA/Speedball formulation of 30/50/20 by wt%

Although this represents a much lower sensitivity to that of the electropolymerized PANI or drop-cast PANI using comparable designs, it is still much higher than current fully screen-printed pH sensors. Additionally, the benefits of having a fully screen-printable sensor greatly compensate for the loss in sensitivity. The response times for this sensor to reach 75%, 90%, and 100% steady state response were approximately 189 seconds, 345 seconds, and 1065 seconds. These response times are slightly less ideal for certain applications requiring immediate responses, but very reasonable for applications such as wound healing where changes occur over a span of many hours.

Adhesion testing revealed no discernible differences between the two composites other than slightly more residues being removed from the PANI-EB composites compared to the PANI-ES composites. However, both maintained conductive pathways even after 10 peelings. Like the plastisol composites, the Speedball composites using ES composite had a much lower resistivity (~10^{-3} Ω·m) than the EB composites (~10^{-1} Ω·m). The amount of residue peeled was also essentially negligible after the first three peelings. It is estimated that the additional residue observed from the PANI-EB adhesion testing came from some of the larger particles which had not been incorporated into the composite.

5.5.5. Flexibility Testing

The results of the original, bent, and unbent sensors are shown in Figure 53. The sensitivities remained nearly identical. However, a potential drift was seen as indicated by the shifting of potential at comparable pH values, even during the same scan as indicated by the recovery level.

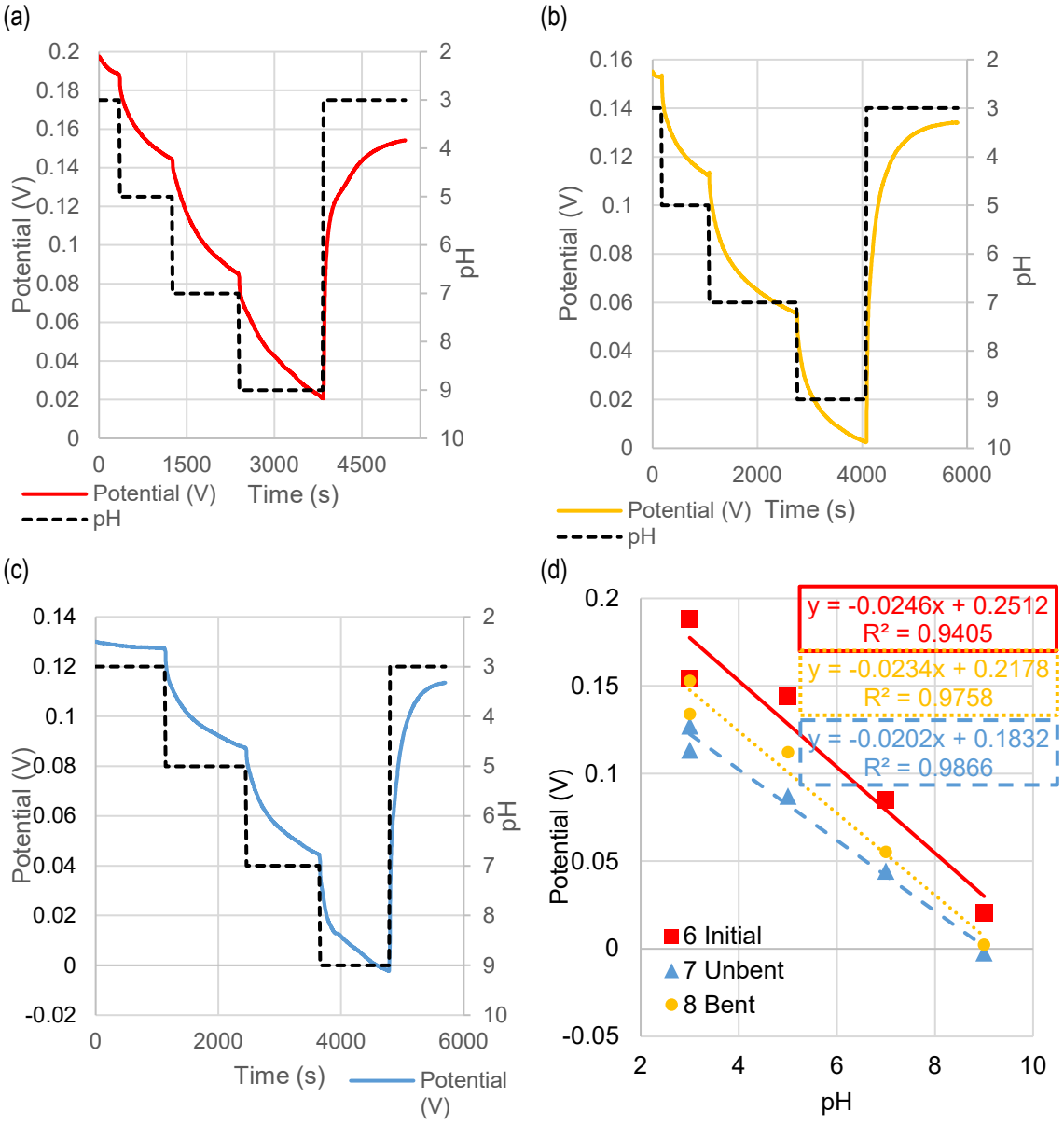

Figure 53. OCP of PANI-EB Composite in (a) initial state, (b) bent state, and (c) unbent state along with (d) corresponding sensitivity curves

The PANI-EB composites showed a slight loss in sensitivity after bending and unbending when compared to the initial response. Additionally, a relatively strong potential

drift was observed over the course of these set of responses This can be seen from the difference between the start and end potentials of the same scan or from scan to scan.

The PANI-ES + DBSA + Speedball composites were also tested. The results of these are shown in Figure 54.

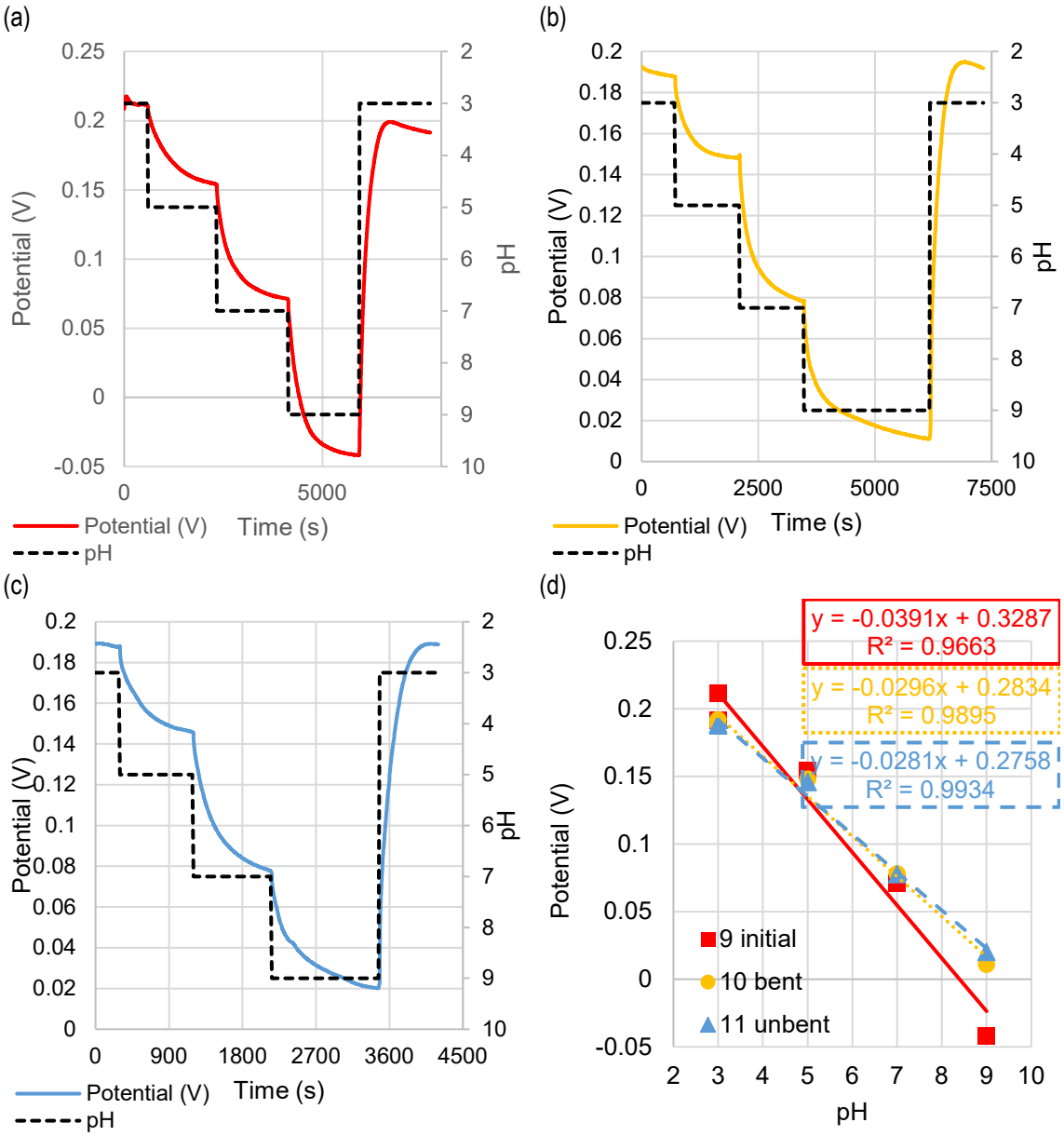

Figure 54. OCP of PANI-ES composite in (a) initial state, (b) bent state, and (c) unbent state along with (d) corresponding sensitivity curves

The PANI-ES composites initially showed higher sensitivity but also higher non-linearity, with increasing potential differences as the pH was decreased. After this first

scan of pH response and bending the sensor, this increasing change was not noticed as a higher potential is seen at a pH of 9. As a result, the overall linearity increased at the expense of a reduction in sensitivity as seen by the R^2 values in Figure 54 (d).

Overall, slightly more successful flexibility results were obtained with the ES composites. This is expected to be a result of the differences in particle sizes of the powders which was mentioned earlier. The differences between the PANI-ES and PANI-EB composites is shown in Figure 55. The PANI-ES shows a much more homogeneous print layer and less cracking compared to the PANI-EB composite.

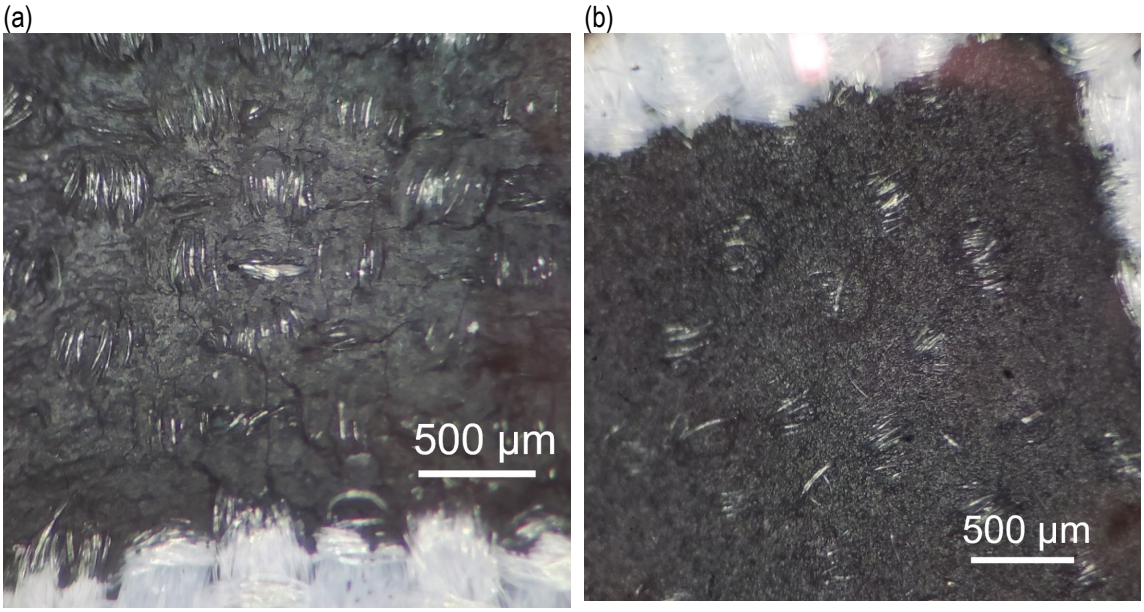

Figure 55. (a) PANI-EB + DBSA + Speedball and (b) PANI-ES + DBSA + Speedball composites screen-printed on textile substrate

Following these results, the PANI-ES + DBSA + Speedball composite samples were tested for 100 bend cycles. The results are shown in Figure 56.

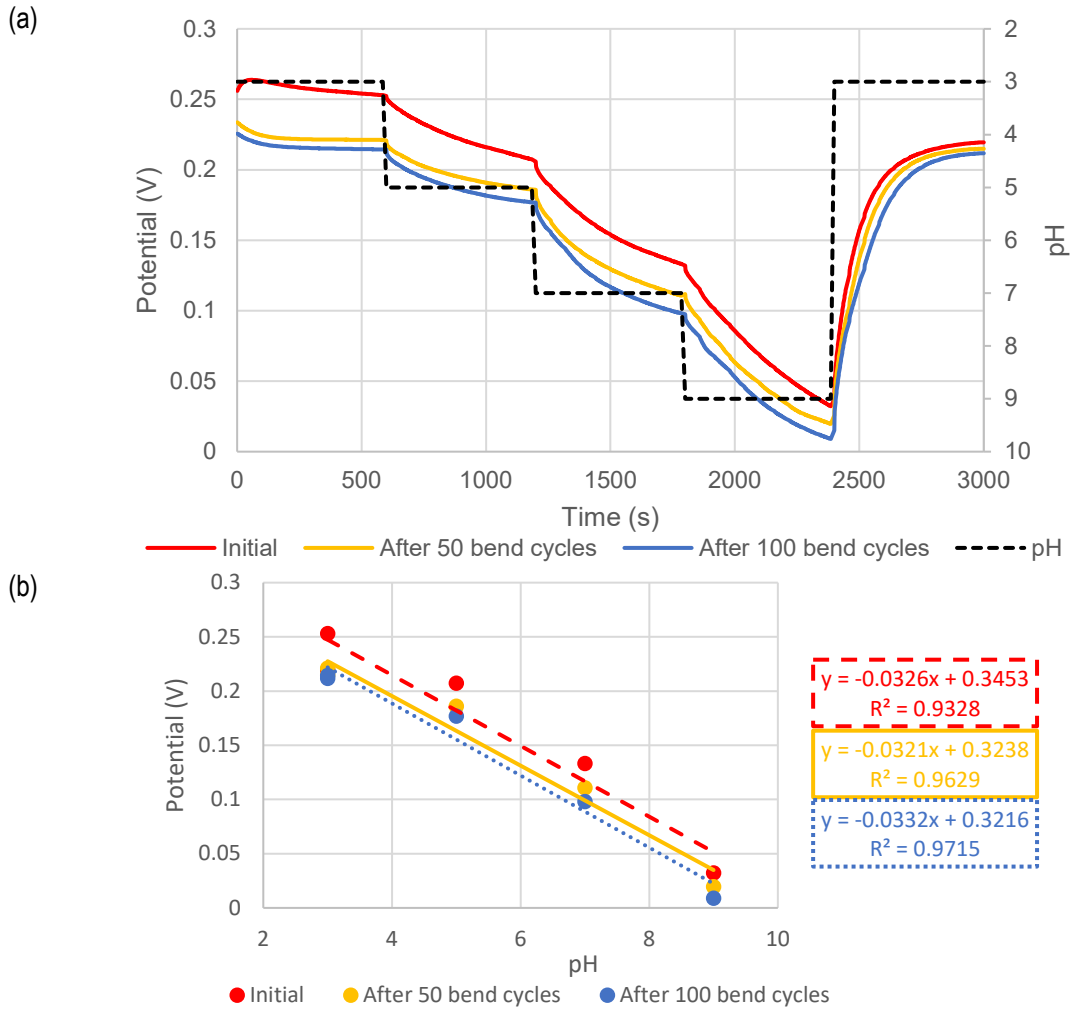

Figure 56. (a) OCP pH Response of PANI-ES + DBSA + Speedball composite after 50 and 100 bend cycles and (b) corresponding sensitivity curves

A slight drift was observed over the course of the experiments as can be seen from the different start and end points of each scan and the decreasing start point in the fitted sensitivity curve. However, the slopes of the PANI-ES + DBSA + Speedball composite show negligible differences and very similar responses after both 50 and 100 bend cycles when compared to the initial measurements.

5.5.6. CV Analysis

The PANI composite was subject to a CV analysis. Figure 57 shows the CV curves obtained in 1M HCl and at various pH levels. The CV curve did not show any significant redox peaks. Although, a slight trend was observed at the extreme potentials when changing potentials but did not recover when the buffer solutions' pH was decreased. In

the end, as was confirmed with the drop-cast and electropolymerized PANI, the PANI composite could not be used as an amperometric sensor.

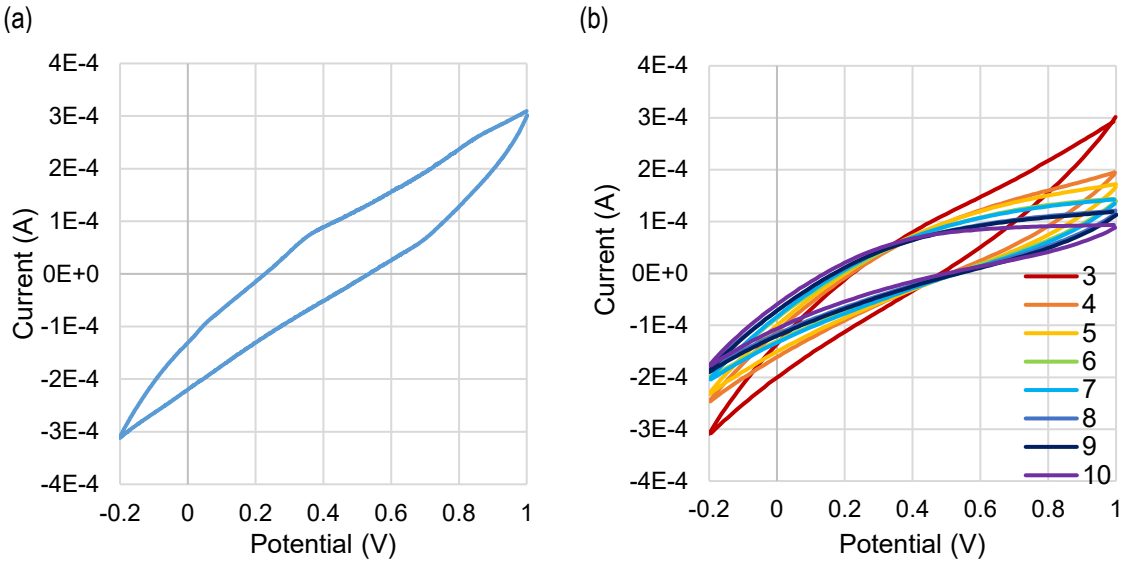

Figure 57. CV of PANI-EB + DBSA + Speedball composite in (a) 1M HCl; and at (b) various pH levels

5.5.7. PANI Composite Discussion

A summary of the results for all the general composite formulations is summarized in Table 14.

Table 14. Sumary of results for PANI composites

Experiment Sequence	Formulation	Sensor Response	Print Quality	Conductivity
1st	PANI-EB + Plastisol	Not tested	Poor	Low
2nd	PANI-ES + Plastisol	Not tested	Poor	High
2nd	PANI-EB + DBSA + Plastisol	Inconsistent / not tested	Ok	Low
2nd	PANI-ES + DBSA + Plastisol	Inconsistent, high sensitivity, slightly non-linear, slow response	Good	High
3rd	PANI-EB + DBSA + Speedball	Moderate sensitivity, linear response, moderate response time	Ok/Good	Low
3rd & 4th	PANI-ES + DBSA + Speedball	High sensitivity, non-linear response, moderate response time	Good	High

Comparing the PANI-EB and PANI-ES composites, the PANI-EB provides a much more linear pH response to pH in the range of pH 3 to 10 with a sensitivity between -20

and -30 mV/pH. The PANI-ES shows a pH response with a slightly non-linear response, but overall, a much greater sensitivity between -30 and -40 mV/pH over the same pH range of 3 to 10 and greater flexibility. Although the measurements were taken over the pH range of 3 to 9 (or 10 in some cases), the physiologically relevant pH for sweat or wound healing is typically between 5 and 8. As such, the non-linearity observed for PANI-ES may be less consequential over this smaller range. The PANI-ES used in this thesis also had more favourable mixing properties given the finer powder size. Theoretically, the PANI-EB would be preferred in terms of chemical interaction with the solvent and polymer matrix given the unknown nature of the proprietary sulfonic acid dopant used to dope the PANI-ES. Moving forward, obtaining a PANI-EB powder with a finer particle size for improving the composite mechanical properties or a PANI-ES synthesized chemically in the presence of DBSA or another dopant which provides a linear pH response would be the preferred conductive, pH-sensitive filler particle of choice.

Beyond the second sequence of experiments, an obvious pH response is observable through the OCP recordings. The second sequence was characterized by a great deal of inconsistency, particularly compared to the third and fourth sequence of experiments. This change may have reflected an improvement in user technique in composite preparation/mixing and screen-printing. Therefore, it is difficult to establish with absolute certainty that one composite formulation was superior to the other. The manual screen-printing method and small sample size (typically less than 4 samples per formulation) leaves room for error. When possible, many samples were tested to validate the results. In the second sequence, many repeat samples showed very different responses. In the third and fourth sequence, the results were much more consistent from sample to sample. As such, given the recorded measurements, the Speedball composites appear to provide an advantage in terms of sensor reliability, response time, and relatively good responses.

In terms of formulations, 30 wt% PANI-EB seems to be a safe threshold for loading into screen-printable composites. For PANI-ES, it could be extended to about 40 wt%. Above these values, increases in PANI loading did not produce any improvement in sensor response and typically results in a decrease in the composite’s print quality. In terms of DBSA and Speedball ink, roughly equal 30 to 40 wt% provided the greatest combination of response and mechanical properties.

5.6. PAPBA Lactate Sensor

5.6.1. Synthesis

As was done with the electropolymerized PANI, the progression of the electropolymerization reaction could be monitored is situ by observing the increase in current with each potential cycle. Figure 58 shows the progression of the electropolymerization reactions.

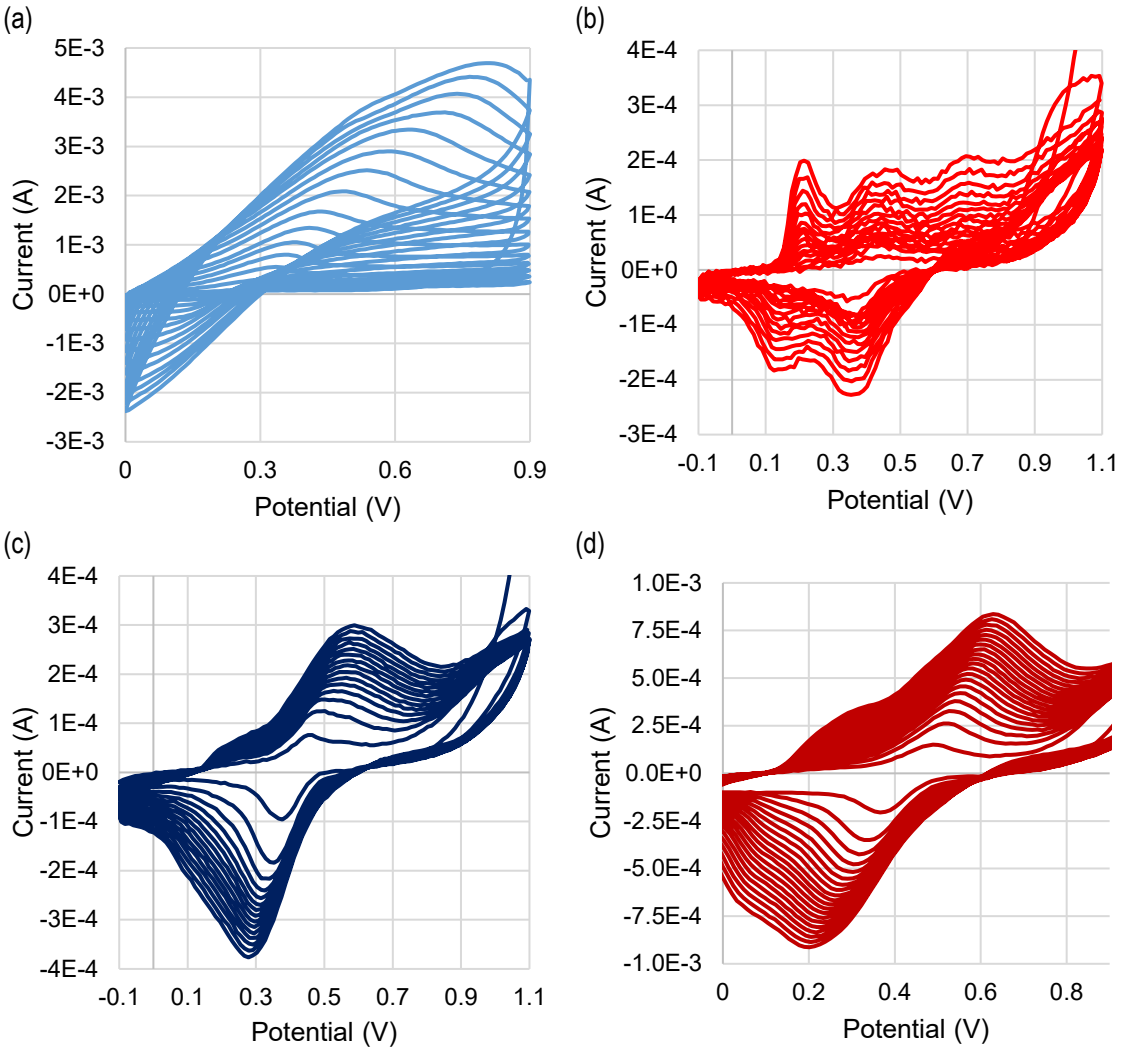

Figure 58. Electropolymerization of PAPBA on Pine SPEs with synthesis conditions (a) 1 and (b) 2; and on textile SPEs with synthesis conditions (c) 1 and (d) 2

The electropolymerization reaction progressions for the different synthesis conditions looked very different, with the second set of conditions displaying a more ideal

shape. Nevertheless, both showed increases in current as the reaction progressed. The final PAPBA film was then further characterized by recording the CV in 1M HCl solution. These CV curves are shown in Figure 59.

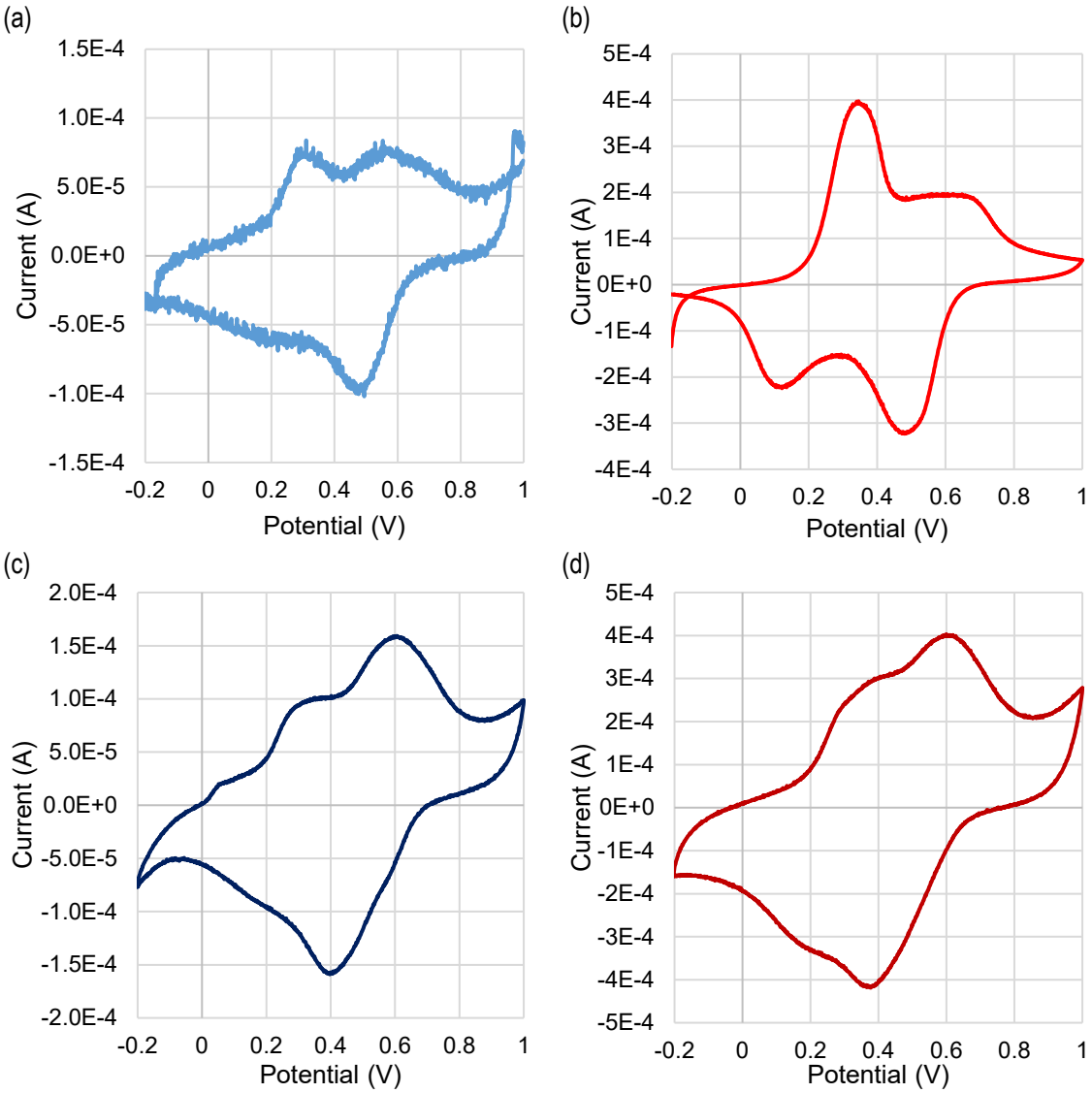

Figure 59. CV curves for electropolymerized PAPBA in 1M HCl for Pine SPEs with synthesis conditions (a) 1 and (b) 2, as well as on textile SPEs with synthesis conditions (c) 1 and (d) 2

Comparing the CV curves of the two synthesis conditions on the Pine Research SPE, the curve shapes are relatively similar, with the second having a much more prominent oxidation peak at about 335 mV. Yet, comparing the CV curves of the textile SPEs under the different conditions revealed very similar curve shapes between the two

conditions. The lactate responses were still characterized despite the differences in CV curves.

5.6.2. Lactate Sensor Response

In terms of lactate sensor response, PAPBA was not very ideal. The second set of synthesis conditions, despite the more defined peaks on the CV curve provided no clear response. The PAPBA from the first set of conditions did display a response, but it had relatively low sensitivity (0.1 mV/mM) between 0.1 mM and 100 mM. Sensitivity improves slightly up to 2.5 mV/mM between concentrations of 0.1 mM to 1 mM, but these are still relatively low for practical applications. These sensitivities were relatively similar to those recorded using PAPBA as a potentiometric sensor for other diols [173]. The OCP lactate response for the PAPBA electropolymerized on the Pine Research and textile SPES are shown in Figure 60.

Additionally, it is worth noting that both the textile and Pine SPEs appeared to have a large drift. The large potential drift observed in both cases was somewhat surprising as the Pine Research SPEs had previously been relatively stable when recording the OCP for the pH sensors. This possibly indicates that a longer wetting time needed to be observed before a stable potential was reached. Overall, this approach was an interesting alternative to enzyme-based sensors, but its linear range and sensitivity are still too low for most practical sensing application.

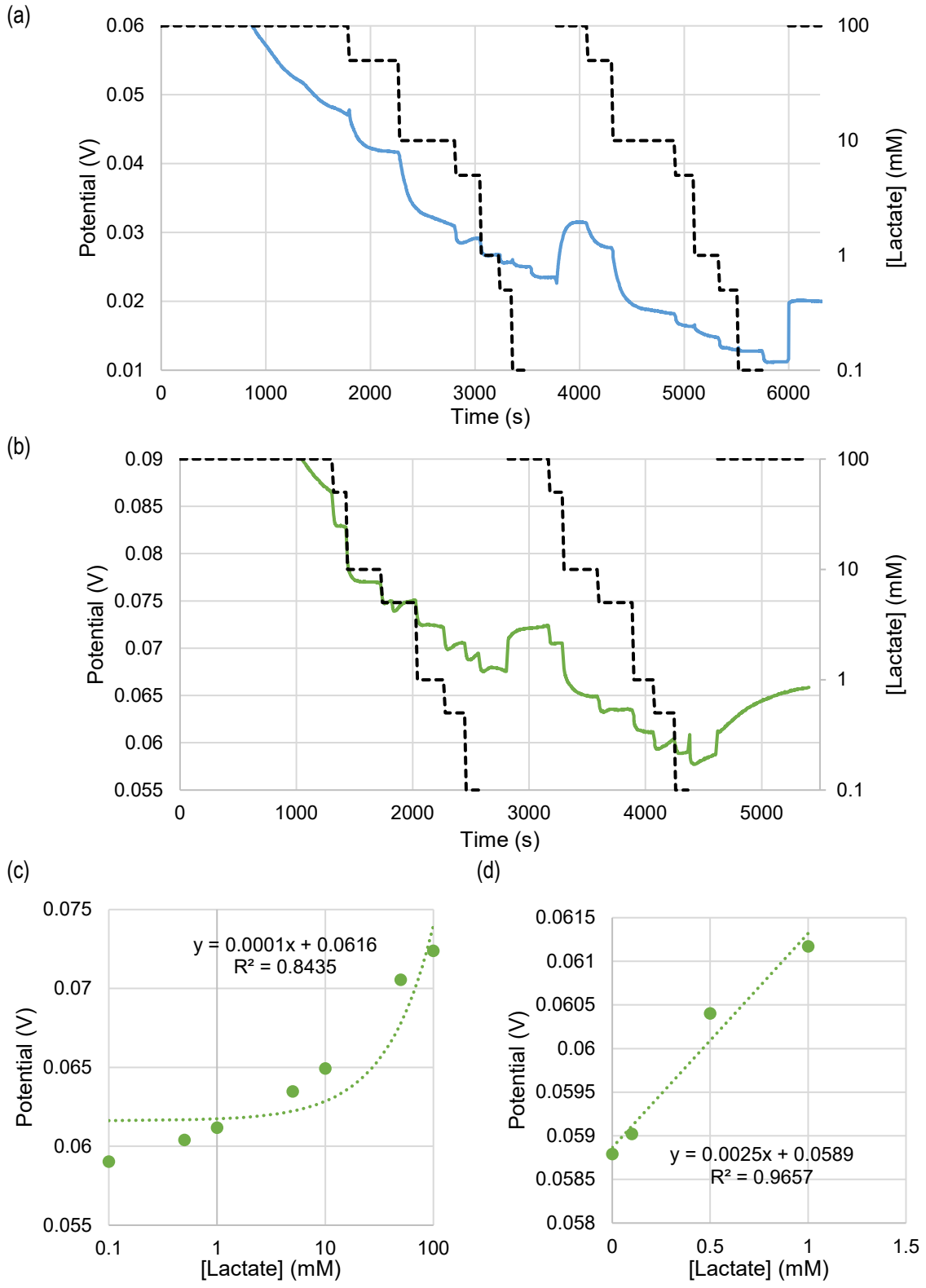

Figure 60. PAPBA (synthesis conditions 1) OCP lactate response on (a) Pine Research SPE and (b) textile SPE with corresponding sensitivity curve for textile SPE in lactate concentration range of (c) 0.1 mM to 100 mM, and (d) 0 to 1 mM

Chapter 6. Future Work and Conclusions

6.1. Future Work

Based on the methodology and results of Chapters 4 and 5, various improvements and suggestions for future study have been outlined in this section.

6.1.1. Real-world Samples

In this thesis, it was shown that PANI and the PANI composites demonstrated a strong pH response. The next step in characterization would be to track the effects of real-world factors which could potentially affect the sensor's performance. To this end, changes in electrolyte concentration and temperature of the sample are of interest within the normal physiological ranges. For electrolytes, this was described earlier in Table 1 in Chapter 2. The main ions to account for would be chloride, potassium, and sodium. In terms of temperature, all experiments were operated at room temperature. However, given that these would likely be in contact with human skin, the temperature might be closer to that of the human body at 37 °C. It would also be subject to environmental conditions. So, monitoring how the response changes in the temperatures range of 10°C to 40 °C would be relevant. Thus, human sweat samples and then on-body samples would be an interesting next step in finding out the real-world applications of the screen-printable PANI composite.

6.1.2. Device Integration

To truly make this sensor into a wearable device, better integration into a functional system is still required. This integration requires the addition of multiple components including wearable electronics which can measure, store, process, and transmit data to a display device such as a computer, smartphone, or smartwatch. For measuring the open circuit potential, a wearable voltmeter is required. Analog voltmeters are composed of wound-up coils in a magnetic field which exhibit a physical shift in an attached dial when a current is passed. This device is not easily integrated into textiles but has been implemented in devices such as smartwatches. However, long conductive traces would still be required. Alternatively, devices like the Arduino Flora present other alternatives for

microcontrollers designed to be sown onto textiles. Enabling Bluetooth or Near-Field Communication (NFC) capability would enable data to be transmitted to other devices for more rigorous data processing and display. Power requirements for these electronics also need to be considered. Flexible lithium polymer batteries are one possible example of wearable power sources which could be integrated with these devices.

Beyond integration with electronics, integration with sample collection systems is also required for reliable sample collection. Human interactions and considerations also need be accounted for. One possibility to help protect the sensor from harm by wearers or incidental contact is to integrate the sensor into isolated channels such that no surface is directly exposed to the outside. Figure 61 (a) below shows examples of plastisol-based microfluidic channels. The first shows a conventional hollow microfluidic channel made from plastisol which can be printed onto textiles through a substrate transfer process [33]. The second draws on concepts of paper microfluidics and applies these to textiles to wick sample fluid through a textile channel. The textile microfluidic channel is created by soaking portions of the textile with less viscous plastisol and covers layers with a more viscous plastisol thus creating impermeable walls around the channel. The textile acts as a pathway for fluids and capillary forces allow for passive movement through the channel. This is shown in Figure 61 (b) and (c).

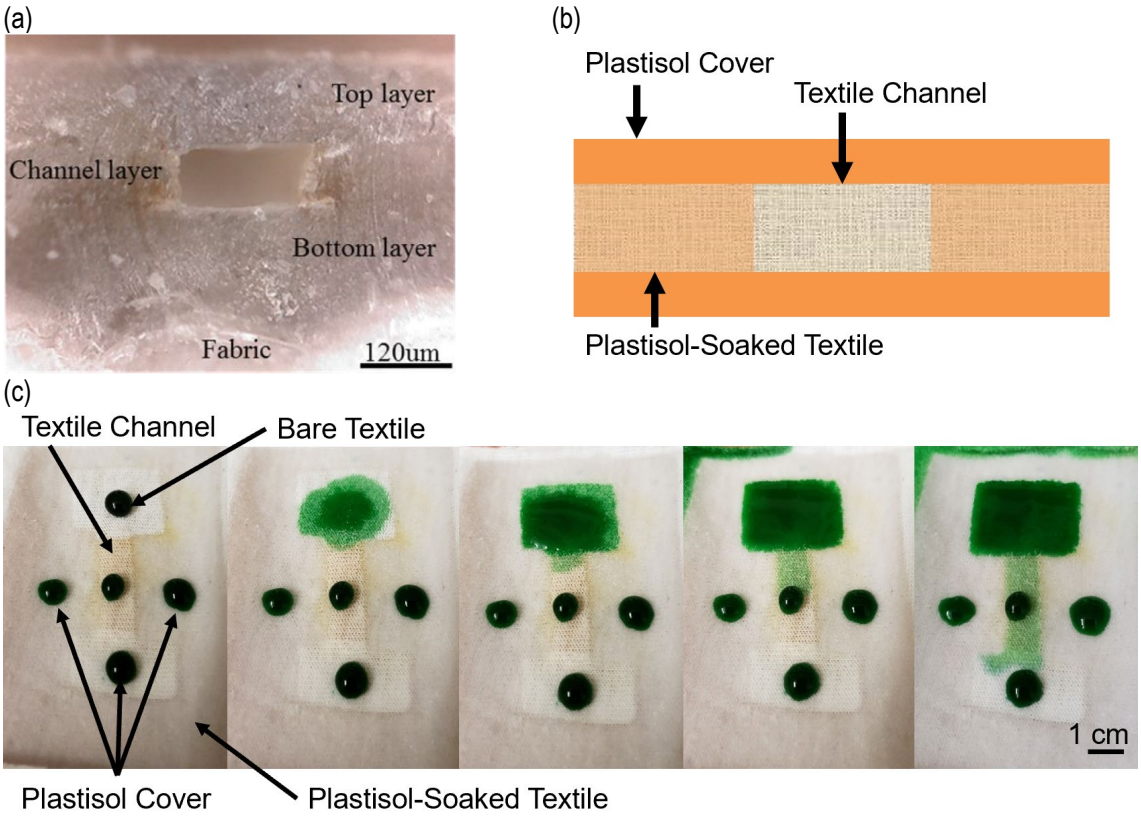

Figure 61. Plastisol microfluidic channel on textile substrate [33]; concept for textile microfluidic channel and example of fluid flow properties

To this end, proper textile substrate selection must also be considered in combination with the ink properties. Textiles with a less dense weave may saturate throughout their entire thickness not allowing for textile channels to be created. Textiles which are too dense may not fully saturate or need more ink to do so. The devices designed in this thesis were not designed to be stretchable as no stretchable inks were commercially available and thus all components would have needed to be reformulated. Nevertheless, composites involving stretchable elastomers like polyurethane have been developed and could be investigated for PANI composites. Corresponding modifications to the substrate would also need to be performed.

6.1.3. Reference Electrodes

Screen-printed reference electrodes still represent an important fabrication challenge. In this thesis, many of the tests were performed using a standard silver/silver chloride RE. Others were performed using the screen-printed Ag/AgCl RE. Although this RE provides an adequate short-term stability, it is prone to drift over long time periods.

This was shown in the drop-cast sensor response in Section 5.4.3. and is shown through another measurement in Figure 62. In this example, there is an initial stabilization period of about 10 to 15 minutes where the potential changes rapidly before being relatively stable for the next 45 minutes, albeit still exhibiting a slight drift. Longer evaluations would be required for longer measurements.

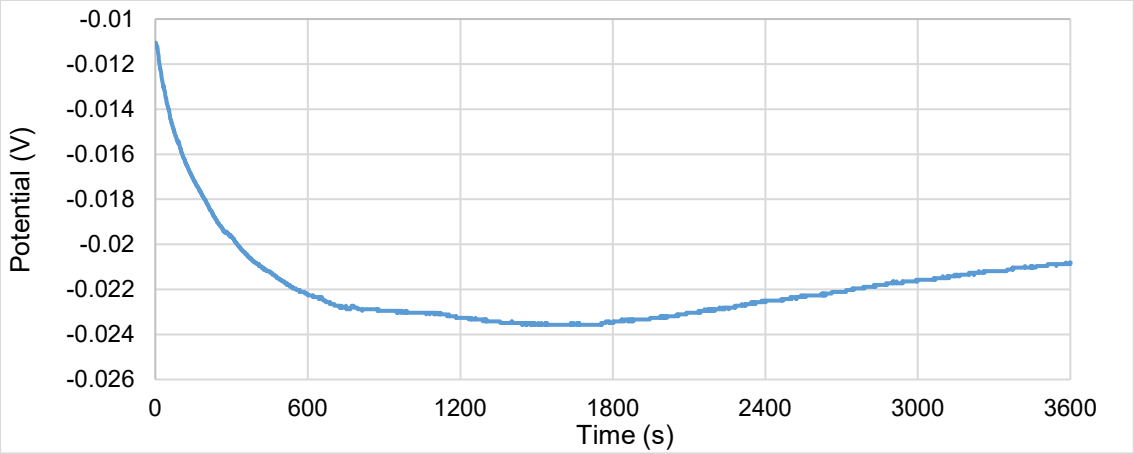

Figure 62. Screen-printed Ag/AgCl RE potential drift in 0.5 M KCl solution pH 6 versus a screen-printed carbon textile RE

To help mitigate this drift, some groups have printed additional layers overtop the screen-printed Ag/AgCl to act as electrolyte reservoirs. These have been reported to be highly beneficial to creating stable long-term REs. This is an important consideration not only for the sensors developed in this thesis but for all screen-printable sensors.

Another potentially interesting approach which has not yet been tested would be to seal the wearable plastisol microfluidic channels developed by our research group [33] with a material like the porous frit. This channel could be used to contain a KCl solution like the way a standard Ag/AgCl RE works. Figure 63 shows a design for this idea. The porous frit could be replaced with some other flexible, porous material.

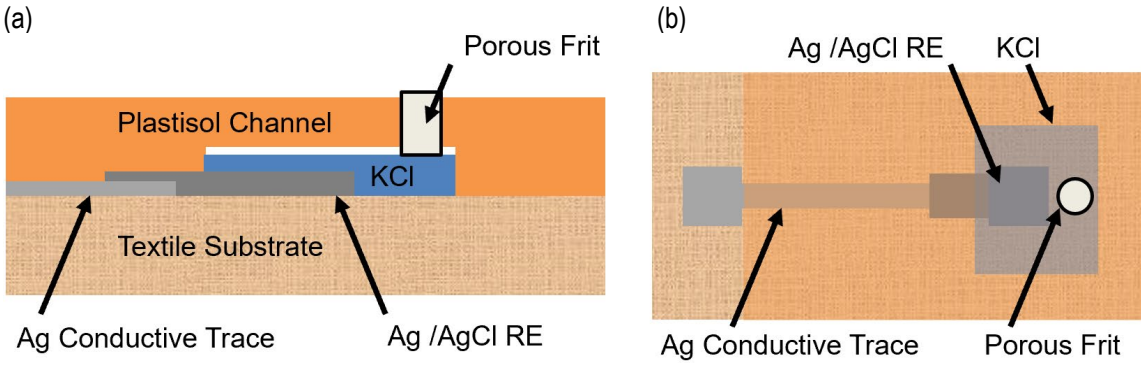

Figure 63. Conceptual screen-printed RE using a plastisol compartment to contain a KCl electrolyte solution: (a) Cross-section view; (b) Top view

6.1.4. PANI Composite Formulation Optimization for Automated Screen-Printer

The screen-printing performed in this thesis was all done manually using a glass slide as a blade and a plastic adhesive sheet patterned via a laser cutter for a mask. To increase repeatability in print properties, and thus sensor properties, the PANI composite should be formulated to be able to be printed using an automated screen-printer. To do so, further characterization and tailoring of the viscosity and surface tension of the PANI composite would be required using a rheometer or viscometer and the print requirement of the automated screen-printer.

6.1.5. Additional Biosensors

Given the interconnection of the human body's systems, the ability to monitor many different physiological parameters allows for a better picture to be obtained of the state of the human body. Incorporating sensors for electrolytes, glucose, sweat rate, uric acid, urea, cortisol, and the numerous other components of sweat would provide additional information which can be used in the diagnosis, monitoring, and management of numerous medical conditions. Chapter 2 highlighted many of the possible applications for which sweat sensors could be applied to. For some of these analytes, a different implementation than the potentiometric sensor may be required to achieve the level of sensitivity required to detect the smaller concentrations of these analytes present in sweat.

6.2. Conclusions

Sweat provides a promising avenue for the development of non-invasive biosensors. As a biofluid, it contains a wealth of information which could be used to diagnose, monitor, and manage numerous medical conditions. Nevertheless, the development of wearable sweat-based biosensors remains a complex challenge in terms of fabrication, materials, electronics, and system integration. The ability to produce flexible, highly sensitive sensors using scalable approaches remains one of the primordial challenges.

In this thesis, a simple, cost-effective fabrication procedure was used to design a textile-based SPE for wearable continuous chemical monitoring applications. This textile SPE design used screen-printable silver, silver/silver chloride, and carbon inks for the conductive traces, RE, and WE, respectively. Plastisol inks with different viscosities were used to pattern the different insulating backing and cover layers of the textile SPE. In a three-electrode design, a third carbon electrode can be added as the CE. Its operation was confirmed using CV and CA with $K_3Fe(CN)_6$ as a test redox probe. The textile SPE could also be used as a platform for the development of multi-analyte textile biosensors by monitoring multiple WEs simultaneously.

Leading up to the development of a screen-printable PANI composite, PANI was electropolymerized and drop-cast onto the textile SPEs and the CV curves were used to confirm proper deposition on the WE. Various solvents were tested and the PANI solubility enhancement through the addition of DBSA was confirmed. The pH response of PANI was then confirmed by recording the OCP using the electropolymerized and drop-cast textile SPEs.

A conductive, screen-printable, pH responsive composite was developed for use with this textile SPE design by mixing PANI, DBSA, and Speedball screen-printing ink. The optimal formulation for this composite was found to be 30 wt% PANI, 40 wt% DBSA, and 30 wt% Speedball ink, although the DBSA and Speedball ink ratios can be modified slightly. Plastisol composites were also tested but showed much slower response times than the Speedball composites.

PANI-EB and PANI-ES were both tested as conductive fillers. The PANI-EB composite showed sensitivities in the range of -20 to -30 mV/pH with a highly linear

response between pH levels of 3 and 10. The flexibility was acceptable but showed occasional breaking when bent to radius of curvature or 4 mm, with some cracks visible in the print. The PANI-ES had a smaller particle size which allowed for it to be mixed more readily and produce more homogeneous films with better print quality, conductivity, and better flexibility as demonstrated after 100 bend cycles with a greater than 90° bend angle. It also provided better sensitivity levels of -30 to -40 mv/pH, albeit with a slightly non-linear response. These represent a significant improvement over existing screen-printed pH sensors and the first instance of a flexible, screen-printable pH-responsive PANI composite. A 75-90% response was typically achievable between 3 and 6 minutes which is suitable for the applications of hydration monitoring, skin disorders, and wound healing. Although the sensitivity and response time of the screen-printed sensor were not as good as that of sensors using drop-casted solutions of PANI or electropolymerized PANI, the ability to have a fully screen-printable system from start to finish provides a significant improvement to the development of these sensors.

Investigation into a non-enzymatic, PAPBA-based potentiometric sensor showed that a response was observable at lactate concentrations with a 2.5 mV/mM sensitivity in the range of 0.1 mM to 1 mM, but only 0.1 mV/pH in the range of 0.1 to 100 mM. This represents the first investigations into PAPBA as a potentiometric lactate sensor, an implementation suitable to wearable sensors. However, this response is likely not adequate for monitoring clinically relevant parameters. Further improvements to synthesis conditions may help improve the response somewhat.

In summary, the overall contributions of this thesis are as follows:

1) Development of a textile-based screen-printed electrode system for continuous chemical/biochemical monitoring.

2) Development of a flexible, screen-printable, pH-sensing composite ink using PANI particles which could be applied to textiles.

3) Investigation of a non-enzymatic, potentiometric lactate sensor based on electrochemically synthesized PAPBA on screen-printed electrodes on textiles.

4) Establishing a platform for the development of a comprehensive multi-analyte textile biosensor system for sweat diagnostics.

References

[1] Canadian Medical Association. (2013). Health and health care for an aging population. *Policy Summary of The Canadian Medical Association, 316*, 1-10.

[2] Larsson, A., Greig-Pylypczuk, R., & Huisman, A. (2015). The state of point-of-care testing: a European perspective. *Upsala journal of medical sciences, 120*(1), 1-10.

[3] da Silva, E. T., Souto, D. E., Barragan, J. T., de F. Giarola, J., de Moraes, A. C., & Kubota, L. T. (2017). Electrochemical biosensors in point-of-care devices: recent advances and future trends. *ChemElectroChem, 4*(4), 778-794.

[4] Vashist, S. K., Luppa, P. B., Yeo, L. Y., Ozcan, A., & Luong, J. H. (2015). Emerging technologies for next-generation point-of-care testing. *Trends in biotechnology, 33*(11), 692-705.

[5] Zarei, M. (2017). Portable biosensing devices for point-of-care diagnostics: Recent developments and applications. TrAC Trends in *Analytical Chemistry, 91*, 26-41.

[6] Crozier, A., Rajan, S., Buchan, I., & McKee, M. (2021). Put to the test: use of rapid testing technologies for covid-19. *bmj, 372*.

[7] Health Quality Ontario. (2018). Continuous monitoring of glucose for type 1 diabetes: a health technology assessment. *Ontario health technology assessment series, 18*(2), 1.

[8] Rodbard, D. (2017). Continuous glucose monitoring: a review of recent studies demonstrating improved glycemic outcomes. *Diabetes technology & therapeutics, 19*(S3), S-25.

[9] Yeo, J. C., & Lim, C. T. (2016). Emerging flexible and wearable physical sensing platforms for healthcare and biomedical applications. *Microsystems & Nanoengineering, 2*(1), 1-19.

[10] Mukhopadhyay, S. C. (2014). Wearable sensors for human activity monitoring: A review. *IEEE sensors journal, 15*(3), 1321-1330.

[11] Heikenfeld, J., Jajack, A., Rogers, J., Gutruf, P., Tian, L., Pan, T., ... & Wang, J. (2018). Wearable sensors: modalities, challenges, and prospects. *Lab on a Chip, 18*(2), 217-248.

[12] Seshadri, D. R., Li, R. T., Voos, J. E., Rowbottom, J. R., Alfes, C. M., Zorman, C. A., & Drummond, C. K. (2019). Wearable sensors for monitoring the physiological and biochemical profile of the athlete. *NPJ digital medicine, 2*(1), 1-16.

[13] Peake, J. M., Kerr, G., & Sullivan, J. P. (2018). A critical review of consumer wearables, mobile applications, and equipment for providing biofeedback, monitoring stress, and sleep in physically active populations. *Frontiers in physiology, 9*, 743.

[14] Bunn, J. A., Navalta, J. W., Fountaine, C. J., & Reece, J. D. (2018). Current state of commercial wearable technology in physical activity monitoring 2015–2017. *International journal of exercise science, 11*(7), 503.

[15] Wong, C., Zhang, Z. Q., Lo, B., & Yang, G. Z. (2015). Wearable sensing for solid biomechanics: A review. *IEEE Sensors Journal, 15*(5), 2747-2760.

[16] Chung, D., Khosla, A., & Gray, B. L. (2014, April). Screen printable flexible conductive nanocomposite polymer with applications to wearable sensors. In *Nanosensors, Biosensors, and Info-Tech Sensors and Systems 2014* (Vol. 9060, p. 90600U). International Society for Optics and Photonics.

[17] Chalmers University of Tecnology. (2019). First dexterous hand prosthesis implanted. https://www.chalmers.se/en/departments/e2/news/Pages/Hand-prosthesis-successfully-implanted.aspx

[18] Osborn, L. E., Dragomir, A., Betthauser, J. L., Hunt, C. L., Nguyen, H. H., Kaliki, R. R., & Thakor, N. V. (2018). Prosthesis with neuromorphic multilayered e-dermis perceives touch and pain. *Science robotics, 3*(19).

[19] Silva de Lima, A. L., Smits, T., Darweesh, S. K., Valenti, G., Milosevic, M., Pijl, M., ... & Bloem, B. R. (2020). Home-based monitoring of falls using wearable sensors in Parkinson's disease. *Movement disorders, 35*(1), 109-115.

[20] Pang, I., Okubo, Y., Sturnieks, D., Lord, S. R., & Brodie, M. A. (2019). Detection of near falls using wearable devices: a systematic review. *Journal of geriatric physical therapy, 42*(1), 48-56.

[21] Frost, M. C., & Meyerhoff, M. E. (2015). Real-time monitoring of critical care analytes in the bloodstream with chemical sensors: progress and challenges. *Annual Review of Analytical Chemistry, 8*, 171-192.

[22] Gahlot, R., Nigam, C., Kumar, V., Yadav, G., & Anupurba, S. (2014). Catheter-related bloodstream infections. *International journal of critical illness and injury science, 4*(2), 162.

[23] Edgeworth, J. (2009). Intravascular catheter infections. *Journal of hospital infection, 73*(4), 323-330.

[24] Gray, M., Meehan, J., Ward, C., Langdon, S. P., Kunkler, I. H., Murray, A., & Argyle, D. (2018). Implantable biosensors and their contribution to the future of precision medicine. *The Veterinary Journal, 239*, 21-29.

[25] Simmers, P., Li, S. K., Kasting, G., & Heikenfeld, J. (2018). Prolonged and localized sweat stimulation by iontophoretic delivery of the slowly-metabolized cholinergic agent carbachol. *Journal of dermatological science, 89*(1), 40-51.

[26] Desax, M. C., Ammann, R. A., Hammer, J., Schoeni, M. H., Barben, J., & Swiss Paediatric Respiratory Research Group. (2008). Nanoduct® sweat testing for rapid diagnosis in newborns, infants and children with cystic fibrosis. *European journal of pediatrics, 167*(3), 299-304.

[27] Dargaville, T. R., Farrugia, B. L., Broadbent, J. A., Pace, S., Upton, Z., & Voelcker, N. H. (2013). Sensors and imaging for wound healing: a review. *Biosensors and Bioelectronics, 41*, 30-42.

[28] Hatano, Y., Man, M. Q., Uchida, Y., Crumrine, D., Scharschmidt, T. C., Kim, E. G., ... & Holleran, W. M. (2009). Maintenance of an acidic stratum corneum prevents emergence of murine atopic dermatitis. *Journal of Investigative Dermatology, 129*(7), 1824-1835.

[29] Patterson, M. J., Galloway, S. D., & Nimmo, M. A. (2000). Variations in regional sweat composition in normal human males. *Experimental physiology, 85*(6), 869-875.

[30] Goodwin, M. L., Harris, J. E., Hernández, A., & Gladden, L. B. (2007). Blood lactate measurements and analysis during exercise: a guide for clinicians. *Journal of diabetes science and technology, 1*(4), 558-569.

[31] Bader, D., & Oomens, C. (2006). Recent advances in pressure ulcer research. *Science and practice of pressure ulcer management, 11*-26.

[32] Brown, M. S., Ashley, B., & Koh, A. (2018). Wearable technology for chronic wound monitoring: current dressings, advancements, and future prospects. *Frontiers in bioengineering and biotechnology, 6*, 47.

[33] Chung, D., & Gray, B. L. (2019). Development of Screen-Printed Flexible Multi-Level Microfluidic Devices with Integrated Conductive Nanocomposite Polymer Electrodes on Textiles. *Journal of The Electrochemical Society, 166*(9), B3116.

[34] Laffitte, Y., & Gray, B.L. (2021). Real-time potentiometric pH-sensor using a screen-printable polyaniline composite on textiles. Poster presented at *International Conference on Flexible, Printable Sensors and Systems*, (2021). Topic 5, Paper ID 6038.

[35] Brasier, N., & Eckstein, J. (2019). Sweat as a source of next-generation digital Biomarkers. *Digital biomarkers, 3*(3), 155-165.

[36] Baker, L. B. (2019). Physiology of sweat gland function: The roles of sweating and sweat composition in human health. *Temperature, 6*(3), 211-259.

[37] https://commons.wikimedia.org/wiki/File:Anatomy_The_Skin_-_NCI_Visuals_Online.jpg

[38] Cystic Fibrosis Foundation. (n.d.). Sweat Test. https://www.cff.org/What-is-CF/Testing/Sweat-Test/

[39] Brothers, M. C., DeBrosse, M., Grigsby, C. C., Naik, R. R., Hussain, S. M., Heikenfeld, J., & Kim, S. S. (2019). Achievements and challenges for real-time sensing of analytes in sweat within wearable platforms. *Accounts of chemical research, 52*(2), 297-306.

[40] Lazzeri, C., Valente, S., Chiostri, M., & Gensini, G. F. (2015). Clinical significance of lactate in acute cardiac patients. *World journal of cardiology, 7*(8), 483.

[41] English, P., & Williams, G. (2004). Hyperglycaemic crises and lactic acidosis in diabetes mellitus. *Postgraduate medical journal, 80*(943), 253-261.

[42] Lee, S. M., & An, W. S. (2016). New clinical criteria for septic shock: serum lactate level as new emerging vital sign. *Journal of thoracic disease, 8*(7), 1388.

[43] Gatenby, R. A., & Gillies, R. J. (2007). Glycolysis in cancer: a potential target for therapy. *The international journal of biochemistry & cell biology, 39*(7-8), 1358-1366.

[44] Sakharov, D. A., Shkurnikov, M. U., Vagin, M. Y., Yashina, E. I., Karyakin, A. A., & Tonevitsky, A. G. (2010). Relationship between lactate concentrations in active muscle sweat and whole blood. *Bulletin of experimental biology and medicine, 150*(1), 83.

[45] Bandodkar, A. J., Gutruf, P., Choi, J., Lee, K., Sekine, Y., Reeder, J. T., ... & Rogers, J. A. (2019). Battery-free, skin-interfaced microfluidic/electronic systems for simultaneous electrochemical, colorimetric, and volumetric analysis of sweat. *Science advances, 5*(1), eaav3294.

[46] Nikolaus, N., & Strehlitz, B. (2008). Amperometric lactate biosensors and their application in (sports) medicine, for life quality and wellbeing. *Microchimica Acta, 160*(1-2), 15-55.

[47] Fellmann, N., Grizard, G., & Coudert, J. (1983). Human frontal sweat rate and lactate concentration during heat exposure and exercise. *Journal of Applied Physiology*, *54*(2), 355-360.

[48] Green, J. M., Bishop, P. A., Muir, I. H., McLester Jr, J. R., & Heath, H. E. (2000). Effects of high and low blood lactate concentrations on sweat lactate response. *International journal of sports medicine*, *21*(08), 556-560.

[49] Derbyshire, P. J., Barr, H., Davis, F., & Higson, S. P. (2012). Lactate in human sweat: a critical review of research to the present day. *The journal of physiological sciences*, *62*(6), 429-440.

[50] Baker, L. B., & Wolfe, A. S. (2020). Physiological mechanisms determining eccrine sweat composition. *European journal of applied physiology*, *120*(4), 719-752.

[51] Gordon Jr, R. S., Thompson, R. H., Muenzer, J., & Thrasher, D. (1971). Sweat lactate in man is derived from blood glucose. *Journal of applied physiology*, *31*(5), 713-716.

[52] Biagi, S., Ghimenti, S., Onor, M., & Bramanti, E. (2012). Simultaneous determination of lactate and pyruvate in human sweat using reversed-phase high-performance liquid chromatography: a noninvasive approach. *Biomedical Chromatography*, *26*(11), 1408-1415.

[53] Falk, B., Bar-Or, O., MacDougall, J. D., McGillis, L., Calvert, R., & Meyer, F. (1991). Sweat lactate in exercising children and adolescents of varying physical maturity. *Journal of Applied Physiology*, *71*(5), 1735-1740.

[54] Knight, S. L., Taylor, R. P., Polliack, A. A., & Bader, D. L. (2001). Establishing predictive indicators for the status of loaded soft tissues. *Journal of applied physiology*, *90*(6), 2231-2237.

[55] Polliack, A., Taylor, R., & Bader, D. (1997). Sweat analysis following pressure ischaemia in a group of debilitated subjects. *Journal of rehabilitation research and development*, *34*, 303-308.

[56] Panther, D. J., & Jacob, S. E. (2015). The importance of acidification in atopic eczema: an underexplored avenue for treatment. *Journal of clinical medicine*, *4*(5), 970-978.

[57] Lambers, H., Piessens, S., Bloem, A., Pronk, H., & Finkel, P. (2006). Natural skin surface pH is on average below 5, which is beneficial for its resident flora. *International journal of cosmetic science*, *28*(5), 359-370.

[58] Levin, J., & Maibach, H. (2008). Human skin buffering capacity: an overview. *Skin Research and Technology*, *14*(2), 121-126.

[59] Lee, H. J., Yoon, N. Y., Lee, N. R., Jung, M., Kim, D. H., & Choi, E. H. (2014). Topical acidic cream prevents the development of atopic dermatitis- and asthma-like lesions in murine model. *Experimental dermatology*, *23*(10), 736-741.

[60] Hanifin, J. M., Reed, M. L., Prevalence, E., & Impact Working Group. (2007). A population-based survey of eczema prevalence in the United States. *Dermatitis*, *18*(2), 82-91.

[61] Patterson, M. J., Galloway, S. D., & Nimmo, M. A. (2000). Variations in regional sweat composition in normal human males. *Experimental physiology*, *85*(6), 869-875.

[62] Morgan, R. M., Patterson, M. J., & Nimmo, M. A. (2004). Acute effects of dehydration on sweat composition in men during prolonged exercise in the heat. *Acta physiologica Scandinavica*, *182*(1), 37-43.

[63] Ranchordas, M. K., Tiller, N. B., Ramchandani, G., Jutley, R., Blow, A., Tye, J., & Drury, B. (2017). Normative data on regional sweat-sodium concentrations of professional male team-sport athletes. *Journal of the International Society of Sports Nutrition*, *14*(1), 40.

[64] Patterson, M. J., Galloway, S. D. R., & Nimmo, M. A. (2002). Effect of induced metabolic alkalosis on sweat composition in men. *Acta physiologica scandinavica*, *174*(1), 41-46.

[65] Curto, V. F., Fay, C., Coyle, S., Byrne, R., O'Toole, C., Barry, C., ... & Benito-Lopez, F. (2012). Real-time sweat pH monitoring based on a wearable chemical barcode micro-fluidic platform incorporating ionic liquids. *Sensors and Actuators B: Chemical*, *171*, 1327-1334.

[66] Lara, B., Gallo-Salazar, C., Puente, C., Areces, F., Salinero, J. J., & Del Coso, J. (2016). Interindividual variability in sweat electrolyte concentration in marathoners. *Journal of the International Society of Sports Nutrition*, *13*(1), 31.

[67] Moyer, J., Wilson, D., Finkelshtein, I., Wong, B., & Potts, R. (2012). Correlation between sweat glucose and blood glucose in subjects with diabetes. *Diabetes technology & therapeutics*, *14*(5), 398-402.

[68] Karpova, E. V., Laptev, A. I., Andreev, E. A., Karyakina, E. E., & Karyakin, A. A. (2020). Relationship between sweat and blood lactate levels during exhaustive physical exercise. *ChemElectroChem*, *7*(1), 191-194.

[69] Keller, R. W., Bailey, J. L., Wang, Y., Klein, J. D., & Sands, J. M. (2016). Urea transporters and sweat response to uremia. *Physiological reports*, *4*(11), e12825.

[70] Tricoli, A., & Neri, G. (2018). Miniaturized bio-and chemical-sensors for point-of-care monitoring of chronic kidney diseases. *Sensors*, *18*(4), 942.

[71] Raiszadeh, M. M., Ross, M. M., Russo, P. S., Schaepper, M. A., Zhou, W., Deng, J., ... & Kirsch, W. M. (2012). Proteomic analysis of eccrine sweat: implications for the discovery of schizophrenia biomarker proteins. *Journal of proteome research, 11*(4), 2127-2139.

[72] Csősz, É., Emri, G., Kalló, G., Tsaprailis, G., & Tőzsér, J. (2015). Highly abundant defense proteins in human sweat as revealed by targeted proteomics and label-free quantification mass spectrometry. *Journal of the European Academy of Dermatology and Venereology, 29*(10), 2024-2031.

[73] Yang, Y., Song, Y., Bo, X., Min, J., Pak, O. S., Zhu, L., ... & Gao, W. (2020). A laser-engraved wearable sensor for sensitive detection of uric acid and tyrosine in sweat. *Nature biotechnology*, *38*(2), 217-224.

[74] Pirovano, P., Dorrian, M., Shinde, A., Donohoe, A., Brady, A. J., Moyna, N. M., ... & McCaul, M. (2020). A wearable sensor for the detection of sodium and potassium in human sweat during exercise. *Talanta*, *219*, 121145.

[75] Jadoon, S., Karim, S., Akram, M. R., Kalsoom Khan, A., Zia, M. A., Siddiqi, A. R., & Murtaza, G. (2015). Recent developments in sweat analysis and its applications. *International journal of analytical chemistry*, *2015*.

[76] Sears, M. E., Kerr, K. J., & Bray, R. I. (2012). Arsenic, cadmium, lead, and mercury in sweat: a systematic review. *Journal of environmental and public health, 2012*.

[77] Sheng, J., Qiu, W., Xu, B., Xu, H., & Tang, C. (2016). Monitoring of heavy metal levels in the major rivers and in residents' blood in Zhenjiang City, China, and assessment of heavy metal elimination via urine and sweat in humans. *Environmental Science and Pollution Research*, *23*(11), 11034-11045.

[78] United Nations Office on Drugs and Crime. (2014). Guidelines for testing drugs under international control in hair, sweat and oral fluid.

[79] Buono, M. J. (1999). Sweat Ethanol Concentrations are Highly Correlated with Co-Existing Blood Values in Humans. *Experimental physiology*, *84*(2), 401-404.

[80] Torrente-Rodríguez, R. M., Tu, J., Yang, Y., Min, J., Wang, M., Song, Y., ... & Gao, W. (2020). Investigation of cortisol dynamics in human sweat using a graphene-based wireless mHealth system. *Matter, 2*(4), 921-937.

[81] Järbrink, K., Ni, G., Sönnergren, H., Schmidtchen, A., Pang, C., Bajpai, R., & Car, J. (2017). The humanistic and economic burden of chronic wounds: a protocol for a systematic review. *Systematic reviews*, *6*(1), 1-7.

[82] Frykberg, R. G., & Banks, J. (2015). Challenges in the treatment of chronic wounds. *Advances in wound care*, *4*(9), 560-582.

[83] Brownrigg, J. R. W., Apelqvist, J., Bakker, K., Schaper, N. C., & Hinchliffe, R. J. (2013). Evidence-based management of PAD & the diabetic foot. *European Journal of Vascular and Endovascular Surgery*, *45*(6), 673-681.

[84] Qin, M., Guo, H., Dai, Z., Yan, X., & Ning, X. (2019). Advances in flexible and wearable pH sensors for wound healing monitoring. *Journal of Semiconductors*, *40*(11), 111607.

[85] Eming, S. A., Martin, P., & Tomic-Canic, M. (2014). Wound repair and regeneration: mechanisms, signaling, and translation. *Science translational medicine*, *6*(265), 265sr6-265sr6.

[86] Schreml, S., Szeimies, R. M., Karrer, S., Heinlin, J., Landthaler, M., & Babilas, P. (2010). The impact of the pH value on skin integrity and cutaneous wound healing. *Journal of the European Academy of Dermatology and Venereology*, *24*(4), 373-378.

[87] Uchino, K. (Ed.). (2017). *Advanced piezoelectric materials: Science and technology*. Woodhead Publishing.

[88] Yurddaskal, M., Erol, M., & Celik, E. (2017). Carbon black and graphite filled conducting nanocomposite films for temperature sensor applications. *Journal of Materials Science: Materials in Electronics*, *28*(13), 9514-9518.

[89] https://commons.wikimedia.org/wiki/File:OSCAL_2017_silkscreen_printed_materials_28.jpg

[90] Tang, J., Guo, H., Zhao, M., Yang, J., Tsoukalas, D., Zhang, B., ... & Zhang, W. (2015). Highly stretchable electrodes on wrinkled polydimethylsiloxane substrates. *Scientific reports*, *5*, 16527.

[91] Abrar, M. A., Dong, Y., Lee, P. K., & Kim, W. S. (2016). Bendable electro-chemical lactate sensor printed with silver nano-particles. *Scientific reports*, *6*(1), 1-9.

[92] Flueckiger, J., Ko, F. K., & Cheung, K. C. (2010). Electrospun Nanofibre Based Chemical Sensor: Electrical Characterization. *CMBES Proceedings*, *33*.

[93] Alam, A. U., Qin, Y., Nambiar, S., Yeow, J. T., Howlader, M. M., Hu, N. X., & Deen, M. J. (2018). Polymers and organic materials-based pH sensors for healthcare applications. *Progress in Materials Science*, *96*, 174-216.

[94] Currano, L. J., Sage, F. C., Hagedon, M., Hamilton, L., Patrone, J., & Gerasopoulos, K. (2018). Wearable sensor system for detection of lactate in sweat. *Scientific reports*, *8*(1), 1-11.

[95] Scheiblin, G., Aliane, A., Coppard, R., Owens, R. M., Mailley, P., & Malliaras, G. G. (2015, August). Fully printed metabolite sensor using organic electrochemical transistor. In *Organic Field-Effect Transistors XIV; and Organic Sensors and Bioelectronics VIII* (Vol. 9568, p. 95681E). International Society for Optics and Photonics.

[96] Cranny, A., Harris, N., & White, N. (2014). Screen printed potentiometric chloride sensors. *Procedia Engineering*, *87*, 220-223.

[97] Manjakkal, L., Dervin, S., & Dahiya, R. (2020). Flexible potentiometric pH sensors for wearable systems. *RSC Advances*, *10*(15), 8594-8617.

[98] Yang, Y., Xing, S., Fang, Z., Li, R., Koo, H., & Pan, T. (2017). Wearable microfluidics: fabric-based digital droplet flowmetry for perspiration analysis. *Lab on a Chip*, *17*(5), 926-935.

[99] Lonsdale, W., Wajrak, M., & Alameh, K. (2018). Manufacture and application of RuO2 solid-state metal-oxide pH sensor to common beverages. *Talanta*, *180*, 277-281.

[100] Kurzweil, P. (2009). Metal oxides and ion-exchanging surfaces as pH sensors in liquids: State-of-the-art and outlook. *Sensors*, *9*(6), 4955-4985.

[101] Huang, W. D., Cao, H., Deb, S., Chiao, M., & Chiao, J. C. (2011). A flexible pH sensor based on the iridium oxide sensing film. *Sensors and Actuators A: Physical*, *169*(1), 1-11.

[102] Nie, C., Frijns, A., Zevenbergen, M., & den Toonder, J. (2016). An integrated flex-microfluidic-Si chip device towards sweat sensing applications. *Sensors and Actuators B: Chemical*, *227*, 427-437.

[103] Koncki, R., & Mascini, M. (1997). Screen-printed ruthenium dioxide electrodes for pH measurements. *Analytica Chimica Acta*, *351*(1-3), 143-149.

[104] Labrador, R. H., Soto, J., Martínez-Máñez, R., Coll, C., Benito, A., Ibáñez, J., ... & Gil, L. (2007). An electrochemical characterization of thick-film electrodes based on RuO2-containing resistive pastes. *Journal of Electroanalytical Chemistry*, *611*(1-2), 175-180.

[105] Chou, J. C., Lin, C. Y., Liao, Y. H., Chen, J. T., Tsai, Y. L., Chen, J. L., & Chou, H. T. (2013). Data fusion and fault diagnosis for flexible arrayed pH sensor measurement system based on LabVIEW. *IEEE Sensors Journal*, *14*(5), 1405-1411.

[106] Diculescu, V. C., Beregoi, M., Evanghelidis, A., Negrea, R. F., Apostol, N. G., & Enculescu, I. (2019). Palladium/palladium oxide coated electrospun fibers for wearable sweat pH-sensors. *Scientific reports*, *9*(1), 1-12.

[107] Mani, G. K., Morohoshi, M., Yasoda, Y., Yokoyama, S., Kimura, H., & Tsuchiya, K. (2017). ZnO-based microfluidic pH sensor: a versatile approach for quick recognition of circulating tumor cells in blood. *ACS applied materials & interfaces*, *9*(6), 5193-5203.

[108] Young, S. J., & Tang, W. L. (2019). Wireless zinc oxide based pH sensor system. *Journal of The Electrochemical Society*, *166*(9), B3047-B3050.

[109] Manjakkal, L., Szwagierczak, D., & Dahiya, R. (2019). Metal oxides based electrochemical pH sensors: Current progress and future perspectives. *Progress in Materials Science*, 100635.

[110] Ghoneim, M. T., Nguyen, A., Dereje, N., Huang, J., Moore, G. C., Murzynowski, P. J., & Dagdeviren, C. (2019). Recent Progress in Electrochemical pH-Sensing Materials and Configurations for Biomedical Applications. *Chemical reviews*, *119*(8), 5248-5297.

[111] Singh, K., Lou, B. S., Her, J. L., Pang, S. T., & Pan, T. M. (2019). Super Nernstian pH response and enzyme-free detection of glucose using sol-gel derived RuOx on PET flexible-based extended-gate field-effect transistor. *Sensors and Actuators B: Chemical*, *298*, 126837.

[112] Khalil, M., Liu, N., & Lee, R. L. (2018). Super-Nernstian potentiometric pH sensor based on the electrodeposition of iridium oxide nanoparticles. *International Journal of Technology*, *9*(3), 446-454.

[113] Salvo, P., Calisi, N., Melai, B., Dini, V., Paoletti, C., Lomonaco, T., ... & Romanelli, M. (2017). Temperature-and pH-sensitive wearable materials for monitoring foot ulcers. *International journal of nanomedicine*, *12*, 949.

[114] Dang, W., Manjakkal, L., Navaraj, W. T., Lorenzelli, L., Vinciguerra, V., & Dahiya, R. (2018). Stretchable wireless system for sweat pH monitoring. *Biosensors and Bioelectronics*, *107*, 192-202.

[115] Sahu, D., Kannan, G. M., & Vijayaraghavan, R. (2014). Carbon black particle exhibits size dependent toxicity in human monocytes. *International journal of inflammation*, *2014*.

[116] Ema, M., Matsuda, A., Kobayashi, N., Naya, M., & Nakanishi, J. (2011). Evaluation of dermal and eye irritation and skin sensitization due to carbon nanotubes. *Regulatory Toxicology and Pharmacology*, *61*(3), 276-281.

[117] Nezakati, T., Seifalian, A., Tan, A., & Seifalian, A. M. (2018). Conductive polymers: opportunities and challenges in biomedical applications. *Chemical reviews*, *118*(14), 6766-6843.

[118] Alam, F., RoyChoudhury, S., Jalal, A. H., Umasankar, Y., Forouzanfar, S., Akter, N., ... & Pala, N. (2018). Lactate biosensing: The emerging point-of-care and personal health monitoring. *Biosensors and Bioelectronics, 117*, 818-829.

[119] Korostynska, O., Arshak, K., Gill, E., & Arshak, A. (2007). Review on state-of-the-art in polymer based pH sensors. *Sensors (Basel, Switzerland), 7*(12), 3027.

[120] Gou, P., Kraut, N. D., Feigel, I. M., Bai, H., Morgan, G. J., Chen, Y., ... & Mickle, M. (2014). Carbon nanotube chemiresistor for wireless pH sensing. *Scientific reports, 4*, 4468.

[121] Sulka, G. D., Hnida, K., & Brzózka, A. (2013). pH sensors based on polypyrrole nanowire arrays. *Electrochimica Acta, 104*, 536-541.

[122] Prissanaroon-Ouajai, W., Pigram, P. J., Jones, R., & Sirivat, A. (2009). A sensitive and highly stable polypyrrole-based pH sensor with hydroquinone monosulfonate and oxalate co-doping. *Sensors and Actuators B: Chemical, 138*(2), 504-511.

[123] Bandodkar, A. J., Hung, V. W., Jia, W., Valdés-Ramírez, G., Windmiller, J. R., Martinez, A. G., ... & Wang, J. (2013). Tattoo-based potentiometric ion-selective sensors for epidermal pH monitoring. *Analyst, 138*(1), 123-128.

[124] Yoon, J. H., Hong, S. B., Yun, S. O., Lee, S. J., Lee, T. J., Lee, K. G., & Choi, B. G. (2017). High performance flexible pH sensor based on polyaniline nanopillar array electrode. *Journal of colloid and interface science, 490*, 53-58.

[125] Sha, R., Komori, K., & Badhulika, S. (2017). Amperometric pH sensor based on graphene–polyaniline composite. *IEEE Sensors Journal, 17*(16), 5038-5043.

[126] Guinovart, T., Valdés-Ramírez, G., Windmiller, J. R., Andrade, F. J., & Wang, J. (2014). Bandage-based wearable potentiometric sensor for monitoring wound pH. *Electroanalysis, 26*(6), 1345-1353.

[127] Rahimi, R., Ochoa, M., Parupudi, T., Zhao, X., Yazdi, I. K., Dokmeci, M. R., ... & Ziaie, B. (2016). A low-cost flexible pH sensor array for wound assessment. *Sensors and Actuators B: Chemical, 229*, 609-617.

[128] Smith, R. E., Totti, S., Velliou, E., Campagnolo, P., Hingley-Wilson, S. M., Ward, N. I., ... & Crean, C. (2019). Development of a novel highly conductive and flexible cotton yarn for wearable pH sensor technology. *Sensors and Actuators B: Chemical, 287*, 338-345.

[129] Lindfors, T., & Ivaska, A. (2002). pH sensitivity of polyaniline and its substituted derivatives. *Journal of Electroanalytical Chemistry*, *531*(1), 43-52.

[130] Kaempgen, M., & Roth, S. (2006). Transparent and flexible carbon nanotube/polyaniline pH sensors. *Journal of Electroanalytical Chemistry, 586*(1), 72-76.

[131] Gill, E., Arshak, A., Arshak, K., & Korostynska, O. (2007). pH sensitivity of novel PANI/PVB/PS3 composite films. *Sensors, 7*(12), 3329-3346.

[132] Gill, E. I., Arshak, A., Arshak, K., & Korostynska, O. (2008). Novel Conducting Polymer Composite pH Sensors for Medical Applications. In *14th Nordic-Baltic Conference on Biomedical Engineering and Medical Physics* (pp. 225-228). Springer, Berlin, Heidelberg.

[133] Gill, E., Arshak, A., Arshak, K., & Korostynska, O. (2010). Response mechanism of novel polyaniline composite conductimetric pH sensors and the effects of polymer binder, surfactant and film thickness on sensor sensitivity. *European polymer journal, 46*(10), 2042-2050.

[134] Gomes, T. C., Constantino, C. J. L., Lopes, E. M., Job, A. E., & Alves, N. (2012). Thermal inkjet printing of polyaniline on paper. *Thin Solid Films, 520*(24), 7200-7204.

[135] Kulkarni, M. V., Apte, S. K., Naik, S. D., Ambekar, J. D., & Kale, B. B. (2013). Ink-jet printed conducting polyaniline based flexible humidity sensor. *Sensors and Actuators B: Chemical, 178*, 140-143.

[136] Kit-Anan, W., Olarnwanich, A., Sriprachuabwong, C., Karuwan, C., Tuantranont, A., Wisitsoraat, A., ... & Pimpin, A. (2012). Disposable paper-based electrochemical sensor utilizing inkjet-printed Polyaniline modified screen-printed carbon electrode for Ascorbic acid detection. *Journal of Electroanalytical Chemistry, 685*, 72-78.

[137] Bao, Q., Yang, Z., Song, Y., Fan, M., Pan, P., Liu, J., ... & Wei, J. (2019). Printed flexible bifunctional electrochemical urea-pH sensor based on multiwalled carbon nanotube/polyaniline electronic ink. *Journal of Materials Science: Materials in Electronics, 30*(2), 1751-1759.

[138] Caldara, M., Colleoni, C., Guido, E., Rosace, G., Re, V., & Vitali, A. (2013, May). A wearable sensor platform to monitor sweat pH and skin temperature. In *2013 IEEE International Conference on Body Sensor Networks* (pp. 1-6). IEEE.

[139] Promphet, N., Rattanawaleedirojn, P., Siralertmukul, K., Soatthiyanon, N., Potiyaraj, P., Thanawattano, C., ... & Rodthongkum, N. (2019). Non-invasive textile based colorimetric sensor for the simultaneous detection of sweat pH and lactate. *Talanta, 192*, 424-430.

[140] L'Oréal. (n.d.). My Skin Track Ph by La Roche-Posay won the CES 2019 Innovation Award. https://mediaroom.loreal.com/en/loreal-unveils-prototype-of-first-ever-wearable-microfluidic-sensor-to-measure-skin-ph-levels/

[141] Jia, W., Bandodkar, A. J., Valdés-Ramírez, G., Windmiller, J. R., Yang, Z., Ramírez, J., ... & Wang, J. (2013). Electrochemical tattoo biosensors for real-time noninvasive lactate monitoring in human perspiration. *Analytical chemistry, 85*(14), 6553-6560.

[142] Anastasova, S., Crewther, B., Bembnowicz, P., Curto, V., Ip, H. M., Rosa, B., & Yang, G. Z. (2017). A wearable multisensing patch for continuous sweat monitoring. *Biosensors and Bioelectronics, 93*, 139-145.

[143] Luo, X., Yu, H., & Cui, Y. (2017). A wearable amperometric biosensor on a cotton fabric for lactate. *IEEE Electron Device Letters, 39*(1), 123-126.

[144] Modali, A., Vanjari, S. R. K., & Dendukuri, D. (2016). Wearable Woven Electrochemical Biosensor Patch for Non-invasive Diagnostics. *Electroanalysis, 28*(6), 1276-1282.

[145] Labroo, P., & Cui, Y. (2013). Flexible graphene bio-nanosensor for lactate. *Biosensors and Bioelectronics, 41*, 852-856.

[146] Venkatraman, P. D., Velusamy, V., Kharel, R., & Collins, S. (2016). Smart wearable biosensor for non-invasive real time detection of sweat lactate using compression garments.

[147] Imani, S., Bandodkar, A. J., Mohan, A. V., Kumar, R., Yu, S., Wang, J., & Mercier, P. P. (2016). A wearable chemical–electrophysiological hybrid biosensing system for real-time health and fitness monitoring. *Nature communications, 7*(1), 1-7.

[148] He, W., Wang, C., Wang, H., Jian, M., Lu, W., Liang, X., ... & Zhang, Y. (2019). Integrated textile sensor patch for real-time and multiplex sweat analysis. *Science advances, 5*(11), eaax0649.

[149] Clark Jr, L. C., & Lyons, C. (1962). Electrode systems for continuous monitoring in cardiovascular surgery. *Annals of the New York Academy of sciences, 102*(1), 29-45.

[150] Dieffenderfer, J., Wilkins, M., Hood, C., Beppler, E., Daniele, M. A., & Bozkurt, A. (2016, January). Towards a sweat-based wireless and wearable electrochemical sensor. In *2016 IEEE Sensors* (pp. 1-3). IEEE.

[151] Nagamine, K., Mano, T., Nomura, A., Ichimura, Y., Izawa, R., Furusawa, H., ... & Tokito, S. (2019). Noninvasive sweat-Lactate Biosensor emplsoying a Hydrogel-Based touch pad. *Scientific reports, 9*(1), 1-8.

[152] Bandodkar, A. J., Gutruf, P., Choi, J., Lee, K., Sekine, Y., Reeder, J. T., ... & Ghaffari, R. (2019). Battery-free, skin-interfaced microfluidic/electronic systems for simultaneous electrochemical, colorimetric, and volumetric analysis of sweat. *Science advances, 5*(1), eaav3294.

[153] Alam, F., RoyChoudhury, S., Jalal, A. H., Umasankar, Y., Forouzanfar, S., Akter, N., ... & Pala, N. (2018). Lactate biosensing: The emerging point-of-care and personal health monitoring. *Biosensors and Bioelectronics, 117*, 818-829.

[154] Rathee, K., Dhull, V., Dhull, R., & Singh, S. (2016). Biosensors based on electrochemical lactate detection: A comprehensive review. *Biochemistry and biophysics reports, 5*, 35-54.

[155] Nikolaus, N., & Strehlitz, B. (2008). Amperometric lactate biosensors and their application in (sports) medicine, for life quality and wellbeing. *Microchimica Acta, 160*(1-2), 15-55.

[156] Garcia, S. O., Ulyanova, Y. V., Figueroa-Teran, R., Bhatt, K. H., Singhal, S., & Atanassov, P. (2016). Wearable sensor system powered by a biofuel cell for detection of lactate levels in sweat. *ECS Journal of Solid State Science and Technology*, *5*(8), M3075.

[157] Chou, J. C., Yan, S. J., Liao, Y. H., Lai, C. H., Wu, Y. X., Wu, C. Y., ... & Wu, T. Y. (2017). Fabrication of flexible arrayed lactate biosensor based on immobilizing LDH-NAD+ on NiO film modified by GO and MBs. *Sensors, 17*(7), 1618.

[158] Berger, A., & Blum, L. J. (1995). Enhancement of lactate oxidase/peroxidase-based fiberoptic sensor. Biosensors and *Bioelectronics, 10*(3-4), vi-vi.

[159] Chan, D., Barsan, M. M., Korpan, Y., & Brett, C. M. (2017). L-lactate selective impedimetric bienzymatic biosensor based on lactate dehydrogenase and pyruvate oxidase. *Electrochimica Acta, 231*, 209-215.

[160] Zaryanov, N. V., Nikitina, V. N., Karpova, E. V., Karyakina, E. E., & Karyakin, A. A. (2017). Nonenzymatic sensor for lactate detection in human sweat. *Analytical chemistry, 89*(21), 11198-11202.

[161] Li, J., Liu, L., Wang, P., & Zheng, J. (2014). Potentiometric detection of saccharides based on highly ordered poly (aniline boronic acid) nanotubes. *Electrochimica Acta*, *121*, 369-375.

[162] Wang, Z., Gui, M., Asif, M., Yu, Y., Dong, S., Wang, H., ... & Liu, H. (2018). A facile modular approach to the 2D oriented assembly MOF electrode for non-enzymatic sweat biosensors. *Nanoscale, 10*(14), 6629-6638.

[163] Sedenho, G. C., Lee, P. T., Toh, H. S., Salter, C., Johnston, C., Stradiotto, N. R., & Compton, R. G. (2015). Nanoelectrocatalytic oxidation of lactic acid using nickel nanoparticles. *The Journal of Physical Chemistry C, 119*(12), 6896-6905.

[164] Kim, S., Kim, K., Kim, H. J., Lee, H. N., Park, T. J., & Park, Y. M. (2018). Non-enzymatic electrochemical lactate sensing by NiO and Ni (OH) 2 electrodes: a mechanistic investigation. *Electrochimica Acta, 276*, 240-246.

[165] Huang, Y. S., Chen, K. Y., Cheng, Y. T., Lee, C. K., & Tsai, H. E. (2020). An Inkjet-Printed Flexible Non-Enzymatic Lactate Sensor for Clinical Blood Plasma Test. *IEEE Electron Device Letters, 41*(4), 597-600.

[166] Schmitt, R. E., Molitor, H. R., & Wu, T. (2012). Voltammetric method for the determination of lactic acid using a carbon paste electrode modified with cobalt phthalocyanine. *Int. J. Electrochem. Sci, 7*(11), 10835-10841.

[167] Dai, G., Hu, J., Zhao, X., & Wang, P. (2017). A colorimetric paper sensor for lactate assay using a cellulose-Binding recombinant enzyme. *Sensors and Actuators B: Chemical, 238*, 138-144.

[168] Promphet, N., Rattanawaleedirojn, P., Siralertmukul, K., Soatthiyanon, N., Potiyaraj, P., Thanawattano, C., ... & Rodthongkum, N. (2019). Non-invasive textile based colorimetric sensor for the simultaneous detection of sweat pH and lactate. *Talanta, 192*, 424-430.

[169] Koh, A., Kang, D., Xue, Y., Lee, S., Pielak, R. M., Kim, J., ... & Manco, M. C. (2016). A soft, wearable microfluidic device for the capture, storage, and colorimetric sensing of sweat. *Science translational medicine, 8*(366), 366ra165-366ra165.

[170] Sartain, F. K., Yang, X., & Lowe, C. R. (2008). Complexation of L-Lactate with Boronic Acids: A Solution and Holographic Analysis. *Chemistry–A European Journal, 14*(13), 4060-4067.

[171] Gallagher, A. J., Ní Annaidh, A., & Bruyère, K. (2012). Dynamic tensile properties of human skin. In *IRCOBI Conference 2012, 12-14 September 2012, Dublin (Ireland)*. International Research Council on the Biomechanics of Injury.

[172] Jeerapan, I., & Poorahong, S. (2020). Flexible and Stretchable Electrochemical Sensing Systems: Materials, Energy Sources, and Integrations. *Journal of The Electrochemical Society, 167*(3), 037573.

[173] Zhou, Y., Dong, H., Liu, L., Liu, J., & Xu, M. (2014). A novel potentiometric sensor based on a poly (anilineboronic acid)/graphene modified electrode for probing sialic acid through boronic acid-diol recognition. *Biosensors and Bioelectronics*, *60*, 231-236.

[174] Aoki, K. J., & Chen, J. (2018). Tips of Voltammetry. In *Voltammetry*. IntechOpen.

[175] Okamoto, Y., & Brenner, W. (1964). Organic Semiconductors, Reinhold Pub. *Co., NY*.

[176] Huang, W. S., Humphrey, B. D., & MacDiarmid, A. G. (1986). Polyaniline, a novel conducting polymer. Morphology and chemistry of its oxidation and reduction in aqueous electrolytes. J*ournal of the Chemical Society, Faraday Transactions 1: Physical Chemistry in Condensed Phases, 82*(8), 2385-2400.

[177] Song, E., & Choi, J. W. (2013). Conducting polyaniline nanowire and its applications in chemiresistive sensing. *Nanomaterials, 3*(3), 498-523.

[178] Baker, C. O., Huang, X., Nelson, W., & Kaner, R. B. (2017). Polyaniline nanofibers: broadening applications for conducting polymers. *Chemical Society Reviews, 46*(5), 1510-1525.

[179] Zare, E. N., Jamaledin, R., Naserzadeh, P., Afjeh-Dana, E., Ashtari, B., Hosseinzadeh, M., ... & Makvandi, P. (2019). Metal-Based nanostructures/PLGA nanocomposites: antimicrobial activity, cytotoxicity, and their biomedical applications. *ACS applied materials & interfaces*, *12*(3), 3279-3300.

[180] Vieira, N. C., Fernandes, E. G., Faceto, A. D., Zucolotto, V., & Guimarães, F. E. (2011). Nanostructured polyaniline thin films as pH sensing membranes in FET-based devices. *Sensors and Actuators B: Chemical*, *160*(1), 312-317.

[181] Kohut-Svelko, N., Reynaud, S., & François, J. (2005). Synthesis and characterization of polyaniline prepared in the presence of nonionic surfactants in an aqueous dispersion. *Synthetic Metals*, *150*(2), 107-114.

[182] Olad, A., Ilghami, F., & Nosrati, R. (2012). Surfactant-assisted synthesis of polyaniline nanofibres without shaking and stirring: effect of conditions on morphology and conductivity. *Chemical Papers*, *66*(8), 757-764.

[183] Carswell, A. D., O'Rea, E. A., & Grady, B. P. (2003). Adsorbed surfactants as templates for the synthesis of morphologically controlled polyaniline and polypyrrole nanostructures on flat surfaces: from spheres to wires to flat films. *Journal of the American Chemical Society*, *125*(48), 14793-14800.

[184] Chuang, C. H., Wu, H. P., Chen, C. H., & Wu, P. R. (2011, November). Flexible pH sensor with polyaniline layer based on impedance measurement. In *2011 Fifth International Conference on Sensing Technology* (pp. 211-216). IEEE.

[185] Karyakin, A. A., Vuki, M., Lukachova, L. V., Karyakina, E. E., Orlov, A. V., Karpachova, G. P., & Wang, J. (1999). Processible polyaniline as an advanced potentiometric pH transducer. Application to biosensors. *Analytical Chemistry, 71*(13), 2534-2540.

[186] Bienkowski, K. (2006). *Polyaniline and its derivatives doped with Lewis acids-synthesis and spectroscopic properites* (Doctoral dissertation, Université Joseph-Fourier-Grenoble I; Warsaw University of Technology).

[187] Krukiewicz, K., & Katunin, A. (2016). The effect of reaction medium on the conductivity and morphology of polyaniline doped with camphorsulfonic acid. *Synthetic Metals*, *214*, 45-49.

[188] Han, Y. G., Kusunose, T., & Sekino, T. (2009). One-step reverse micelle polymerization of organic dispersible polyaniline nanoparticles. *Synthetic Metals*, *159*(1-2), 123-131.

[189] Babazadeh, M. (2009). Aqueous dispersions of DBSA-doped polyaniline: One-pot preparation, characterization, and properties study. *Journal of applied polymer science*, *113*(6), 3980-3984.

[190] Pine Research. (2020). Screen-Printed Electrode Information. https://pineresearch.com/shop/products/electrodes/screen-printed-electrodes/carbon-spes/#documentation

[191] Abu-Thabit, N. Y. (2016). Chemical oxidative polymerization of polyaniline: A practical approach for preparation of smart conductive textiles. *Journal of chemical education, 93*(9), 1606-1611.

[192] Gul, S., & Bilal, S. (2013, June). Synthesis and characterization of processable polyaniline salts. In *Journal of Physics: Conference Series* (Vol. 439, No. 1, p. 012002). IOP Publishing.

[193] Brooks, W. L., & Sumerlin, B. S. (2016). Synthesis and applications of boronic acid-containing polymers: from materials to medicine. *Chemical reviews*, *116*(3), 1375-1397.

[194] Çiftçi, H., Alver, E., Çelik, F., Metin, A. Ü., & Tamer, U. (2016). Non-enzymatic sensing of glucose using a glassy carbon electrode modified with gold nanoparticles coated with polyethyleneimine and 3-aminophenylboronic acid. *Microchimica Acta*, *183*(4), 1479-1486.

[195] Kim, D. M., Moon, J. M., Lee, W. C., Yoon, J. H., Choi, C. S., & Shim, Y. B. (2017). A potentiometric non-enzymatic glucose sensor using a molecularly imprinted layer bonded on a conducting polymer. *Biosensors and Bioelectronics*, *91*, 276-283.

[196] Dorledo de Faria, R. A., Iden, H., Heneine, L. G. D., Matencio, T., & Messaddeq, Y. (2019). Non-enzymatic impedimetric sensor based on 3-aminophenylboronic acid functionalized screen-printed carbon electrode for highly sensitive glucose detection. *Sensors*, *19*(7), 1686.

[197] Li, L., Li, Y., Qin, W., & Qian, Y. (2020). Potentiometric detection of glucose based on oligomerization with a diboronic acid using polycation as an indicator. *Analytical Methods*, *12*(36), 4422-4428.

[198] Wustoni, S., Savva, A., Sun, R., Bihar, E., & Inal, S. (2019). Enzyme-free detection of glucose with a hybrid conductive gel electrode. *Advanced Materials Interfaces*, *6*(1), 1800928.

[199] Bunnfors, K. (2015). Synthesis and electrochemical characterisation of processable polypyrrole boronic acid derivatives for carbohydrate binding.

[200] Andreev, E. A., Komkova, M. A., Nikitina, V. N., & Karyakin, A. A. (2019). Reagentless Impedimetric Sensors Based on Aminophenylboronic Acids. *Journal of Analytical Chemistry*, *74*(2), 153-171.

[201] Ouyang, J., Chen, M., Bao, W. J., Zhang, Q. W., Wang, K., & Xia, X. H. (2015). Morphology controlled poly (aminophenylboronic acid) nanostructures as smart substrates for enhanced capture and release of circulating tumor cells. *Advanced Functional Materials, 25*(38), 6122-6130.

[202] Li, G., Li, Y., Peng, H., & Chen, K. (2011). Synthesis of poly (anilineboronic acid) nanofibers for electrochemical detection of glucose. *Macromolecular rapid communications, 32*(15), 1195-1199.

[203] Deore, B. A., Yu, I., Woodmass, J., & Freund, M. S. (2008). Conducting Poly (anilineboronic acid) nanostructures: controlled synthesis and characterization. *Macromolecular Chemistry and Physics, 209*(11), 1094-1105.

[204] Deore, B. A., & Freund, M. S. (2009). Self-doped polyaniline nanoparticle dispersions based on boronic acid− phosphate complexation. *Macromolecules, 42*(1), 164-168.

[205] Zou, F., Kong, Y., & Cui, B. (2020). Fluoride-free electropolymerization of 3-aminophenylboronic acid in room temperature ionic liquids without exogenous protons. *Journal of Molecular Liquids*, *317*, 114141.

[206] Chaubey, A., & Malhotra, B. (2002). Mediated biosensors. *Biosensors and bioelectronics*, *17*(6-7), 441-456.